University of Stuttgart
Institute of Aerodynamics and Gas Dynamics

NRG

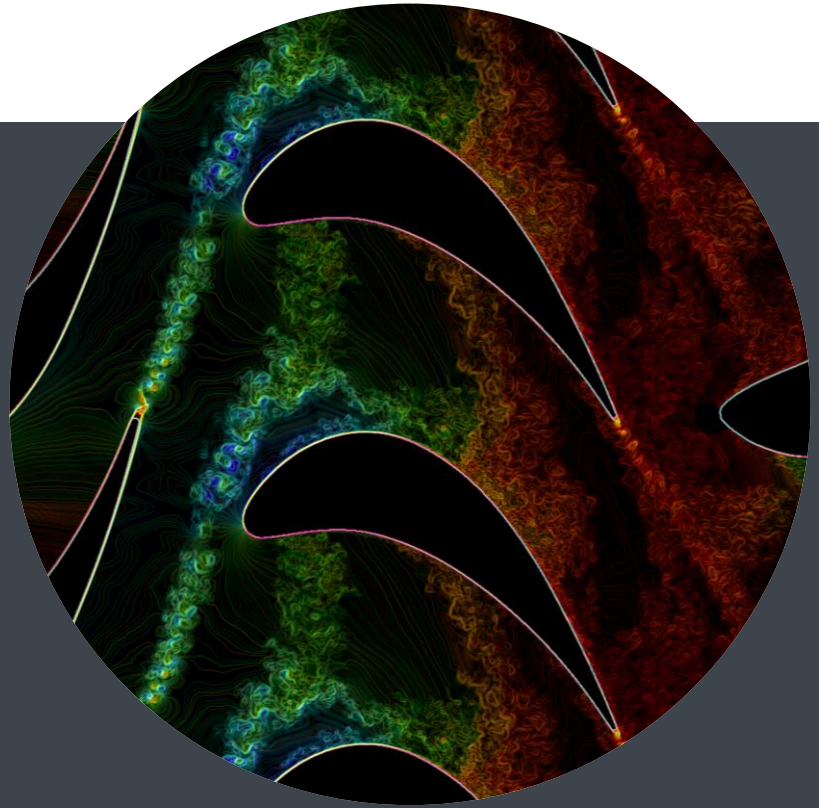

Efficient solution strategies for multiscale flow problems: combining adaptive high order discretizations, models and data

LLNL Seminar, 02/2026

Andrea Beck
Institute of Aerodynamics and Gas Dynamics (IAG) &
Stuttgart Center for Simulation Science (SC SimTech)

All simulations shown here are conducted with FLEXI by members of the Numerics Research Group unless stated otherwise. I would like to thank all my present and former Ph.D. students, M.Sc. students, PostDocs and all the other colleagues I have had the pleasure of working with.

www.numericsresearchgroup.org

All computations shown here are done with our code framework FLEXI unless specified

NRG

Overview

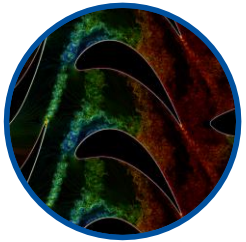

Motivation

Discretization schemes for multi-X problems

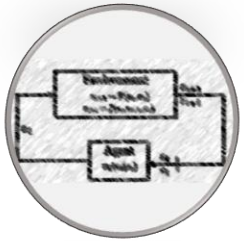

From data-driven to integrated CFD/ML

Definition

High Order Numerical Schemes for PDEs

- Consider a PDE with exact solution u(x,t).
- A numerical scheme with grid spacing h (and time step Δt) produces an approximation u_h.
- The scheme is said to be of order p if there exists a constant C, independent of h, such that for an appropriate norm

$$|u - u_h| \leq Ch^p \; as \; h \to 0,$$

- Higher p implies faster convergence as the grid is refined.
- High-order schemes achieve a given accuracy with fewer grid points.
- Common examples:
  - High-order finite difference methods
  - Finite volume schemes with p-th order reconstruction
  - Discontinuous Galerkin methods

High Order Numerical Schemes for PDEs

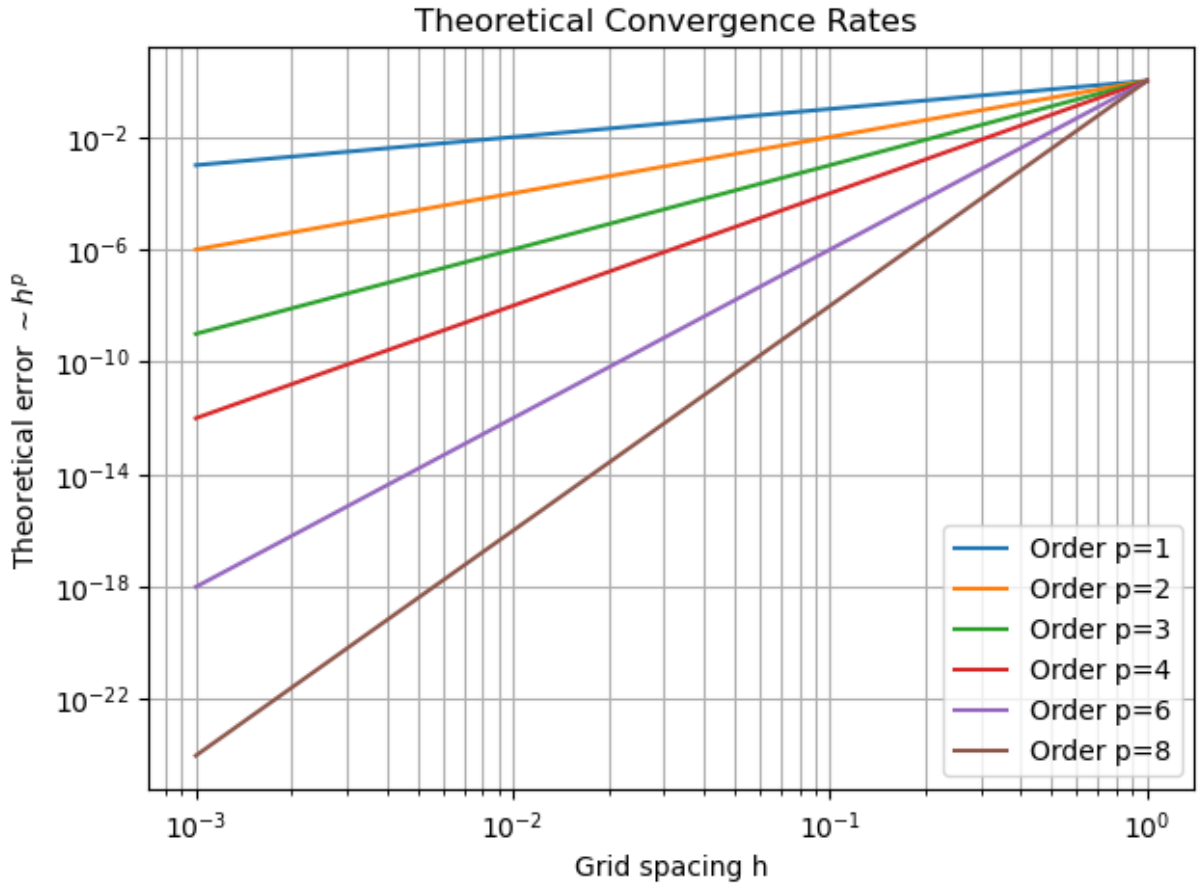

High Order Numerical Schemes for PDEs

- Are sometimes said to be….
  - Very difficult to analyze, understand, code and parallelize
  - Accurate but really slow
  - For single phase incompressible flows only
  - **Really only good for TBLs on flat plates!**

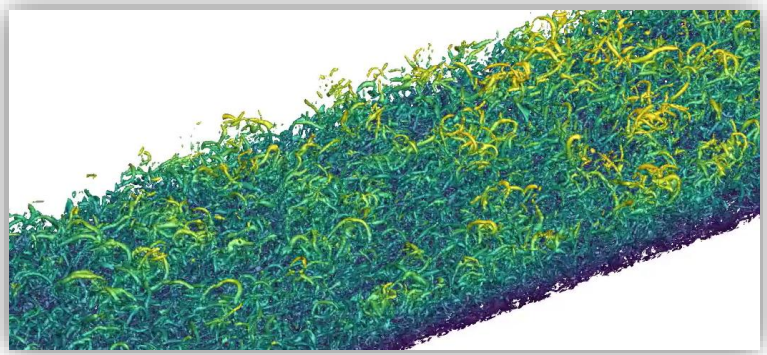

By Wenzel, Rist, Kloker at IAG

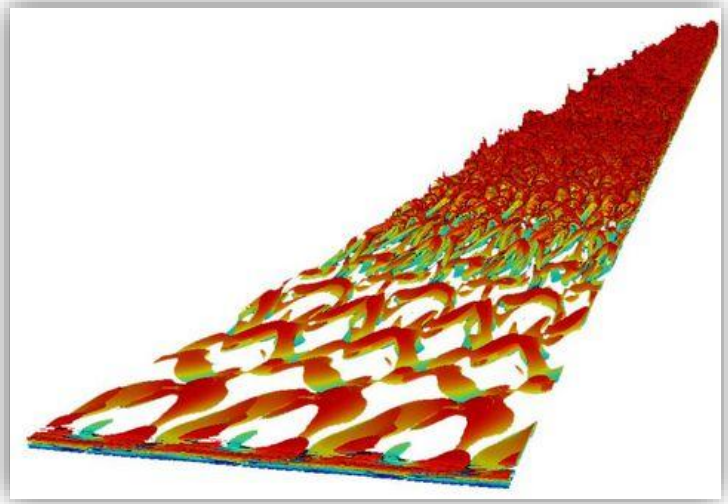

By Atak, Beck, Munz at IAG

(Almost) Real World Problems

Multiphase, Multiscale, Multimethod: Rocket Engine

- Spacecraft propulsion / Raptor Engine

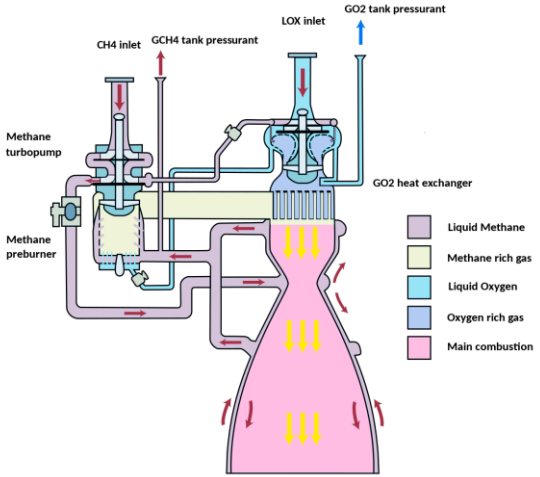

- Cryogenic fuel and oxidizer
- Full-flow staged combustion cycle
- Preburners provide oxygen- and methane-rich gas
- Non-equilibrium: Vaporization in preburners
- Compressibility: Extreme ambient conditions
- Close understanding vital
- Achieve stable combustion
- Avoid cavitation in fuel lines

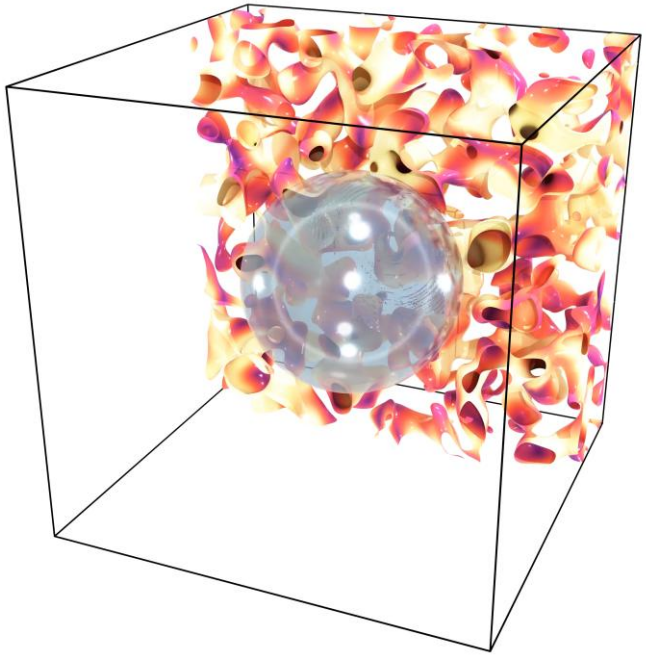

- Droplet in compressible turbulence

- Shock-Droplet Interaction

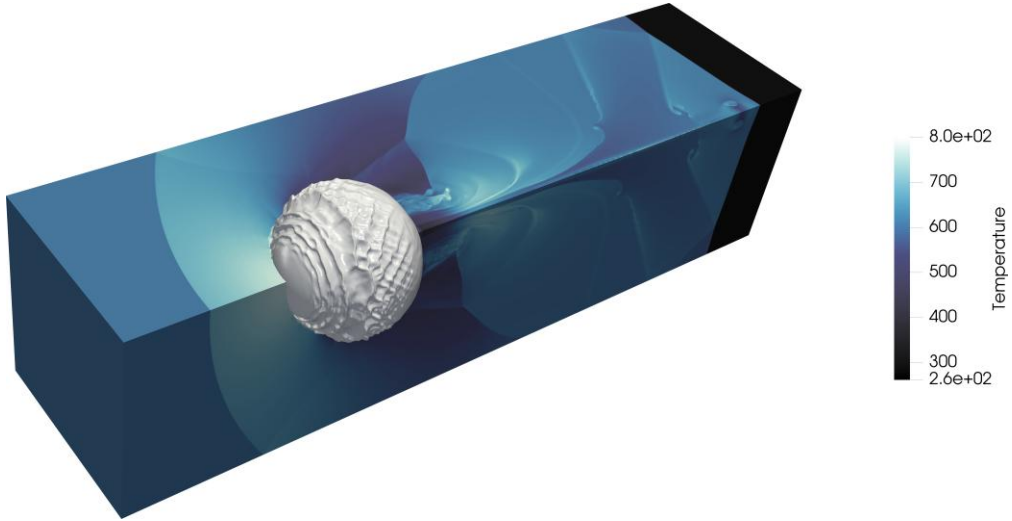

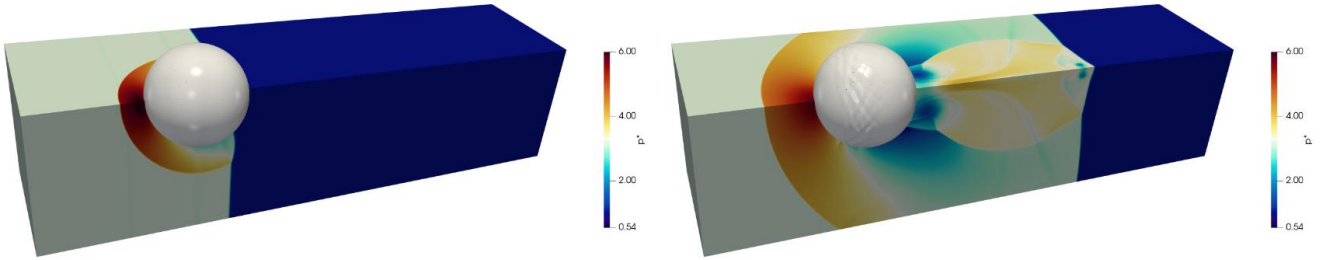

(a) $t^* = 0.8$ (b) $t^* = 2.4$

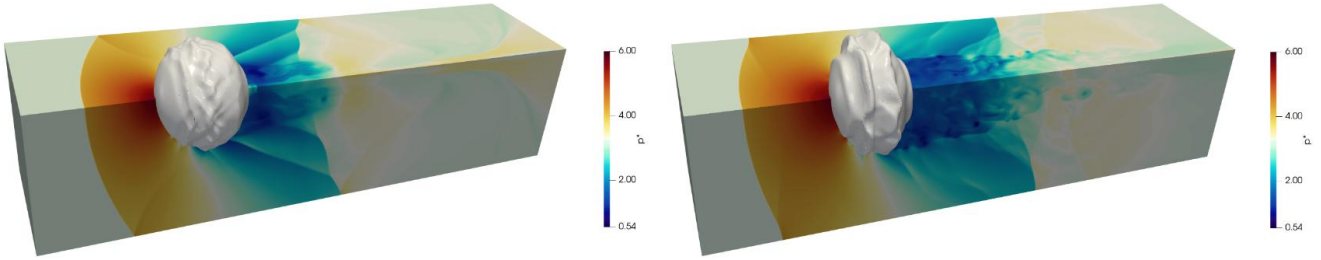

(c) $t^* = 4.7$ (d) $t^* = 7.0$

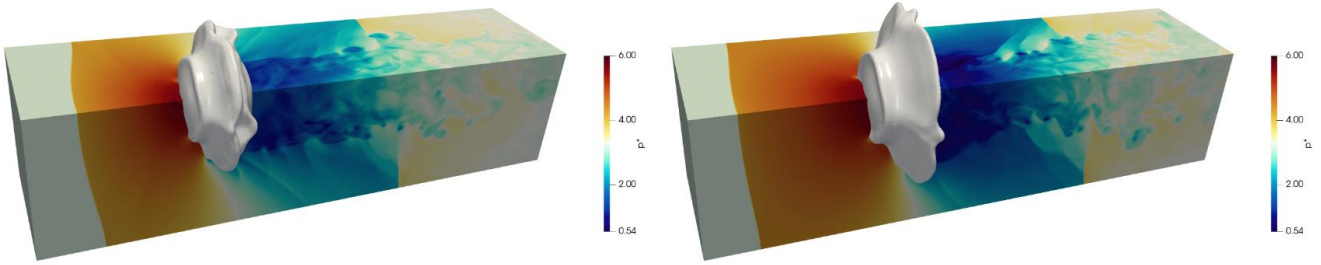

(e) $t^* = 9.4$ (f) $t^* = 11.8$

Icing on Wings

Stefano Fornasier via http://tesi.cab.unipd.it/50432/1/STEFANO_FORNASIER_1147354_assignsubmission_file_Fornasier_Stefano_1056548.pdf

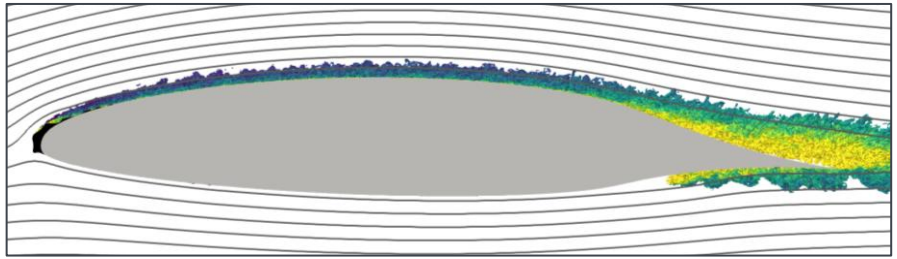

Turbulent Boundary Layer

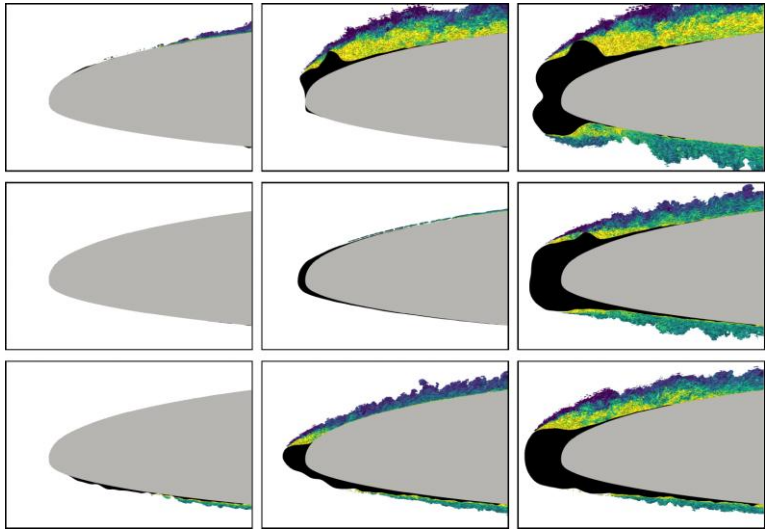

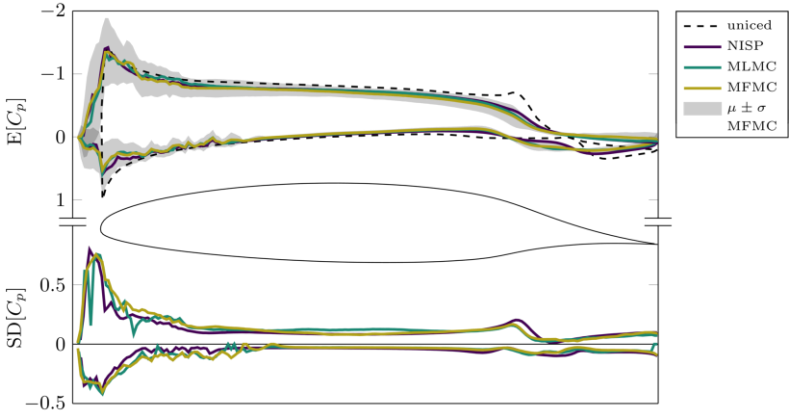

Sandstorm on Mars

Copyright by NASA

- High sand concentration, compressible flow (Ma=0.8), Martian atmospheric conditions
- Modulation of shock structures, strengths and wake turbulence by particles
- DGSEM N4, four-way coupling Euler-Lagrange

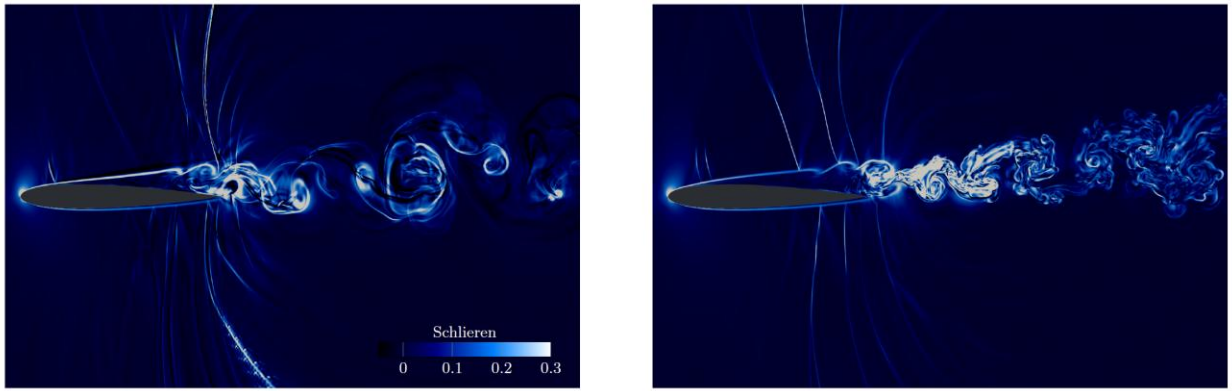

Figure 12: Comparison of pseudo-Schlieren as a representation of density gradients for the unladen (left) and particle-laden (right) flow around a NACA 0012 airfoil at $Ma = 0.8$ and $Re = 50\,000$.

Multiphase, Multiscale, Multimethod: Wake / HTP interaction under buffet

FOR 2895

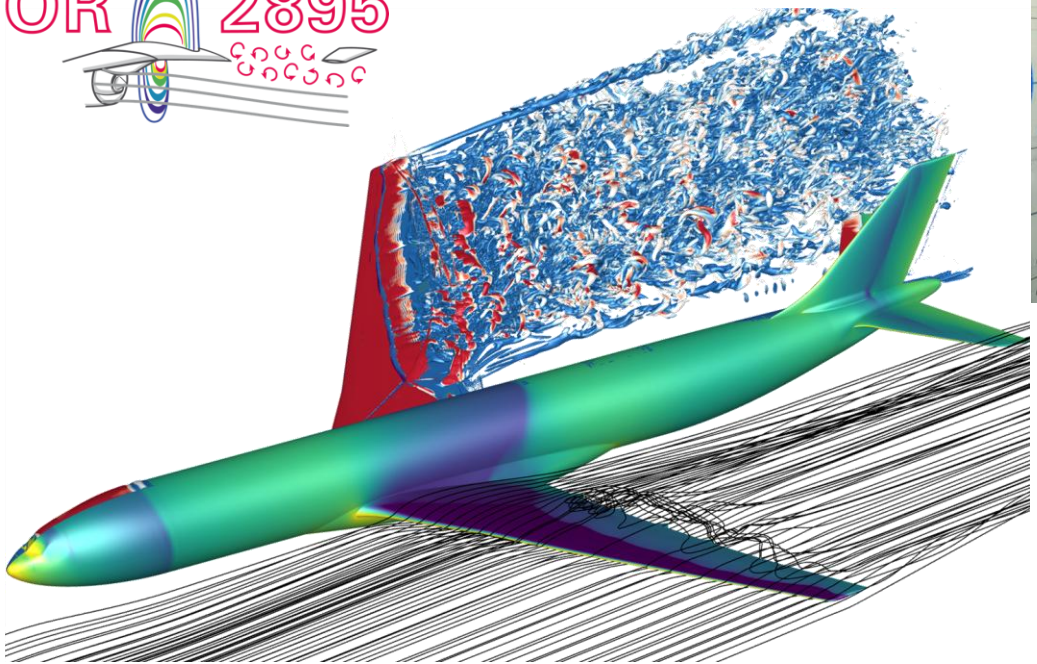

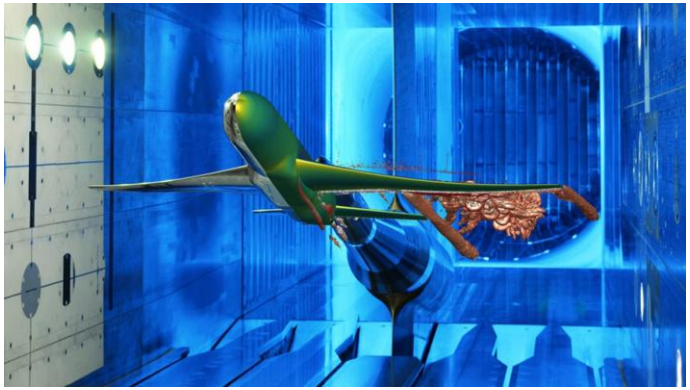

ETW EUROPEAN TRANSONIC WINDTUNNEL

HELMHOLTZ

AIRBUS

Multiphase, Multiscale, Multimethod: Wake / HTP interaction under buffet

FOR 2895

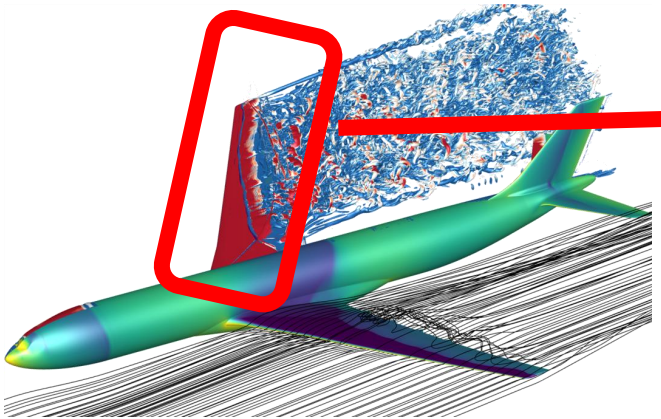

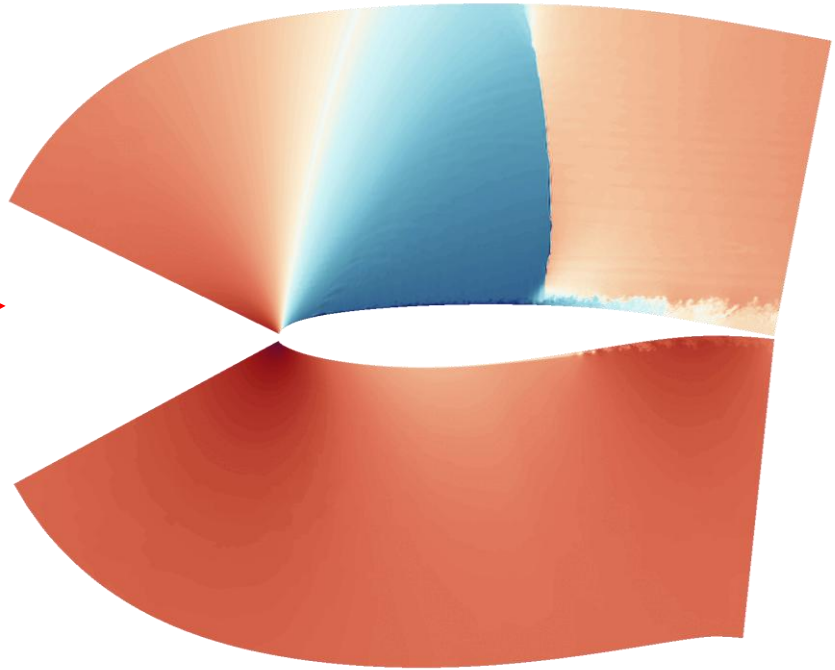

Multiphase, Multiscale, Multimethod: Wake / HTP interaction under buffet

FOR 2895

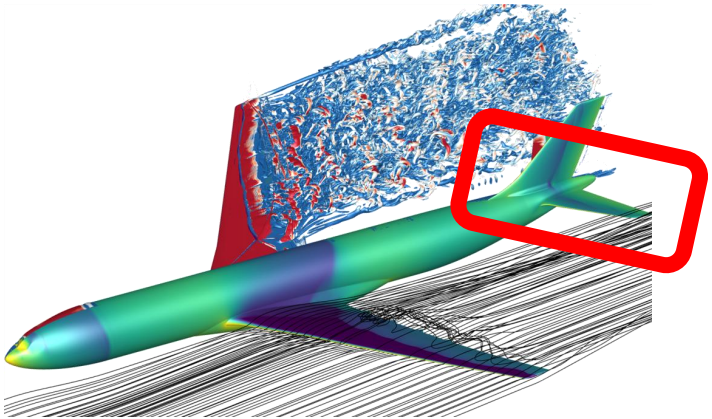

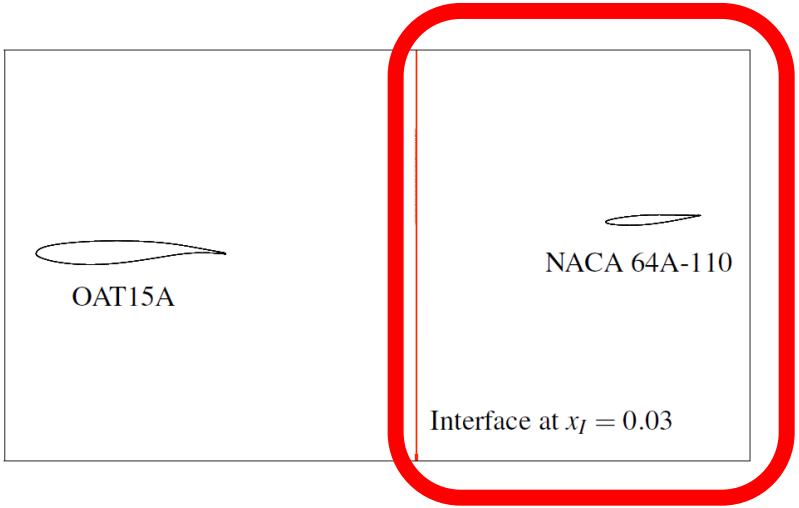

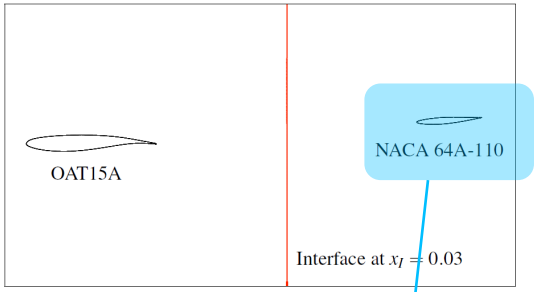
OAT15A
NACA 64A-110
Interface at $x_I = 0.03$

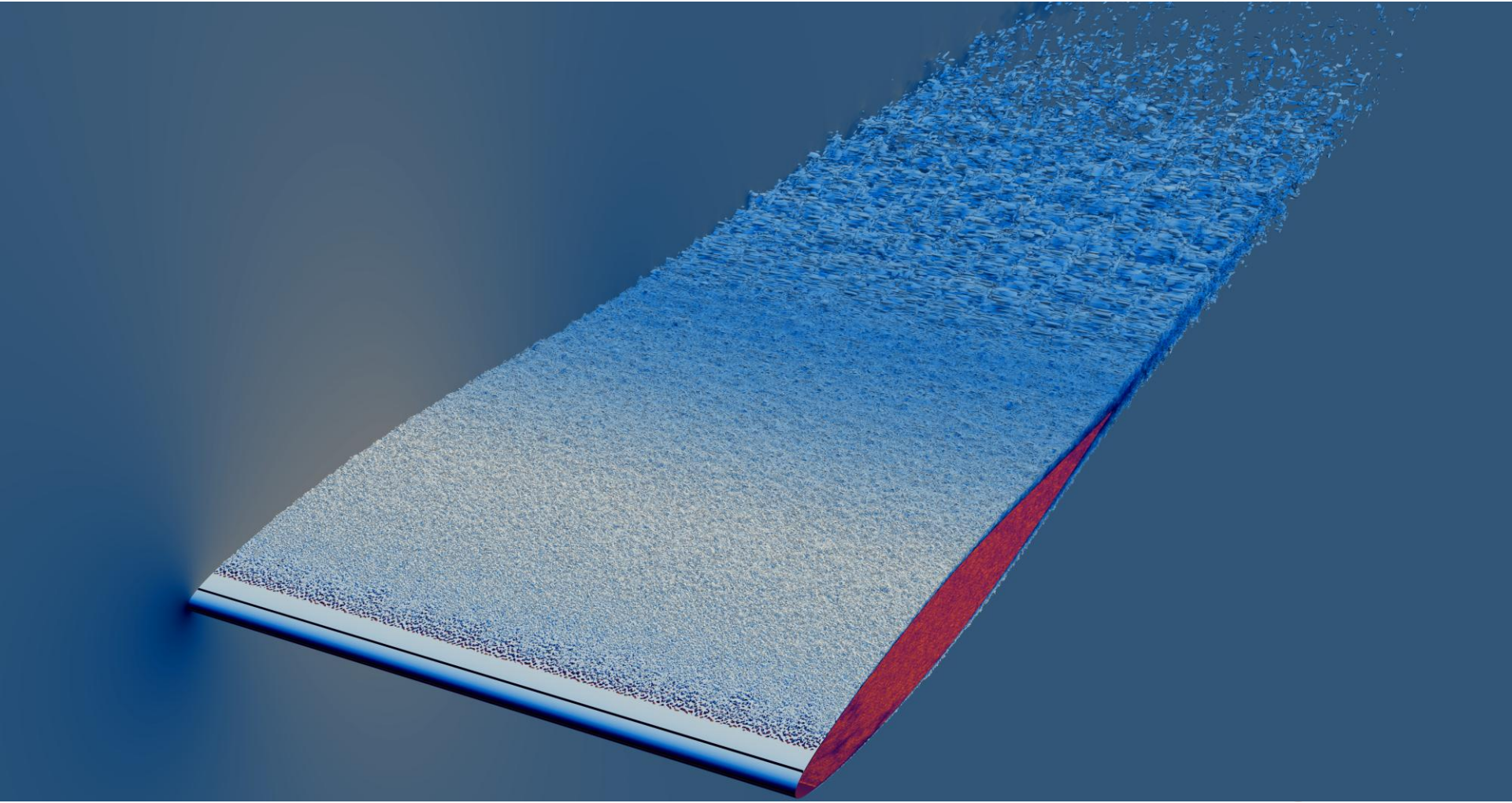

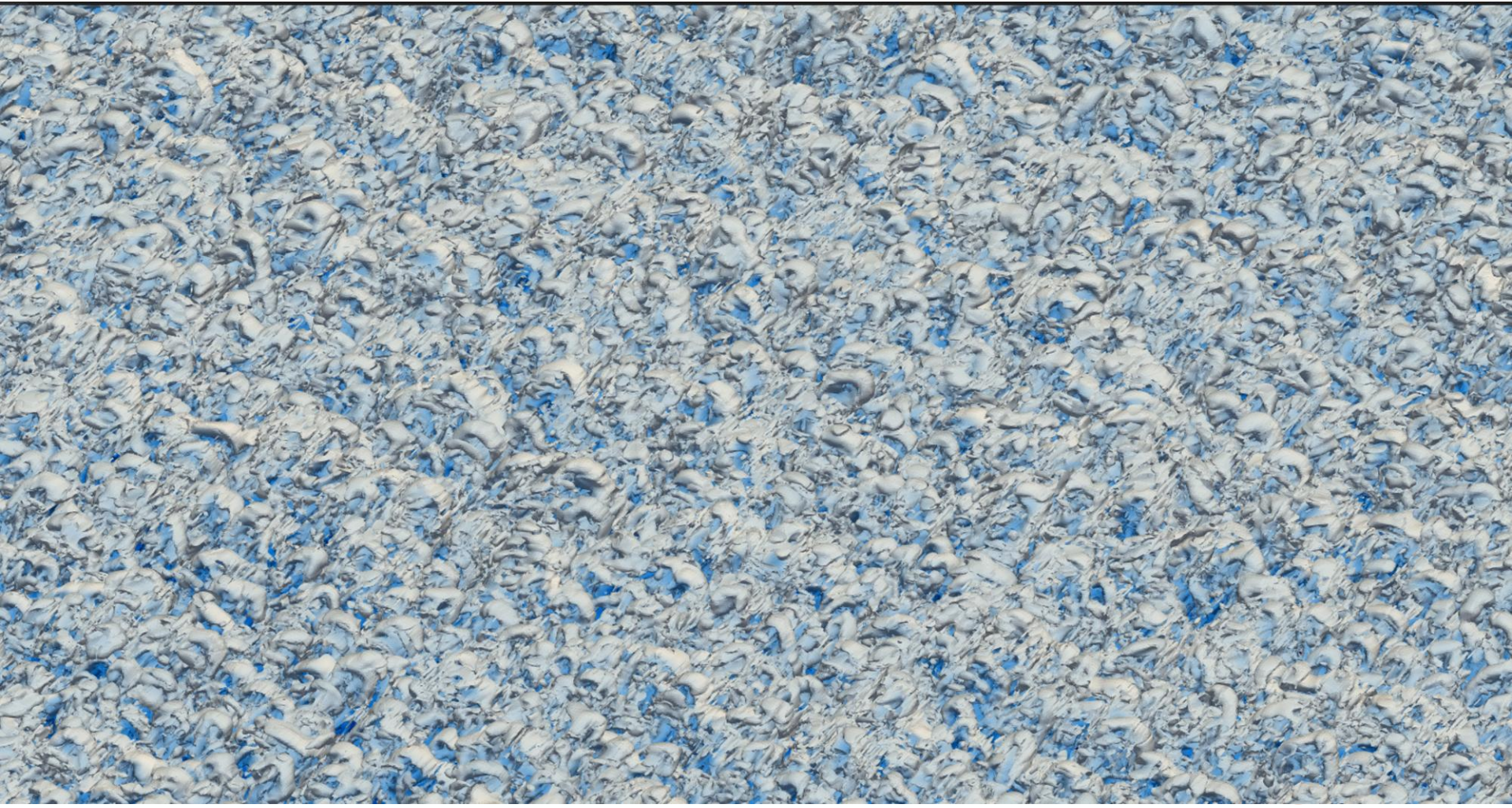

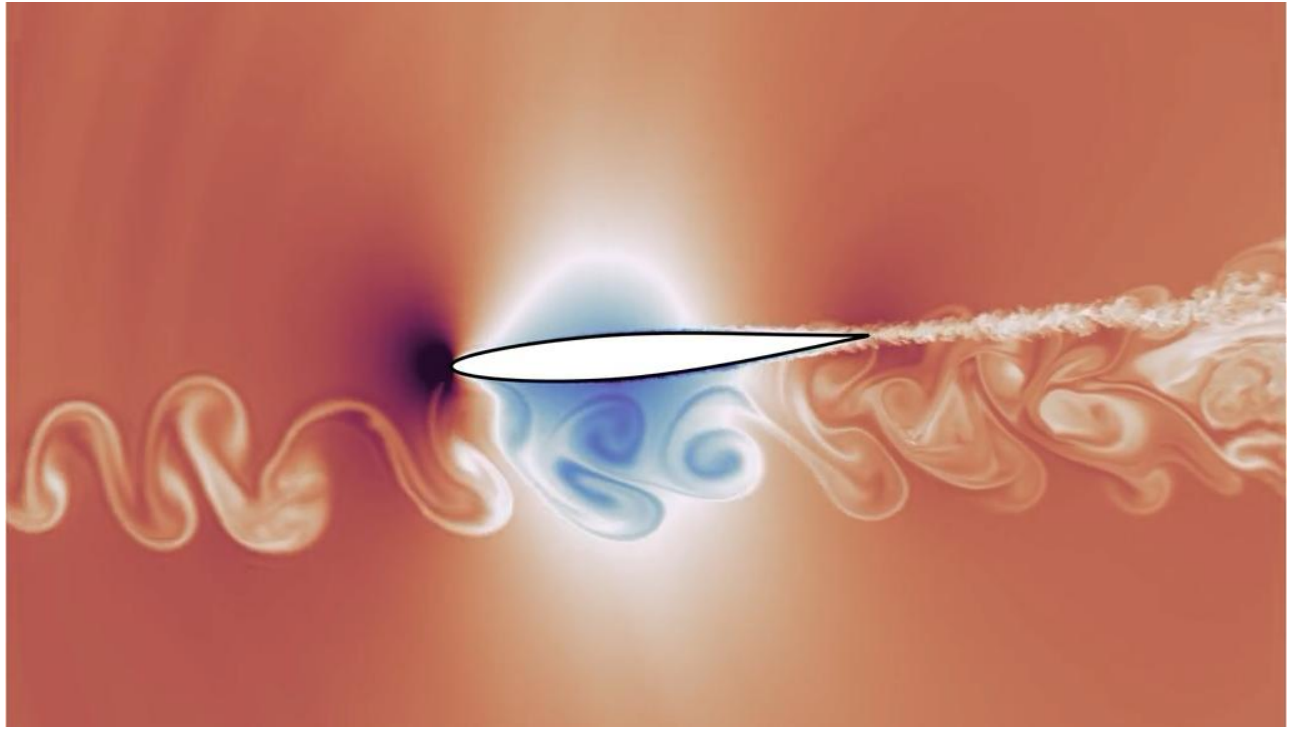

- Approx. 1 Billion DOF, N=7, 70 CTU
- One of a kind simulation for previously not accessible problems

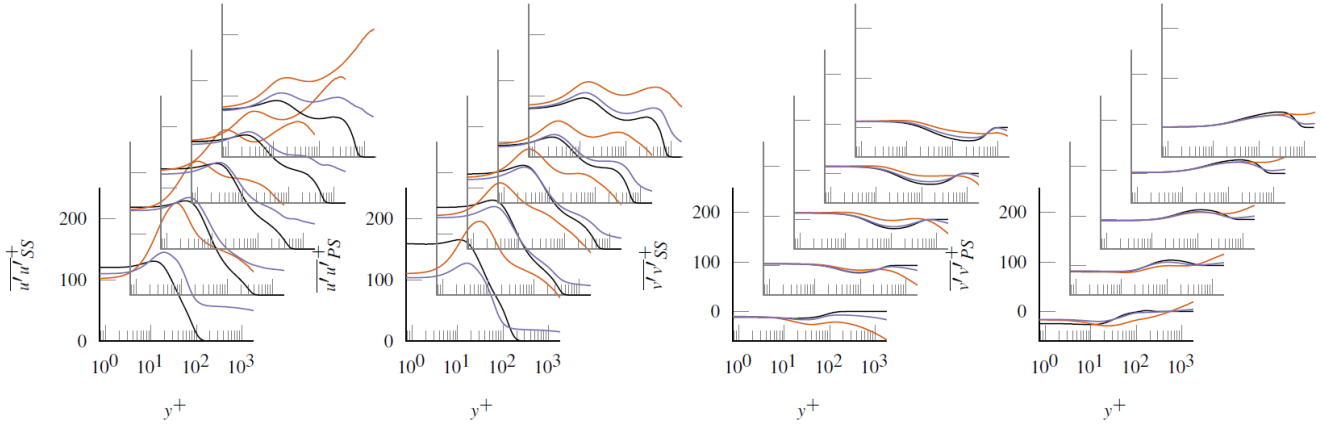

(c) Streamwise mean velocity fluctuations

(d) Wall-normal mean velocity fluctuations.

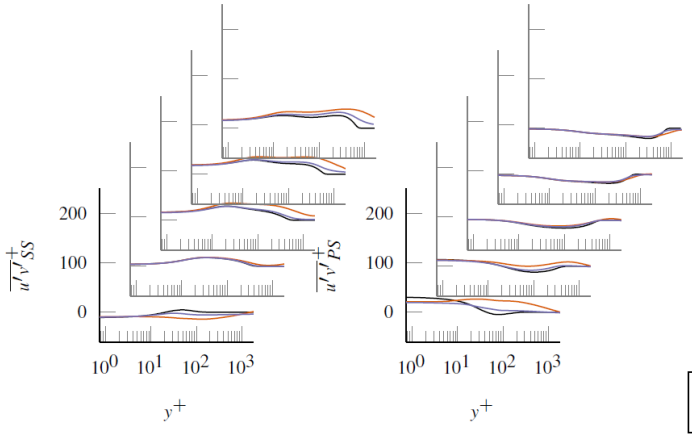

(e) $\overline{u'v'}^{+}$ velocity fluctuation.

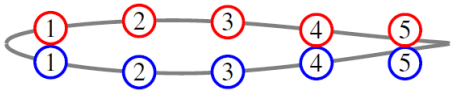

suction side pressure side

steady unsteady: Phase 1 unsteady: Phase 2

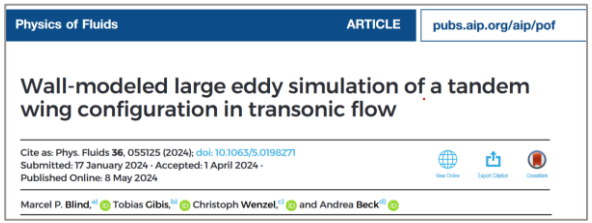

Problems we are interested in…

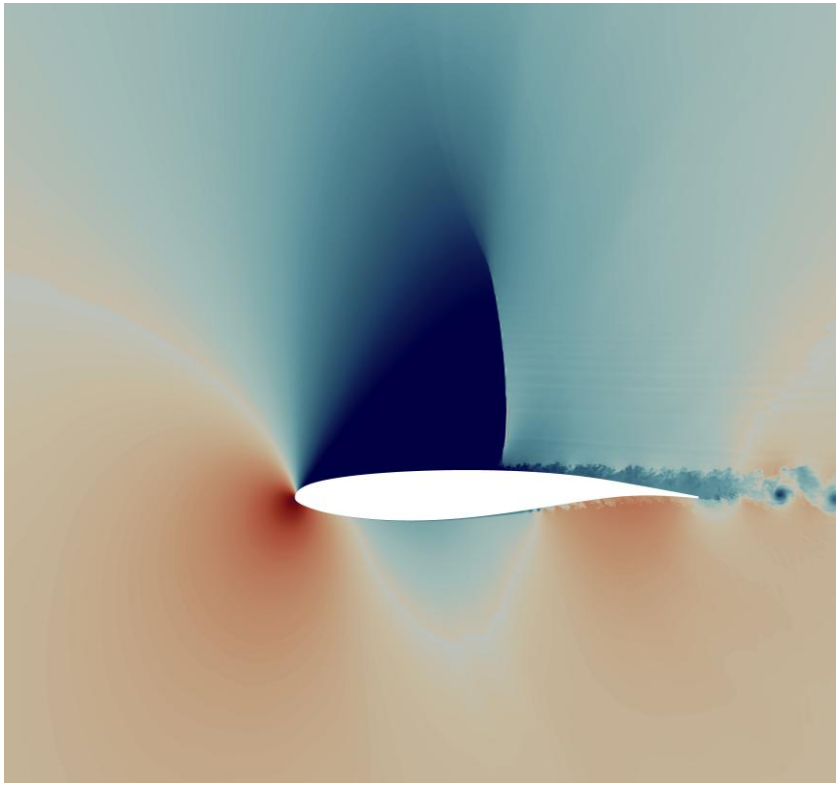

- Are “beyond the flat plate”.
- Dominated by “Multi-X” physics.
- Require “Multi-Model” numerics.
- On the edge of what is currently possible.
- Require the resolution powers of HO schemes!

Overview

Motivation

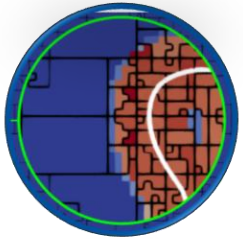

Discretization schemes for multi-X problems

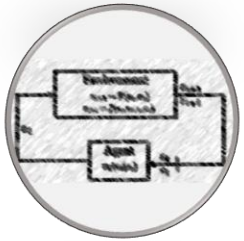

From data-driven to integrated CFD/ML

$$\int_E J(\vec{\xi}) U_t \phi \, d\vec{\xi} = \int_{-1}^{1}\int_{-1}^{1}\int_{-1}^{1} J(\vec{\xi}) \left(\frac{\partial}{\partial t} \sum_{r,s,t=0}^{N} \hat{U}_{rst}(t) \psi^N_{rst}(\vec{\xi}) \right) \psi^N_{ijk}(\vec{\xi}) d\vec{\xi^1} d\vec{\xi^2} d\vec{\xi^3}$$

$$= \sum_{\alpha,\beta,\gamma=0}^{N} J(\vec{\xi}_{\alpha\beta\gamma}) \left(\frac{\partial}{\partial t} \sum_{r,s,t=0}^{N} \hat{U}_{rst}(t) \underbrace{\ell^N_r(\xi^1_\alpha)}_{=\delta_{r\alpha}} \underbrace{\ell^N_s(\xi^2_\beta)}_{=\delta_{s\beta}} \underbrace{\ell^N_t(\xi^3_\gamma)}_{=\delta_{t\gamma}} \right) \psi^N_{ijk}(\vec{\xi}_{\alpha\beta\gamma}) \omega_\alpha \omega_\beta \omega_\gamma$$

$$= \sum_{\alpha,\beta,\gamma=0}^{N} J(\vec{\xi}_{\alpha\beta\gamma}) \frac{\partial}{\partial t} \hat{U}_{\alpha\beta\gamma}(t) \underbrace{\ell^N_i(\xi^1_\alpha)}_{=\delta_{i\alpha}} \underbrace{\ell^N_j(\xi^2_\beta)}_{=\delta_{j\beta}} \underbrace{\ell^N_k(\xi^3_\gamma)}_{=\delta_{k\gamma}} \omega_\alpha \omega_\beta \omega_\gamma$$

Building Block I: High Order Schemes

For a smooth solution and a consistent scheme of order N, we have an error bound

$$\|u - u_h\|_{h,\Omega} \leq Ch^{N+1}$$

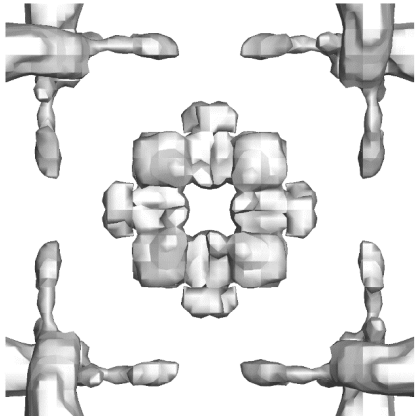

N=1, 64 DOF

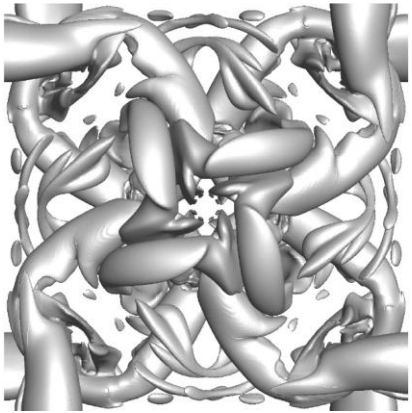

DNS

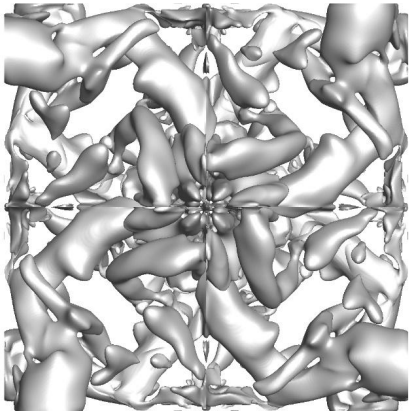

N=15, 64 DOF

For a smooth solution and a consistent scheme of order N, we have an error bound

$$\|u - u_h\|_{h,\Omega} \leq Ch^{N+1}$$

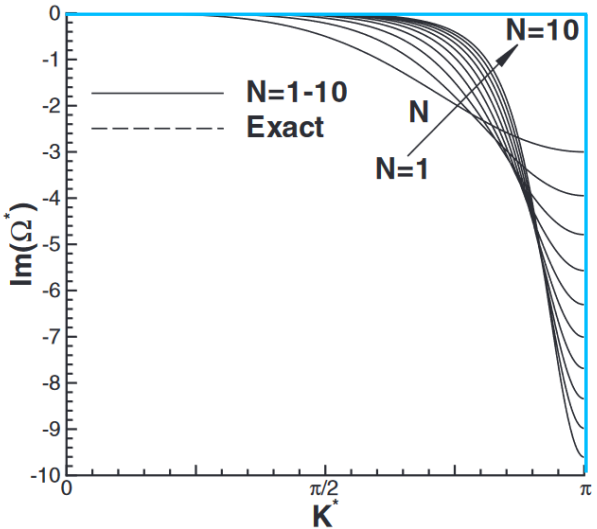

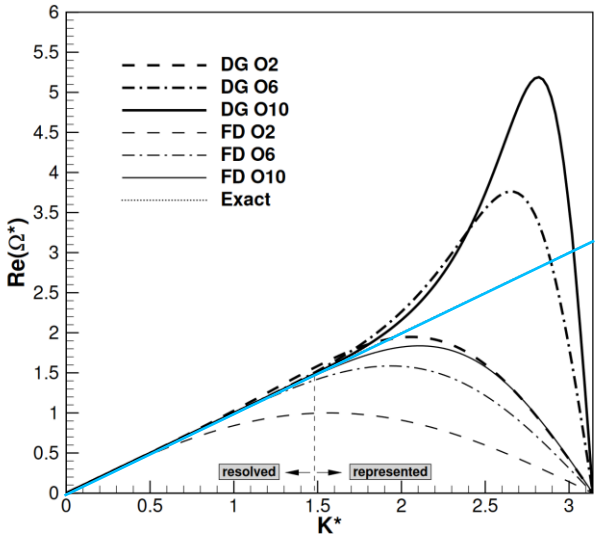

For a sufficiently smooth solution and an appropriate numerics, HO schemes are fast

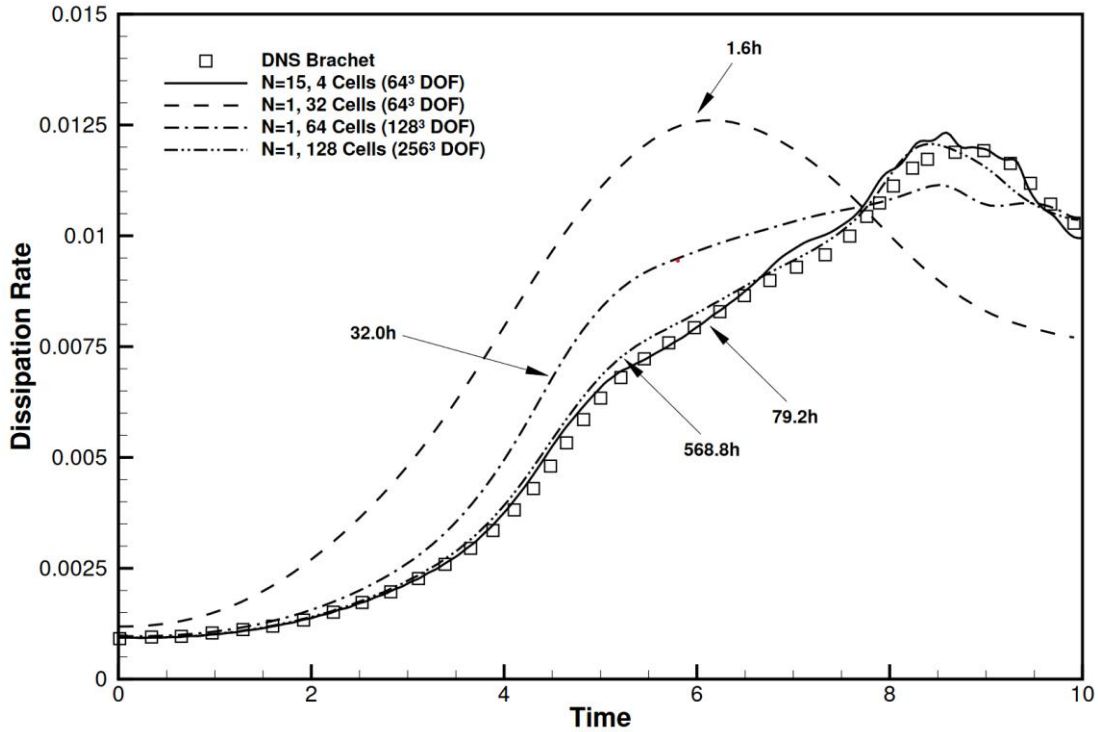

HO schemes are accurate, but can they be fast?

Number of points per wavelength for a given error: Measure of information efficiency

$$N_{total} \sim n_{PPW}^4 \, Re^3$$

64^3 DOF
nppw ≈ 4
DG, N=7

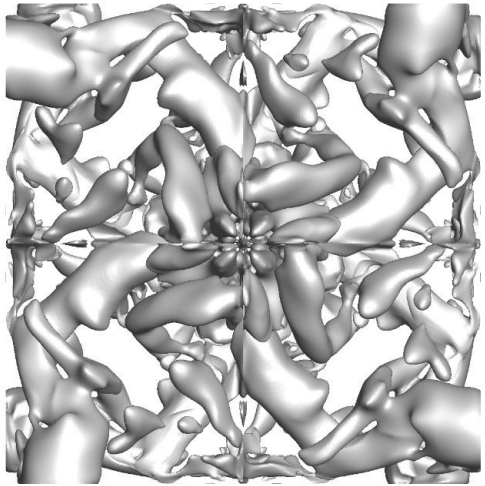

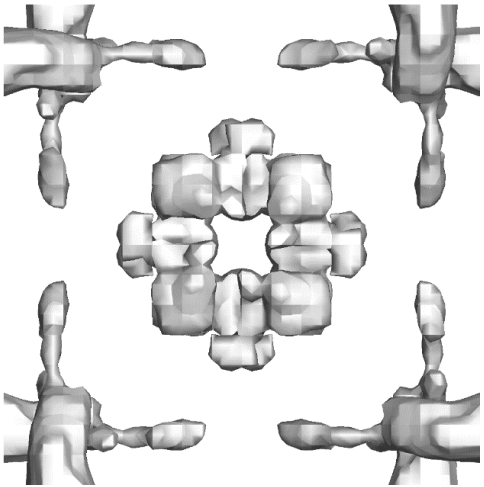

64^3 DOF
nppw ≈ 16
FV, N=1

1 Billion DOF
nppw ≈ 4

256 Billion DOF
nppw ≈ 16

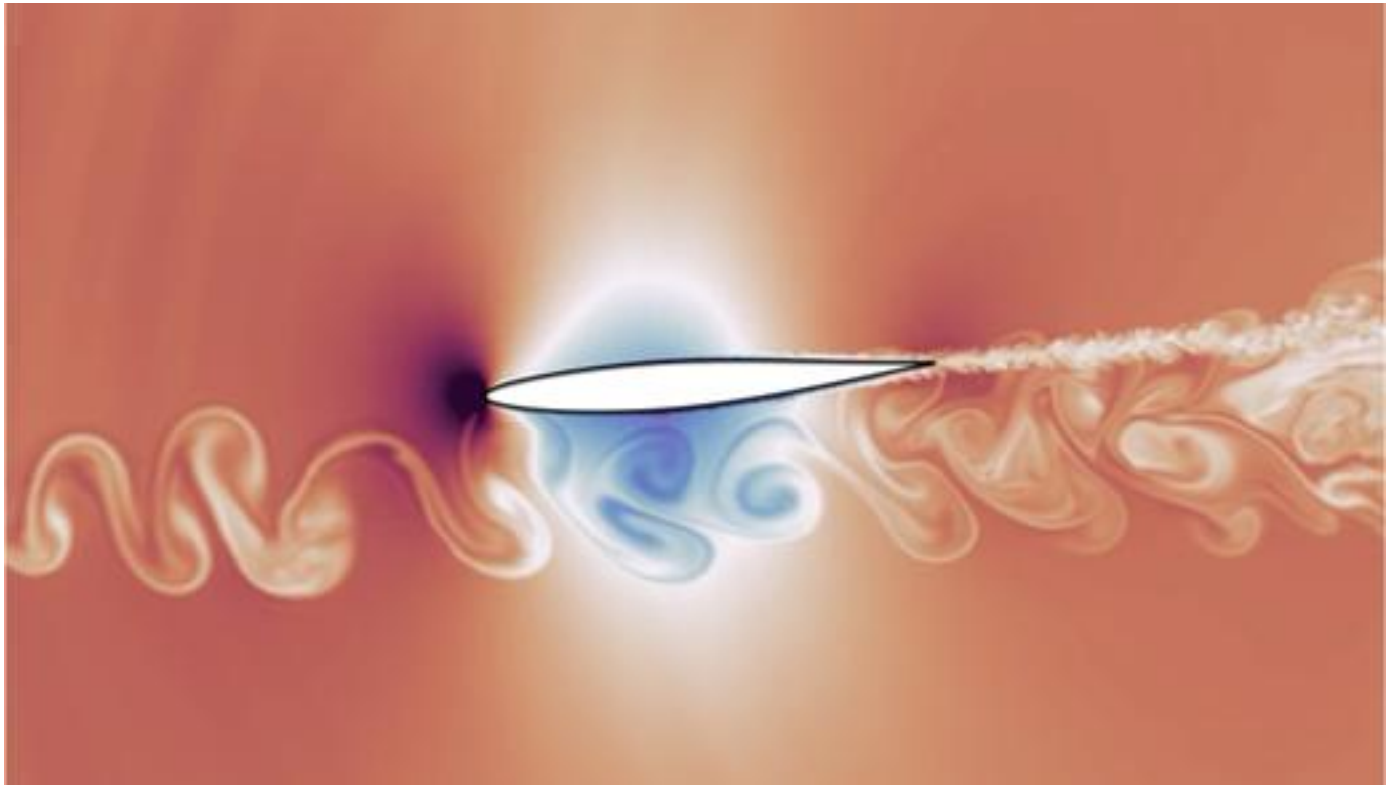

Discontinuous Galerkin Schemes

- Different Roads to High Order: Higher Derivatives, wider stencils: From local to global
- Discontinuous Galerkin schemes combine useful properties for multiscale problems
- Basic ideas:
  - High order polynomial basis with compact support
  - L_2 projection is optimal
  - Hybrid FE and FV scheme
- This gives flexibility, locality, conservation and stability (FV) and accuracy (FE)

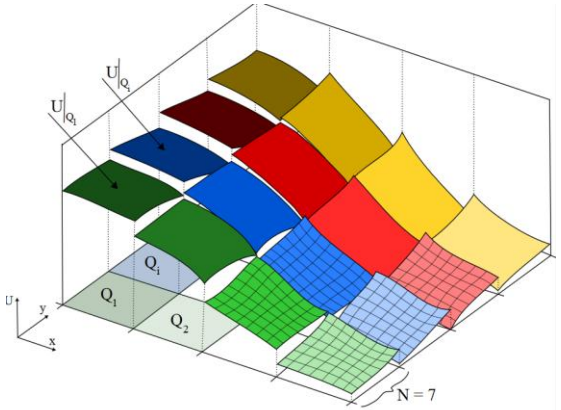

Discontinuous Galerkin Schemes

- A hyperbolic / parabolic conservation law of the form

$$\frac{\partial \vec{U}(\vec{x},t)}{\partial t} + \nabla \cdot \left(\vec{F}^c\left(\vec{U}\right) - \vec{F}^v\left(\vec{U}, \nabla \vec{U}\right)\right) = 0$$

- Mapping to a suitable reference space

$$\mathcal{J}\frac{\partial \vec{U}(\vec{x},t)}{\partial t} + \nabla_\xi \cdot \vec{\mathcal{F}} = 0$$

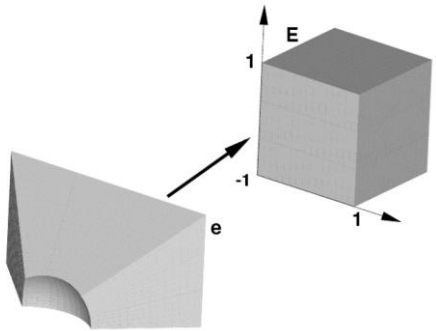

- Variational formulation and weak DG form per element

$$\left\langle \mathcal{J}\frac{\partial \vec{U}}{\partial t}, \phi \right\rangle + \iint_{\partial E} \phi \left(\vec{\mathcal{F}} \cdot \mathcal{N}\right)^* \, \mathrm{d}S - \left\langle \vec{\mathcal{F}}, \nabla_\xi \phi \right\rangle = 0$$

Discontinuous Galerkin Schemes: Spectral Element

- Ansatz: Tensorproduct formulation of 1D-Lagrange Polynomials
- Collocation of integration and interpolation on LGL or LG-nodes

Two triple sums for the mass matrix: Efficiency?

$$\left\langle \mathcal{J}\frac{\partial \vec{U}}{\partial t}, \phi \right\rangle = \frac{\partial}{\partial t} \sum_{\alpha,\beta,\gamma=1}^{N} \mathcal{J}(\xi_{\alpha\beta\gamma}) \sum_{m,n,o}^{N} \left(\vec{U}_{mno}(t) \ell_m(\xi_\alpha^1) \ell_n(\xi_\beta^2) \ell_o(\xi_\gamma^3) \right) \psi_{ijk}(\xi_{\alpha\beta\gamma}) \omega_\alpha \omega_\beta \omega_\gamma,$$

$$= \frac{\partial}{\partial t} \sum_{m,n,o=1}^{N} \mathcal{J}(\xi_{mno}) \vec{U}_{mno} \ell_i(\xi_m^1) \ell_j(\xi_n^2) \ell_k(\xi_o^3) \omega_m \omega_n \omega_o$$

Cardinal Property and Collocation

$$= \mathcal{J}(\xi_{ijk}) \frac{\partial \vec{U}_{ijk}}{\partial t} \omega_i \omega_j \omega_k, \quad \forall i, j, k.$$

Single product per DOF

Discontinuous Galerkin Schemes: Spectral Element

- Ansatz: Tensorproduct formulation of 1D-Lagrange Polynomials
- Collocation of integration and interpolation on LGL or LG-nodes
- Tensorproduct structure of the Ansatz transfers to the operator
- In Multi-D: Line-by-line operations

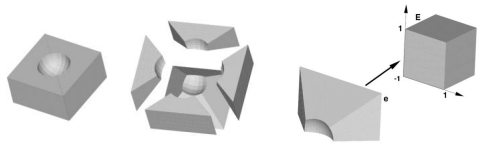

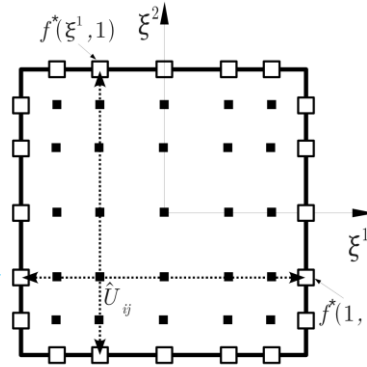

1D Operator along “1”-direction

$$\frac{\partial \vec{\mathbf{U}}_{ijk}}{\partial t} = -\frac{1}{\mathcal{J}_{ijk}}\left[\sum_{\alpha=0}^{N} \vec{\mathcal{F}}^{1}_{\alpha jk}\hat{D}_{i\alpha} + \left(\left[\vec{f}^{*}\hat{s}\right]_{j,k}^{+\xi^1}\hat{\ell}_i(1) + \left[\vec{f}^{*}\hat{s}\right]_{j,k}^{-\xi^1}\hat{\ell}_i(-1)\right)\right.$$
$$+\sum_{\beta=0}^{N} \vec{\mathcal{F}}^{2}_{i\beta k}\hat{D}_{j\beta} + \left(\left[\vec{f}^{*}\hat{s}\right]_{i,k}^{+\xi^2}\hat{\ell}_j(1) + \left[\vec{f}^{*}\hat{s}\right]_{i,k}^{-\xi^2}\hat{\ell}_j(-1)\right)$$
$$\left.+\sum_{\gamma=0}^{N} \vec{\mathcal{F}}^{3}_{ij\gamma}\hat{D}_{k\gamma} + \left(\left[\vec{f}^{*}\hat{s}\right]_{i,j}^{+\xi^3}\hat{\ell}_k(1) + \left[\vec{f}^{*}\hat{s}\right]_{i,j}^{-\xi^3}\hat{\ell}_k(-1)\right)\right] \quad \forall\, i,j,k.$$

Volume integral

Surface integral: Riemann solvers

Discontinuous Galerkin Spectral Element Method (DG-SEM)

- DG-SEM:
  - Type of grid cells: Hexahedrons (curved elements, unstructured, hanging nodes)

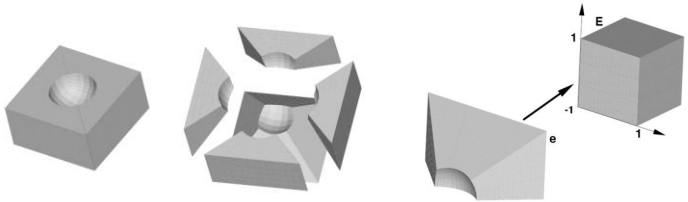

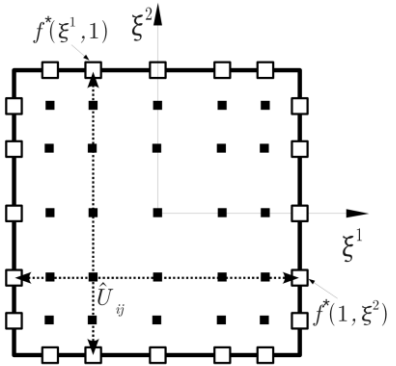

  - Set of basis functions: Tensor product, Lagrange polynomials at Gauß / Gauß-Lobatto points

$$U_h(\xi,t)\sum_{i,j=1}^{N}\hat{U}_{i,j}(t)\psi_i^N(\xi^1)\psi_j^N(\xi^2)$$

  - Numerical integration: Collocation approach (SEM approach)
  - Time approximation: Explicit Runge-Kutta, IMEX
  - Numerical flux: Riemann solver, BR1/2
  - Stability: De-Aliasing, Split form (entropy / energy stable fluxes)
  - Shock-capturing: Finite volume sub-cells, h/p adaptivity

Tensorproduct restricts to (approximately) flat plates.

Recent developments

By my PostDocs Anna Schwarz & Jens Keim et al.

- Entropy-stable DGSEM on heterogeneous grids

$$\frac{\partial \hat{\mathcal{J}}^{(\kappa)}_{ijk} \mathcal{J}^{(\kappa)}_{ijk} \hat{\mathbf{q}}^{(\kappa)}_{ijk}}{\partial t} = -\Bigg[\sum_{\alpha=0}^{N} \boldsymbol{\mathcal{F}}^{(\kappa,1)}_{\alpha jk} \hat{D}_{\alpha i} + \left(\left[\mathbf{f}^* \hat{\mathcal{J}}^{(\kappa,\zeta)} \mathcal{J}^{(\kappa,\zeta)} \right]^{+\eta^1}_{j,k} \hat{l}_i(1) + \left[\mathbf{f}^* \hat{\mathcal{J}}^{(\kappa,\zeta)} \mathcal{J}^{(\kappa,\zeta)} \right]^{-\eta^1}_{j,k} \hat{l}_i(-1) \right)$$
$$+ \sum_{\beta=0}^{N} \boldsymbol{\mathcal{F}}^{(\kappa,2)}_{i\beta k} \hat{D}_{\beta j} + \left(\left[\mathbf{f}^* \hat{\mathcal{J}}^{(\kappa,\zeta)} \mathcal{J}^{(\kappa,\zeta)} \right]^{+\eta^2}_{i,k} \hat{l}_j(1) + \left[\mathbf{f}^* \hat{\mathcal{J}}^{(\kappa,\zeta)} \mathcal{J}^{(\kappa,\zeta)} \right]^{-\eta^2}_{i,k} \hat{l}_j(-1) \right)$$
$$+ \sum_{\gamma=0}^{N} \boldsymbol{\mathcal{F}}^{(\kappa,3)}_{ij\gamma} \hat{D}_{\gamma k} + \left(\left[\mathbf{f}^* \hat{\mathcal{J}}^{(\kappa,\zeta)} \mathcal{J}^{(\kappa,\zeta)} \right]^{+\eta^3}_{i,j} \hat{l}_k(1) + \left[\mathbf{f}^* \hat{\mathcal{J}}^{(\kappa,\zeta)} \mathcal{J}^{(\kappa,\zeta)} \right]^{-\eta^3}_{i,j} \hat{l}_k(-1) \right) \Bigg]$$

with

$$\hat{D}_{\alpha i} = -\frac{\omega_\alpha}{\omega_i} \frac{\partial l_i(\eta^1_\alpha)}{\partial \eta^1}, \qquad \hat{l}_i = \frac{l_i}{\omega_i}, \qquad \mathcal{J}^{(\kappa,\zeta)} = \left\| \mathrm{adj}\left(\mathbf{J}^{(\kappa)}\right)^\top \hat{\mathbf{n}}^{(\kappa,\zeta)} \right\|, \qquad \hat{\mathcal{J}}^{(\kappa,\zeta)} = \left\| \mathrm{adj}\left(\hat{\mathbf{J}}^{(\kappa)}\right)^\top \tilde{\mathbf{n}}^{(\zeta)} \right\|,$$

$$\mathbf{f}^*\left(\mathbf{q}_L, \mathbf{q}_R, \mathbf{n}^{(\kappa,\zeta)}\right) \hat{\mathcal{J}}^{(\kappa,\zeta)} \mathcal{J}^{(\kappa,\zeta)} = \left(\boldsymbol{\mathcal{F}} \cdot \tilde{\mathbf{n}}^{(\zeta)}\right)^*, \quad \boldsymbol{\mathcal{F}}^{(\kappa)} = \hat{\boldsymbol{\mathcal{M}}}^{(\kappa)} \left(\boldsymbol{\mathcal{M}}^{(\kappa)}\right)^\top \mathbb{F}^{(\kappa)}$$

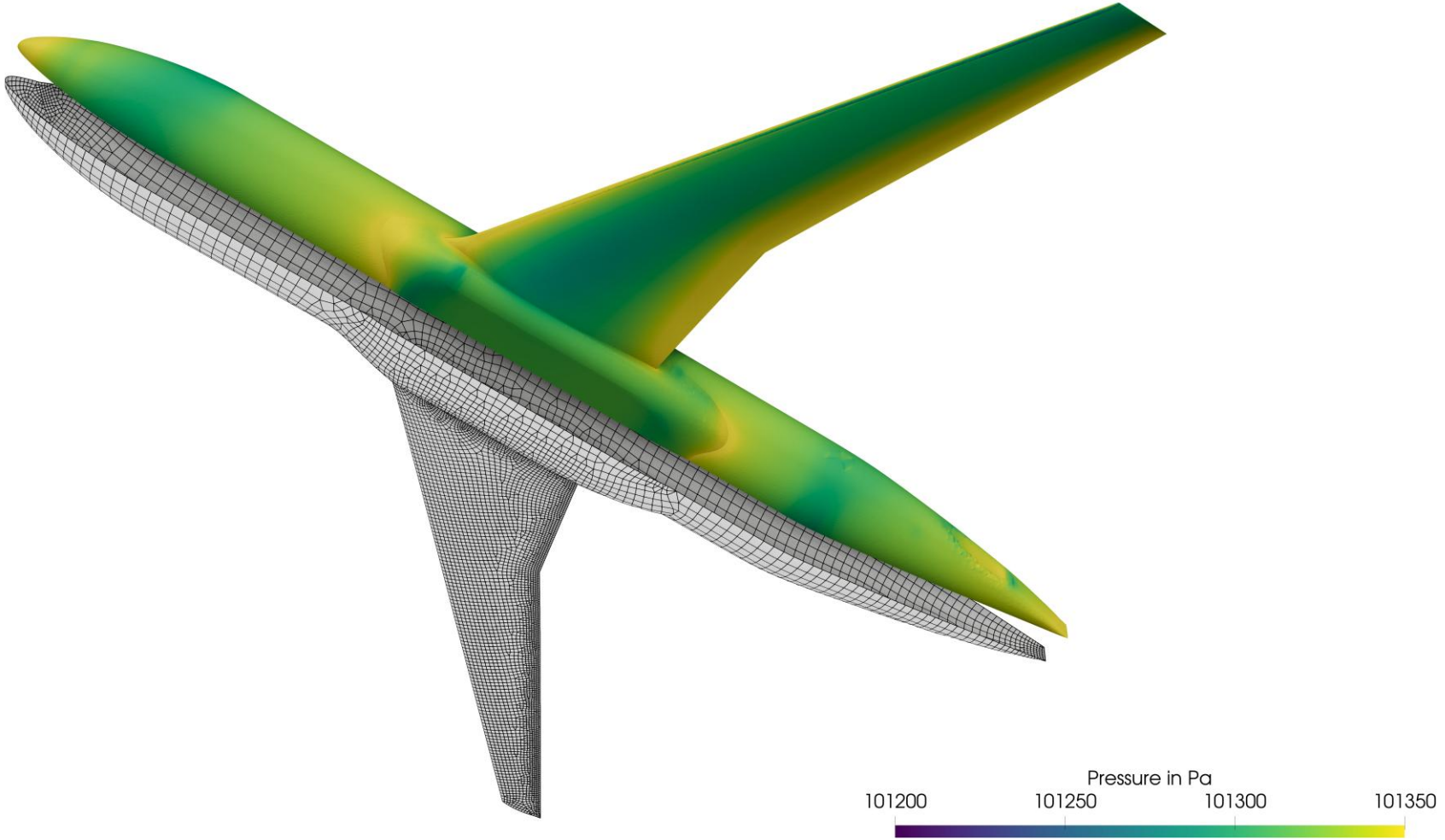
Pressure in Pa
101200
101250
101300
101350

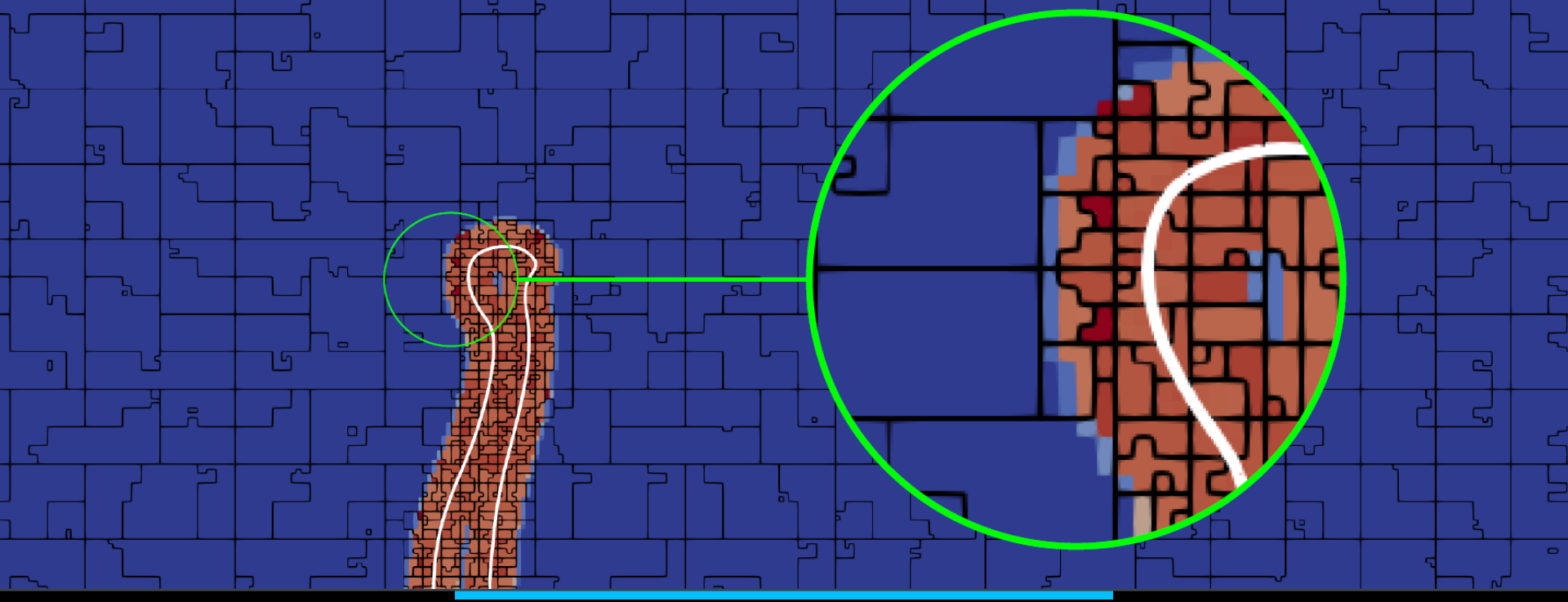

Building Block II: Flexibility, Efficiency and Robustness

For a smooth solution and a consistent scheme of order N, we have an error bound

$$\|u - u_h\|_{h,\Omega} \leq Ch^{N+1}$$

Put differently, HO schemes can leverage the smoothness of the underlying solution

What if the solution is not smooth (enough)?

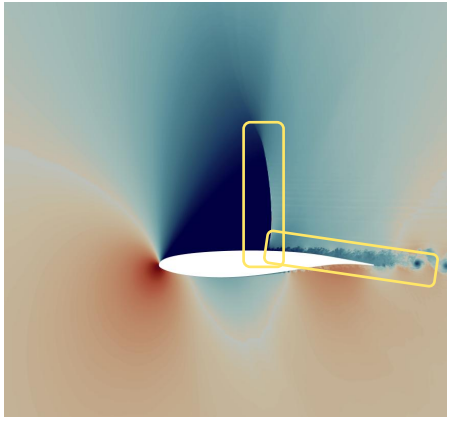

Adaptivity

$$\|u - u_h\|_{h,\Omega} \leq Ch^{N+1}$$

P-REFINEMENT

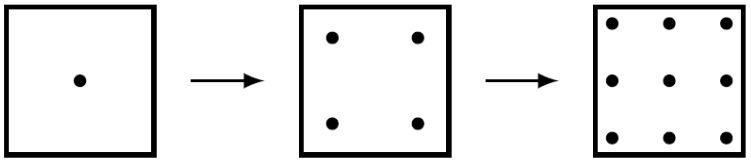

- For smooth, underresolved solutions
- Higher ansatz order: Reduced numerical dissipation and dispersion
- Reduced stability

H-REFINEMENT

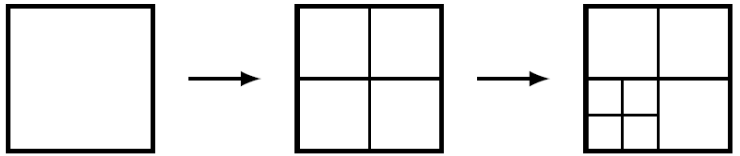

- For non-smooth solutions
- Lower ansatz order: Higher numerical dissipation and dispersion
- Enhanced stability

hp-Adaptive Hybrid DG/FV Approach

SMOOTH REGIONS

- Method of choice: High order DGSEM
- Piecewise polynomial solution
- Local p-refinement / coarsening
- Governed by modal decay indicator

$$Q(\xi) = \underbrace{\sum_{i,j,k=0}^{N} \hat{Q}_{ijk} \Psi_{ijk}(\xi)}_{\text{Ansatz}} + \underbrace{\sum_{i,j,k=N+1}^{\infty} \hat{Q}_{ijk} \Psi_{ijk}(\xi)}_{\text{Truncation error}}$$

$$w_m = \left[\frac{(\sum_{j,k=0}^{N} \hat{Q}_{ijk}^2)^{i=m}}{\sum_{i,j,k=0}^{N} \hat{Q}_{ijk}^2} \right]$$

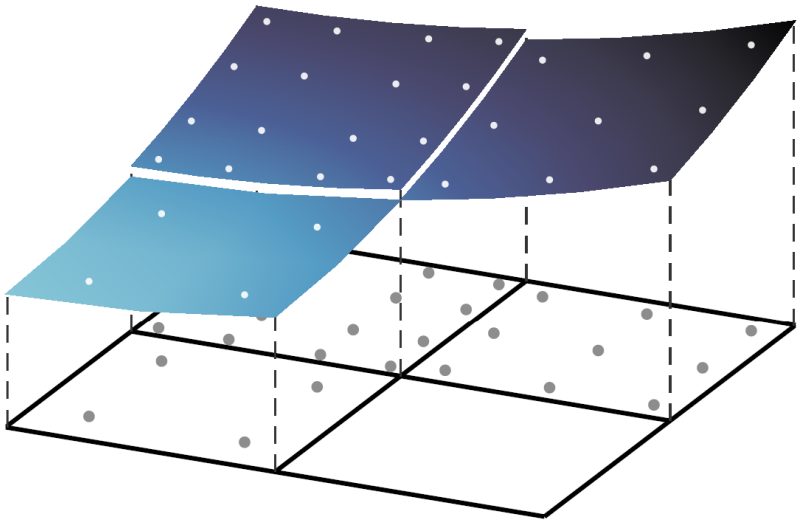

Mavriplis, C.: Nonconforming Discretizations and a Posteriori Error Estimators for Adaptive Spectral Element Techniques.

hp-Adaptive Hybrid DG/FV Approach

DISCONTINUITIES

- Method of choice: Limited Second order Finite Volume method on an embedded grid
- Piecewise linear solution representation
- Local h-refinement

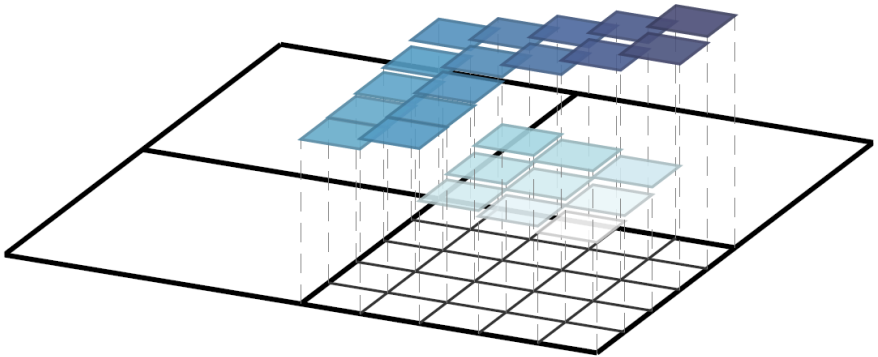

Dumbser et al.: A posteriori subcell limiting of the discontinuous Galerkin finite element method for hyperbolic conservation laws
Sonntag and Munz: Shock capturing for discontinuous Galerkin methods using finite volume subcells

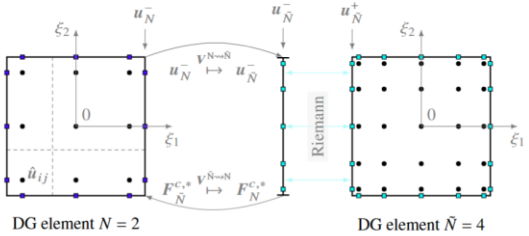

DG element $N = 2$ DG element $\tilde{N} = 4$

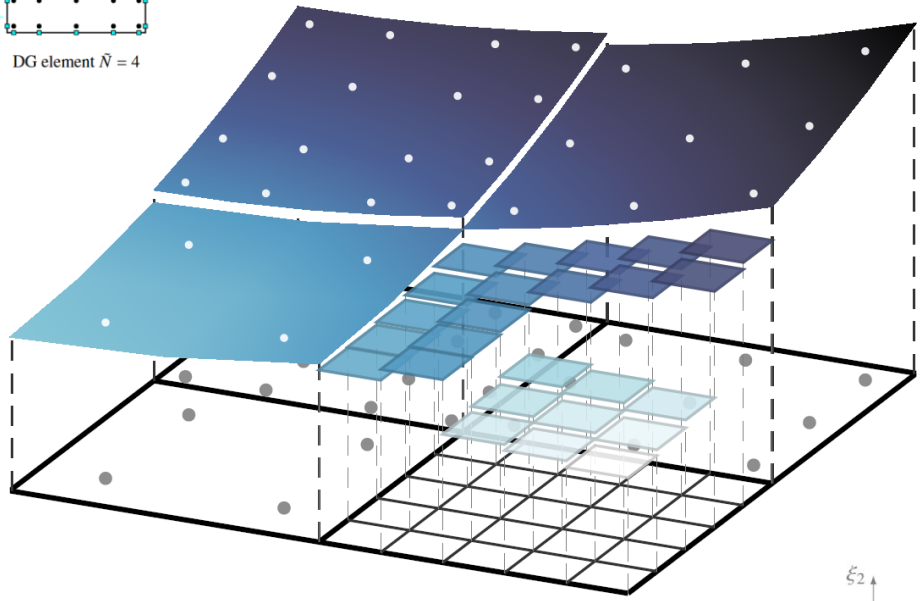

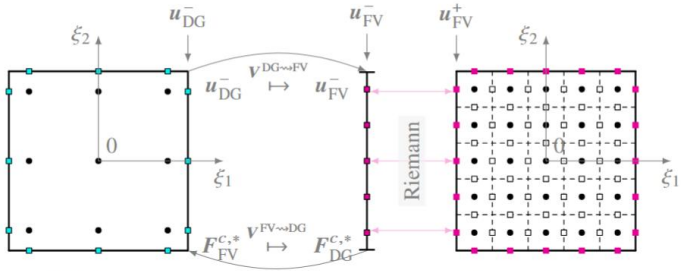

DG element FV sub-cell element

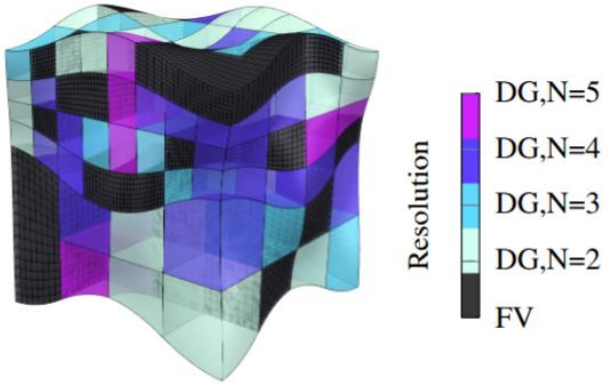

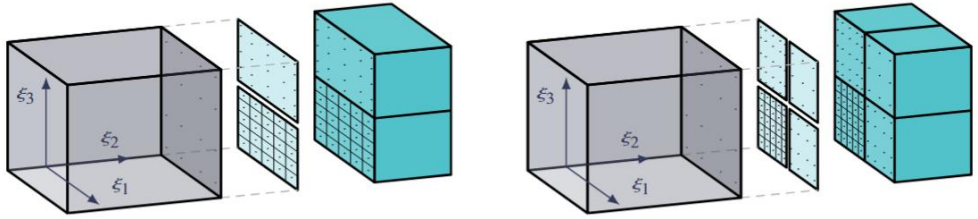

(a) Mortar Type 1 and 2 (b) Mortar Type 3

Figure 5: Schematic of the supported mortar types with Types 1 and 2 differing only in their orientation to the reference direction. The image illustrates the mapping of the big mortar side to *virtual* small mortar sides, that allow a flux computation on conforming surface data.

	u_1	u_2	u_3	u_4	u_5
$\mathbb{L}_2$	$1.42e^{-14}$	$1.13e^{-14}$	$1.15e^{-14}$	$1.16e^{-14}$	$4.36e^{-14}$
$\mathbb{L}_\infty$	$3.91e^{-14}$	$2.88e^{-14}$	$2.96e^{-14}$	$3.03e^{-14}$	$9.81e^{-14}$

Table 1: L_2 and L_∞ free-stream error with a hybrid DG/FV discretization after 180 time steps.

- See *Tackling Compressible Turbulent Multi-Component Flows with Dynamic hp-Adaptation* by Mossier, Oestringer, Keim, Mavriplis, Beck and Munz. 10.13140/RG.2.2.24216.92163 for convergence plots and free-stream preservation on non-conforming, h/p adaptive grids

Shocks and Discontinuities

Projection of discontinuity (shock, interface) onto smooth function (polynomials) induces Gibb's oscillations

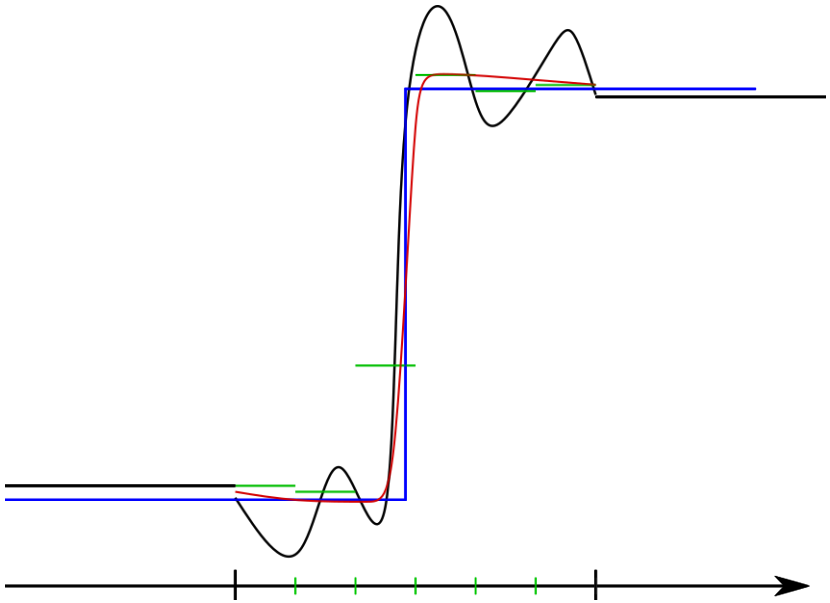

HO schemes and discontinuities (shocks, phase interface etc) do not work well

Shock Capturing for HO schemes

- Nonlinear limiters (TVD, slope, moment): Locally reduce order near shocks while retaining high-order accuracy in smooth regions
  - Disadvantages: loss of formal order near extrema; excessive dissipation; difficult design in multiple dimensions

- ENO / WENO schemes: ENO: adaptive stencil selection (Harten et al.), WENO: nonlinear weighted stencil combination (Jiang–Shu)
  - Disadvantages: high computational cost; complex implementation; accuracy degradation at critical points; parameter sensitivity

Shock Capturing for HO schemes

- Artificial viscosity / filtering: Controlled dissipation near discontinuities
  - Disadvantages: problem-dependent tuning; smearing of shocks; reduced accuracy if dissipation is poorly localized

- • Discontinuous Galerkin (DG) limiting strategies: Limiters, subcell finite-volume methods, MOOD-type a posteriori limiting
  - Disadvantages: algorithmic complexity; high memory (and CPU) cost

- Essential reading:

1. A. Harten, B. Engquist, S. Osher, S. R. Chakravarthy, "Uniformly High Order Accurate Essentially Non-Oscillatory Schemes", J. Comput. Phys., 1987.
2. G.-S. Jiang, C.-W. Shu, "Efficient Implementation of Weighted ENO Schemes", J. Comput. Phys., 1996.
3. C.-W. Shu, "Essentially Non-Oscillatory and Weighted ENO Schemes", Acta Numerica, 2009.
4. B. Cockburn, C.-W. Shu, "Runge–Kutta Discontinuous Galerkin Methods", J. Comput. Phys., 2001.
5. M. Dumbser, O. Zanotti, A. Hidalgo, D. S. Balsara, "ADER-WENO Finite Volume Schemes with A Posteriori Subcell Limiting", J. Comput. Phys., 2014.

Comparison of Shock-Capturing Methods

Method	Accuracy (smooth)	Shock resolution	Robustness	Computational cost
Nonlinear limiters (TVD, slope)	Moderate	Good	High	Low
ENO / WENO	High	Very good	High	High, restriction to structured grids
Artificial viscosity / filtering	Moderate–Low	Moderate	Moderate	Low
DG limiters / subcell methods	Very high	Very good	High	Very high

NRG

Comparison of Shock-Capturing Methods

Method	Accuracy (smooth)	Shock resolution	Robustness	Computational cost
Nonlinear limiters (TVD, slope)	Moderate	Good	High	Low
ENO / WENO	High	Very good	High	High, restriction to structured grids
Artificial viscosity / filtering	Moderate–Low	Moderate	Moderate	Low, but trial and error
DG limiters / subcell methods	Very high	Very good	High	Very high

NRG

Data-informed Shock Capturing for High Order Methods

- Stable numerical approximation through Shock Capturing: improves stability, decreases accuracy: use sparingly!
- Detecting the occurrence of shocks: non-trivial, empiricism, many parameters
- For HO methods: Just detecting a “troubled cell” is not good enough: We need localization on the element subscale

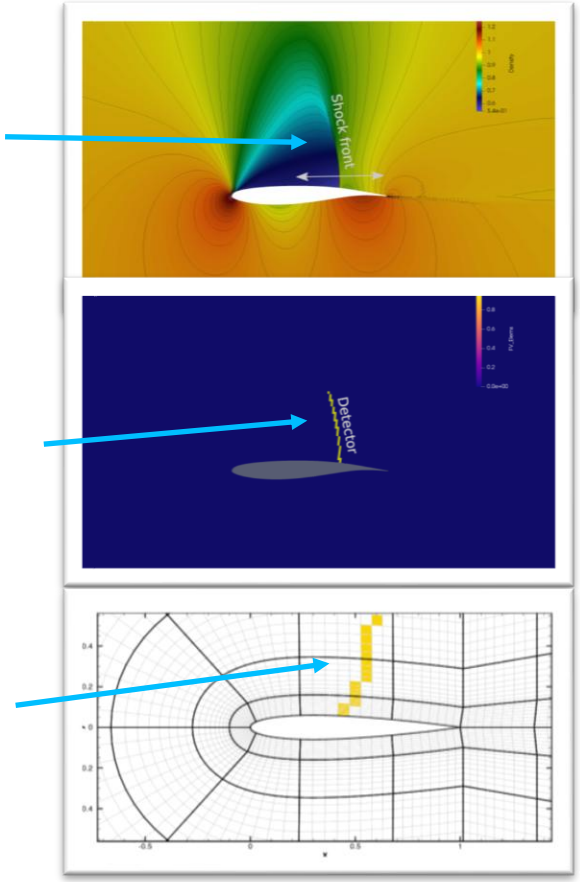

- Is there a shock?
- Where exactly is it?
- How much dissipation is to be added, and where?

Data-informed Shock Capturing for High Order Methods

- Multiscale-CNNs for edge detection: Supervised learning on analytical data
- Consistent subscale localization, contiguous shock fronts: On different grids, for different problems (same model)
- On ”bad but practical” grids: stable & accurate

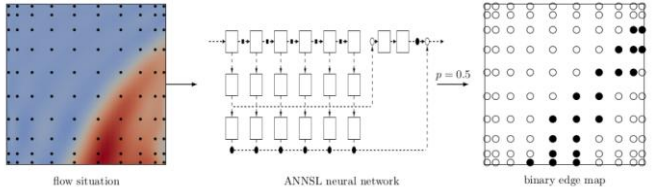

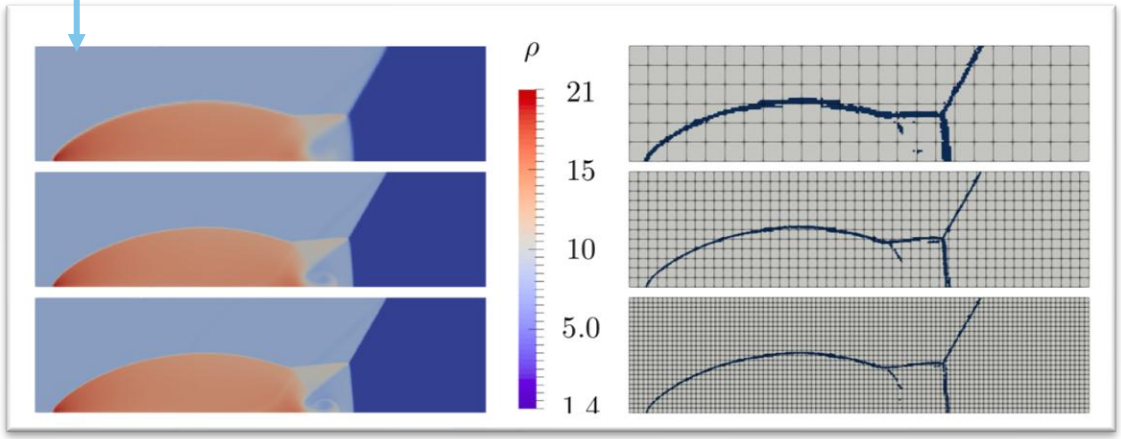

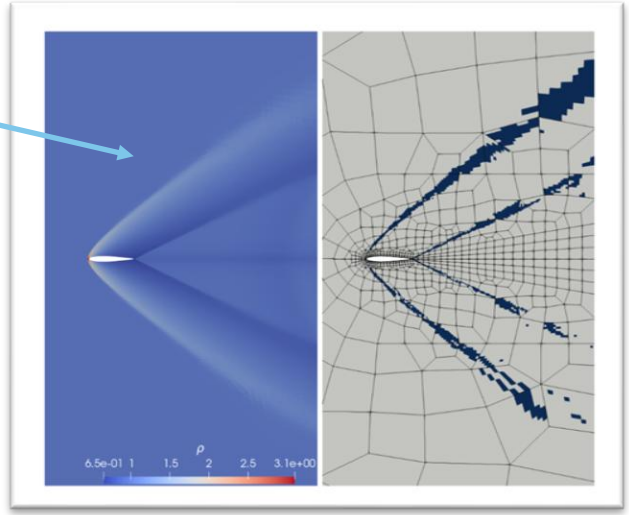

Sub-element Shock Capturing through data-informed AV

- Artificial viscosity approach: $\partial_t \vec{w} + \nabla \cdot \vec{F}(\vec{w}) = \nabla \cdot \mu_a \nabla \vec{w},$
- Shape, amplitude and position of AV need to be specified: Empiricism and trial and error!
- SotA: In DG and related methods: element-wise constant AV with a linear continuous reconstruction, PDE- or filterbased smoothing methods
- We seek: A highly localized, smooth distribution
- Use prediction of ”shocked nodes” (binary edge map) and smooth with high order Radial Basis functions (RBF) interpolation

$$\mu_a(\vec{x}) = \mu_{a\text{scale}} \sum_{i=1}^{n_s} \alpha_i \phi_r \left(\|\vec{x} - \vec{x}_{s_i}\|_2 \right),$$

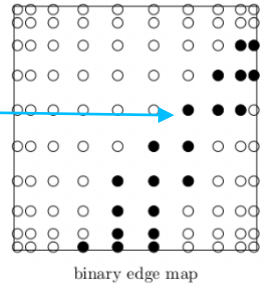

binary edge map

- This leads to a global, but weakly coupled Vandermonde matrix.

Sub-element Shock Capturing through data-informed AV

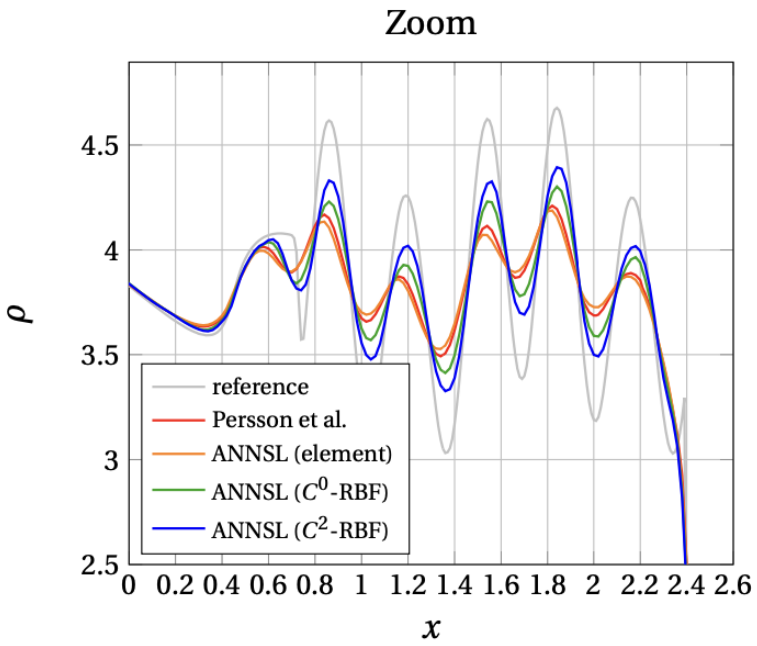

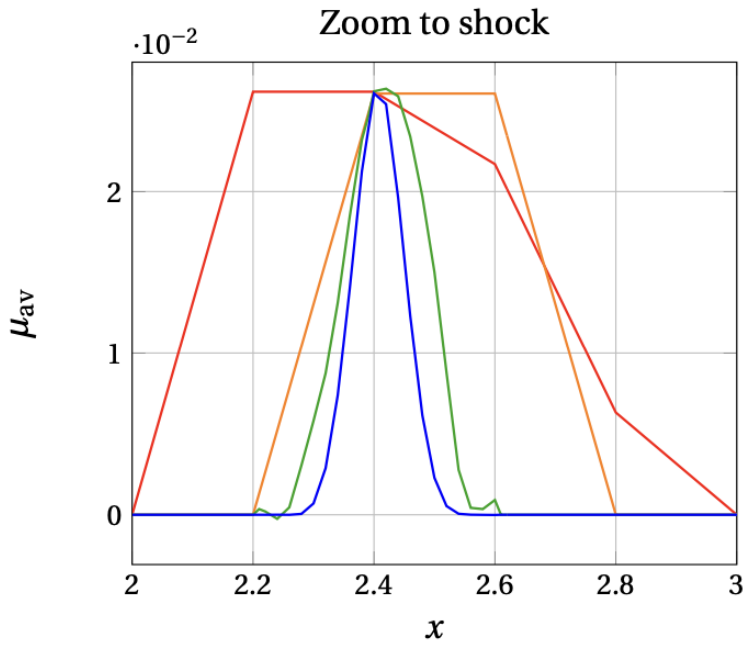

A successful augmentation and improvement of CFD for compressible flows with ML

Sub-element Shock Capturing through data-informed AV

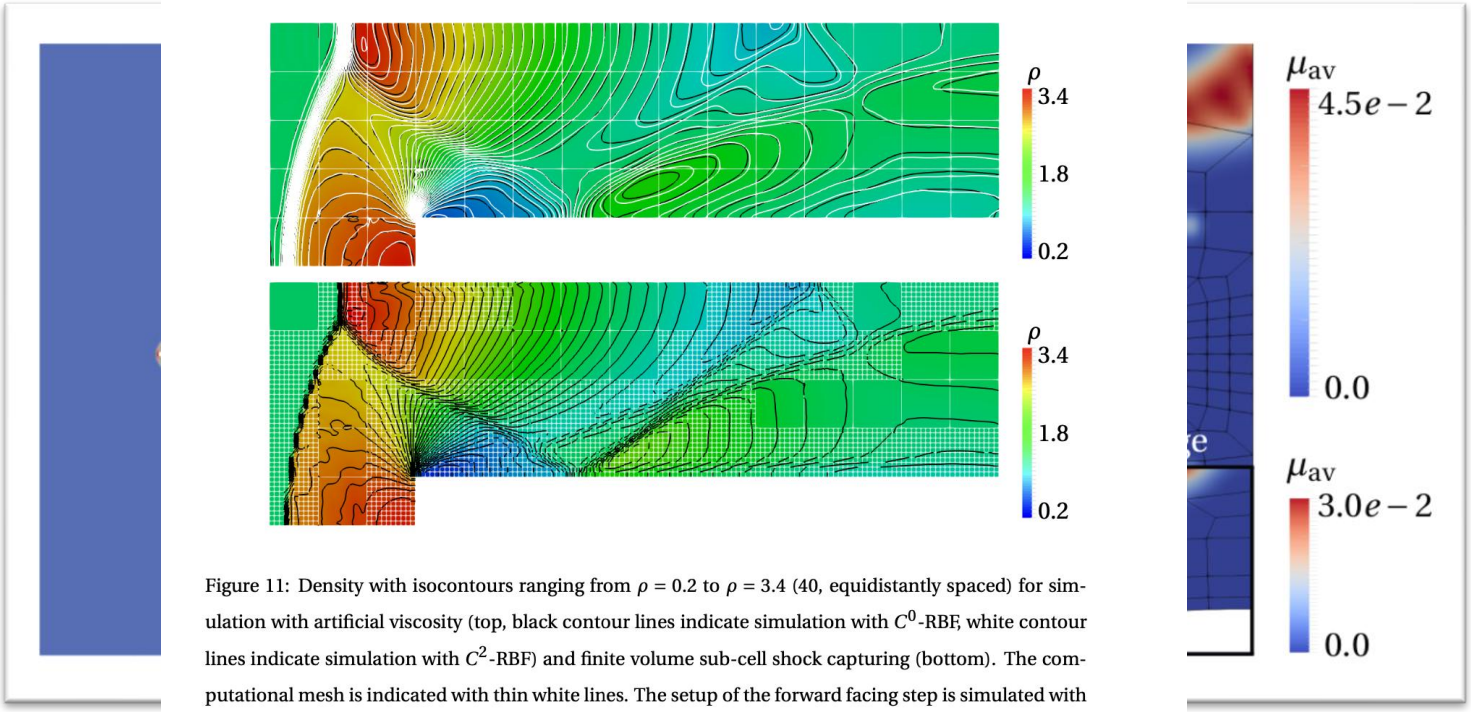

Figure 11: Density with isocontours ranging from $\rho = 0.2$ to $\rho = 3.4$ (40, equidistantly spaced) for simulation with artificial viscosity (top, black contour lines indicate simulation with C^0-RBF, white contour lines indicate simulation with C^2-RBF) and finite volume sub-cell shock capturing (bottom). The computational mesh is indicated with thin white lines. The setup of the forward facing step is simulated with $\Delta x = 0.2$ and $N = 9$.

A successful augmentation and improvement of CFD for compressible flows with ML

Comparison of Shock-Capturing Methods

Method	Accuracy (smooth)	Shock resolution	Robustness	Computational cost
Nonlinear limiters (TVD, slope)	Moderate	Good	High	Low
ENO / WENO	High	Very good	High	High, restriction to structured grids
Artificial viscosity / filtering	Moderate–Low	Moderate	Moderate	Low, but trial and error
DG limiters / subcell methods	Very high	Very good	High	Very high

Discontinuities and Underresolution: h/p/d-adaptivity

- Hybrid discretization operator: TVD FV scheme on subgrid
  - 1. Conservative switching between DG and FV operator based on h/p indicators; efficient implementation on $(N+1)^3$ DOF, CFL-consistent implementation on $(2N+1)^3$ DOF
  - 2. Convex blending on Gauss-Lobatto nodes; entropy stability and global conservation

$$\frac{\partial}{\partial t}\hat{\boldsymbol{U}} = (1-\alpha)\boldsymbol{R}^{DG}(\hat{\boldsymbol{U}}) + \alpha\boldsymbol{R}^{FV}(\hat{\boldsymbol{U}}),$$

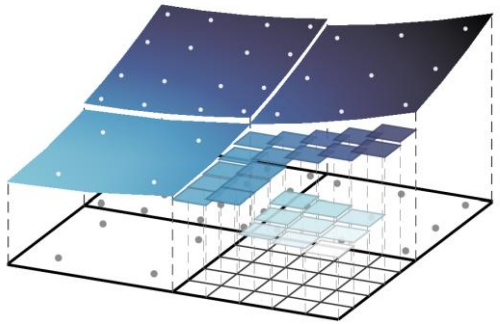

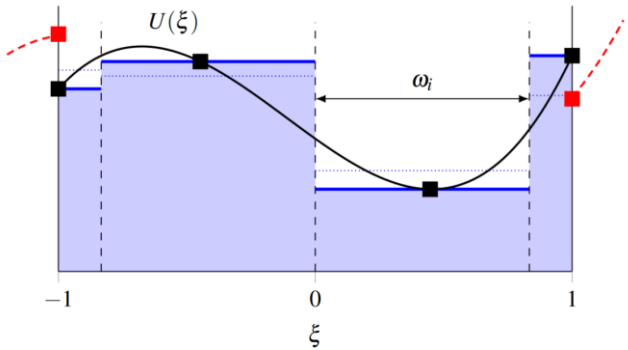

Hennemann, et al: A provably entropy stable subcell shock capturing approach for high order split form DG for the compressible Euler equations

P-Adaptive DG scheme with FV on h-refined subgrid

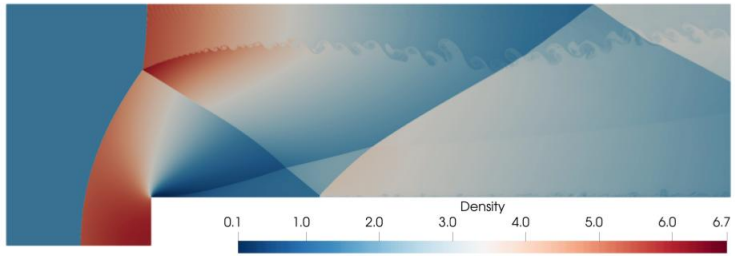

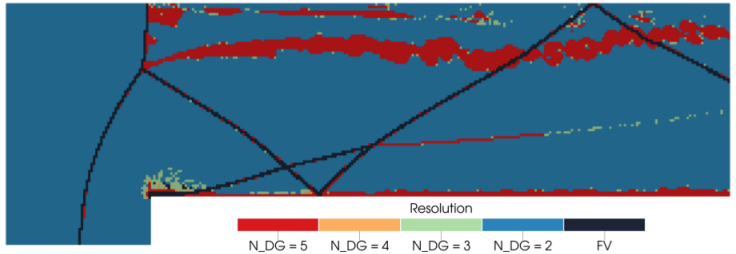

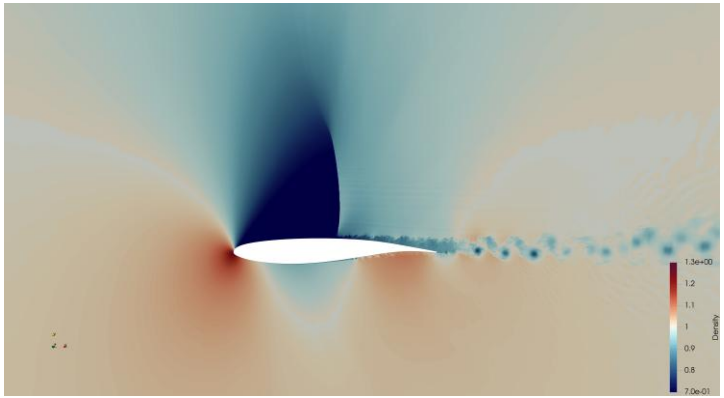

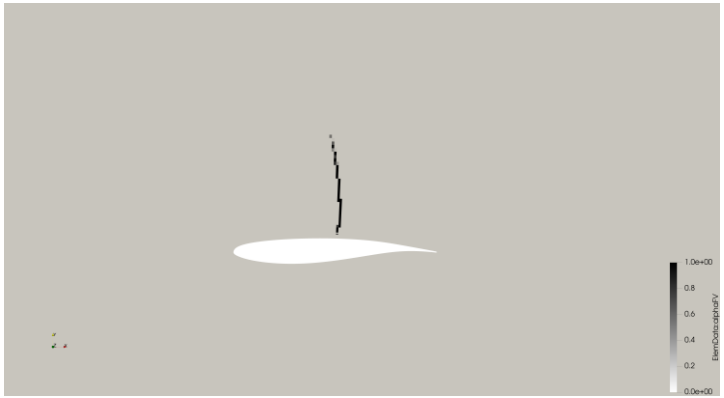

Convex blending of DG and FV scheme on LGL nodes

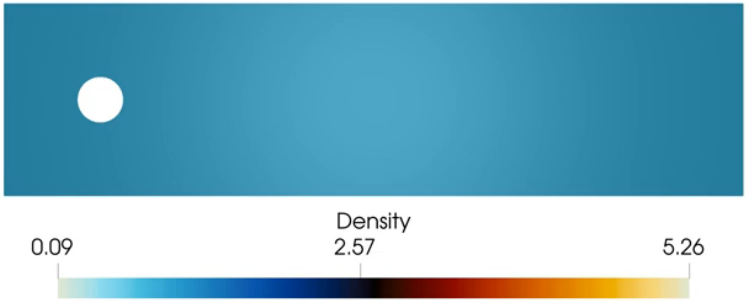
Density
0.09
2.57
5.26

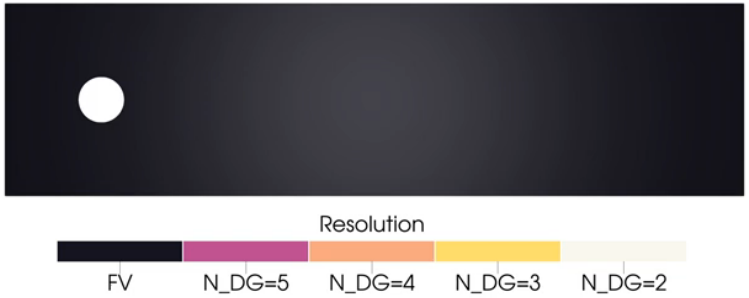
Resolution
FV
N_DG=5
N_DG=4
N_DG=3
N_DG=2

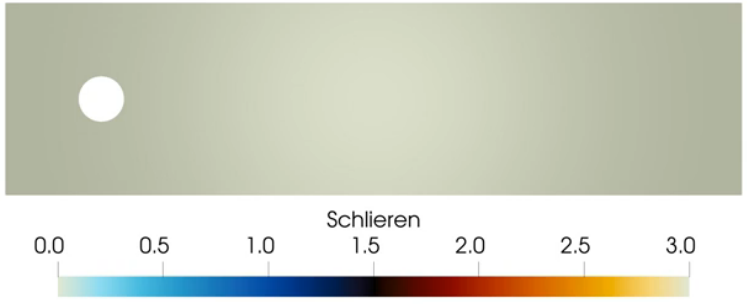
Schlieren
0.0
0.5
1.0
1.5
2.0
2.5
3.0

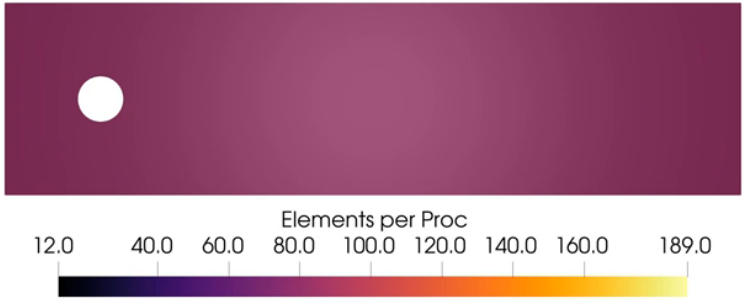
Elements per Proc
12.0
40.0
60.0
80.0
100.0
120.0
140.0
160.0
189.0

WMLES of a plunging NACA 64A-110 airfoil

- Plunging motion replicated with moving mesh approach
  - ↳ ALE formulation of the compressible NSE
- Plunging Amplitude: $h(t) = h_0 \sin(2kF(t)t)$
- Ramping function $F(t)$ to restart from stationary state
- Algebraic wall model for Spalding's law of the wall

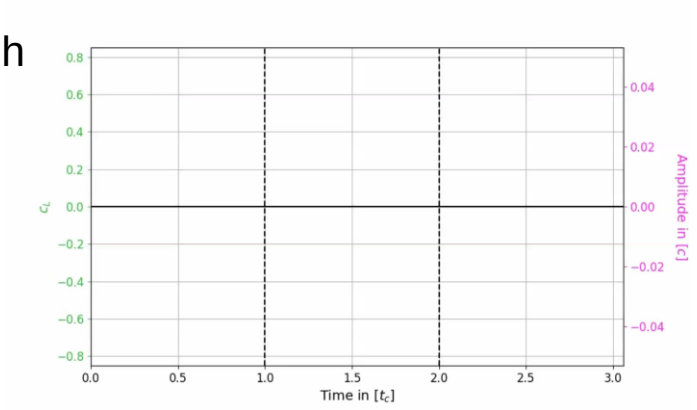

Boundary Cond.	Value
M	0.72
Re	9.3×10^5
amplitude h_0 [c]	$0.05\ c$
nondim. freq. k	1
Geometric Trip	$x = 0.05\ c$
DOFs	3.9×10^8

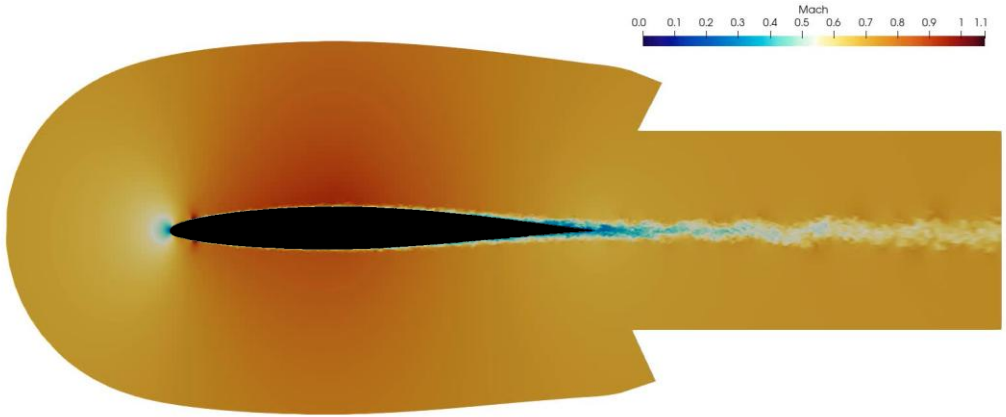

Reasons for adaptivity

Hybrid DG / FV scheme for compressible turbulence
Taylor-Green vortex at Ma=1.25

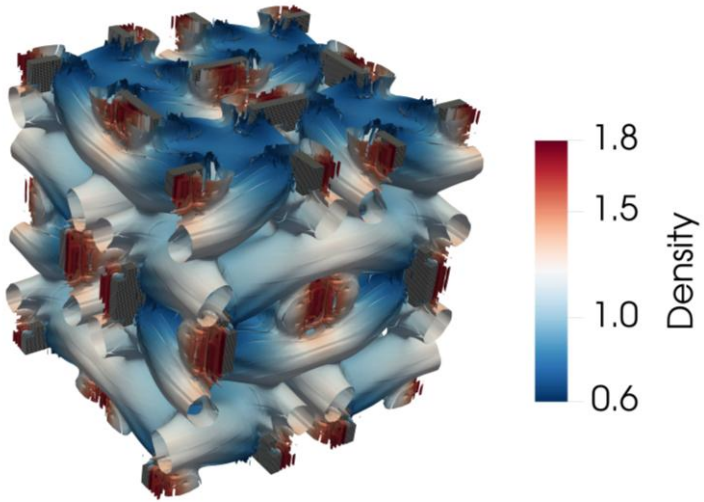

- NATO AVT-352

Physics of Fluids ARTICLE pubs.aip.org/aip/pof

Comparison of high-order numerical methodologies for the simulation of the supersonic Taylor–Green vortex flow

Cite as: Phys. Fluids **36**, 055146 (2024); doi: 10.1063/5.0206359
Submitted: 1 March 2024 · Accepted: 29 April 2024 ·
Published Online: 17 May 2024

Jean-Baptiste Chapelier,[1,a] David J. Lusher,[2,b] William Van Noordt,[3,c] Christoph Wenzel,[4,d] Tobias Gibis,[4,e] Pascal Mossier,[4,f] Andrea Beck,[4,g] Guido Lodato,[5,h] Christoph Brehm,[6,i] Matteo Ruggeri,[7,j] Carlo Scalo,[7,k] and Neil Sandham[2,l]

- Compressible turbulence
  - Scale resolution
  - Shock capturing

Hybrid DG / FV scheme for compressible turbulence

Taylor-Green vortex at Ma=1.25

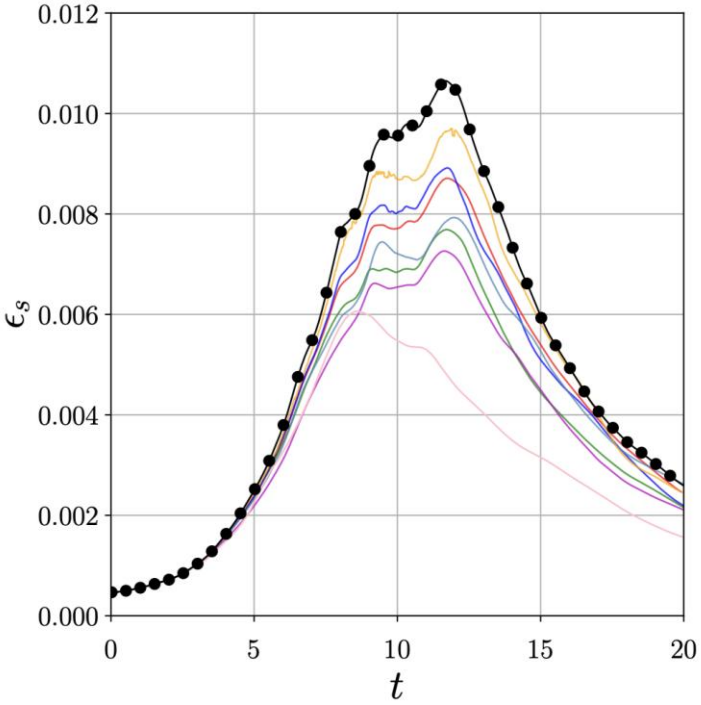

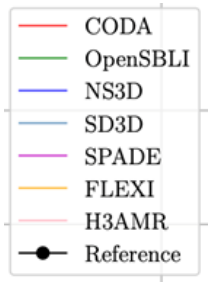

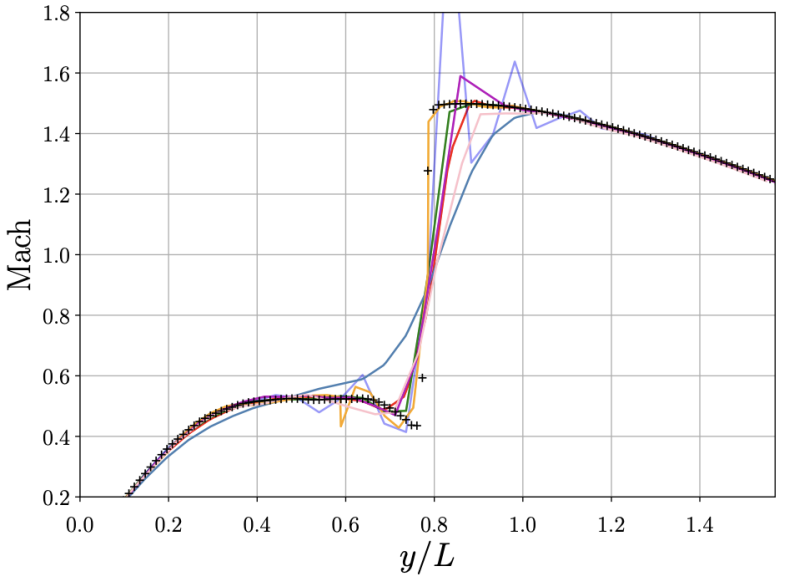

Hydrogen / air injection mixing

- Supersonic injection of hydrogen into air
- Chocked nozzle flow: shocktrain
- NPR = 10

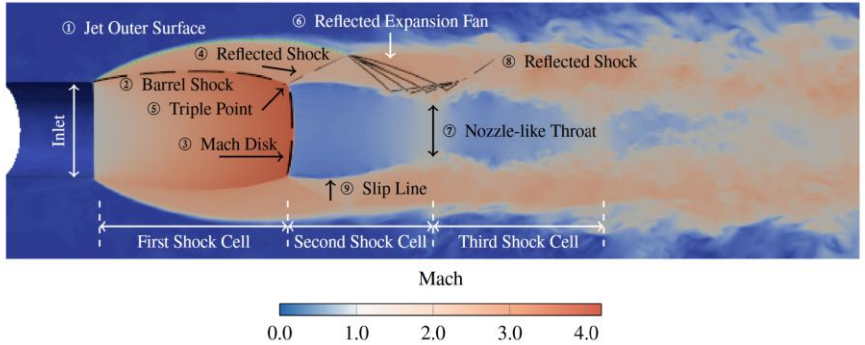

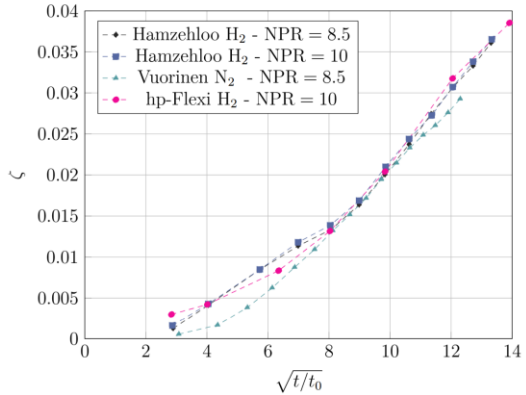

Figure 16: Normalized centerline jet-tip penetration $\mathcal{Z}^*_{\text{tip}}$ over the non-dimensional time t^*. The present study is compared against the results for H_2-jets of Hamzehloo et al. [15] and an N_2-jet of Vuorinen et al. [50].

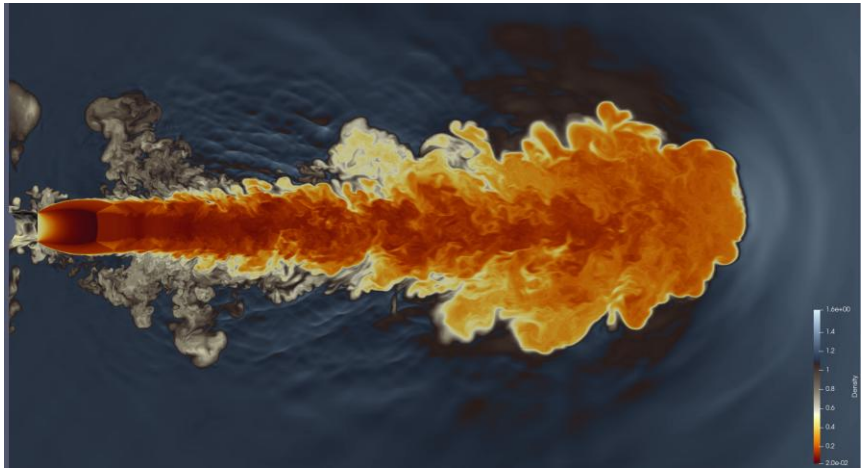

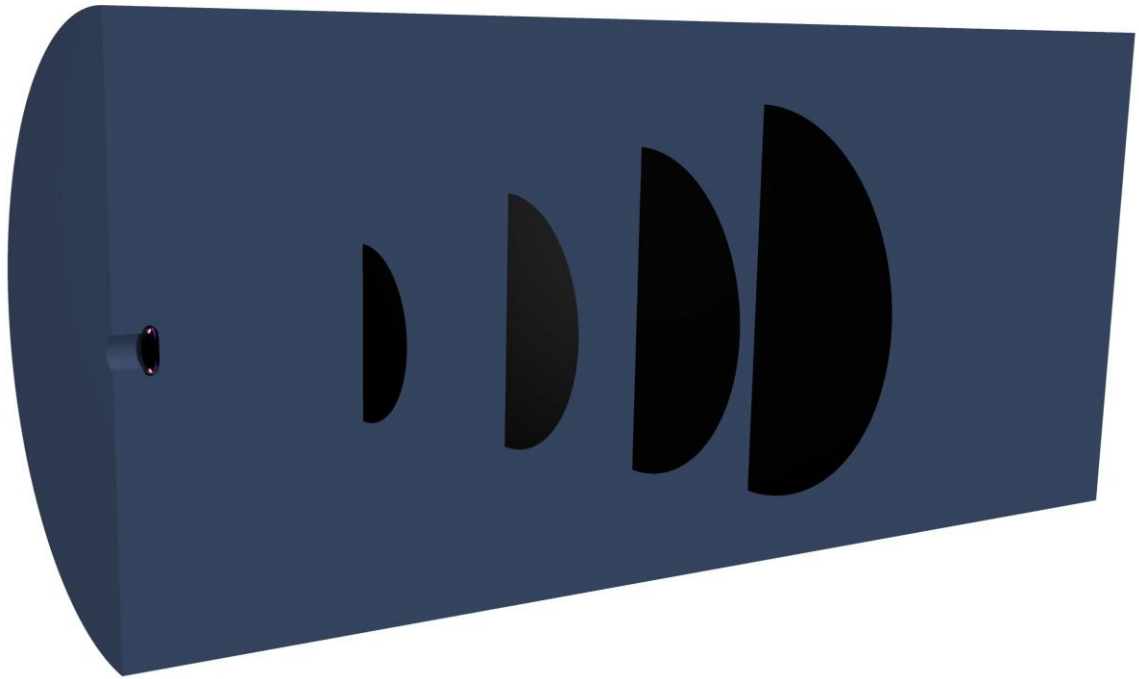
Vorticity
0.
5.e+6
1.e+7
2.e+7
2.e+07
Pressure
5.e+03
1.e+4
2.e+4
5.e+4
1.e+5
2.e+05
H2 Massfraction
0.0
0.2
0.4
0.6
0.8
1.0

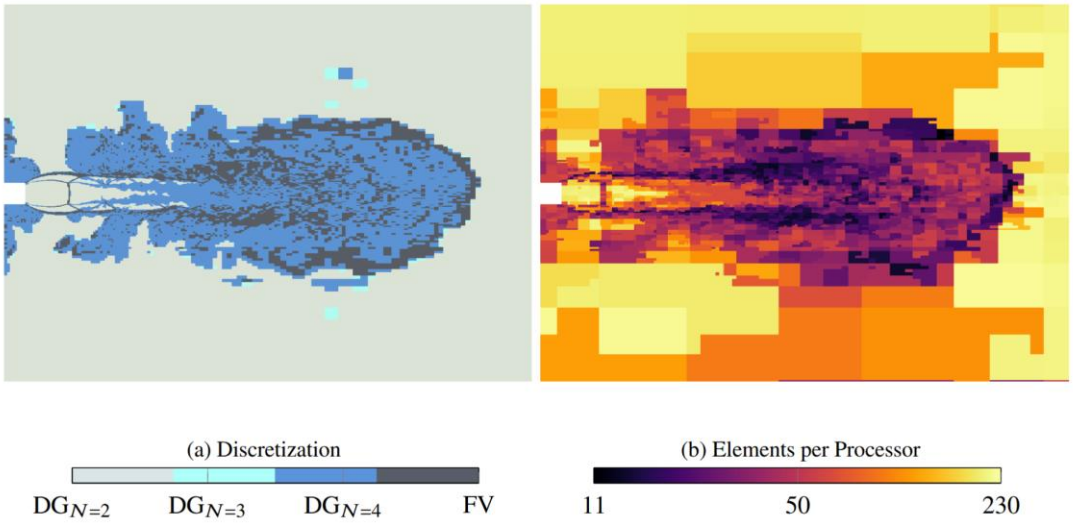

Figure 17: Depiction of the hp-adaptive element-local discretization and domain-decomposition in a slice of the H_2-jet simulation at $t^* = 161$. In (a), a snapshot of the FV sub-cell element distribution and the local ansatz degree of the p-adaptive DG operator is shown. Figure (b) illustrates the decomposition of the domain into sub-partitions for every processor. The color indicates the number of elements within each partiton.

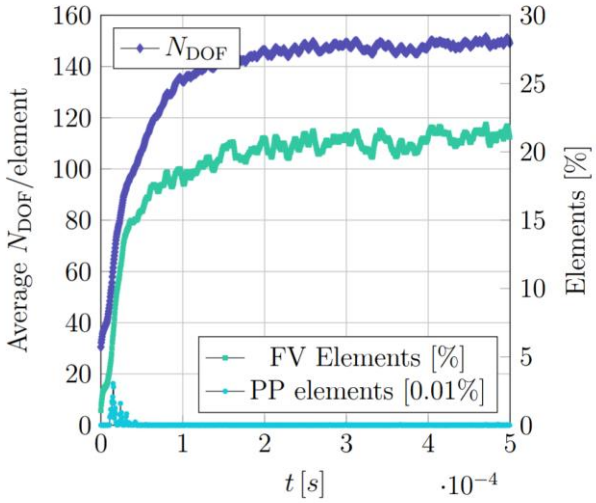

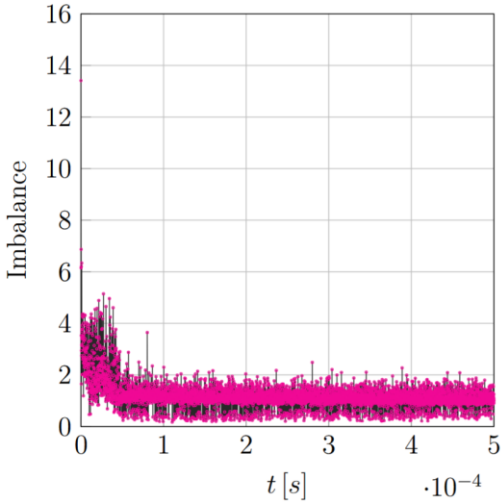

Mixing of H2 in air

N_DG= [2,4], 50 Mio DoF, 0.3 Mio CPUh

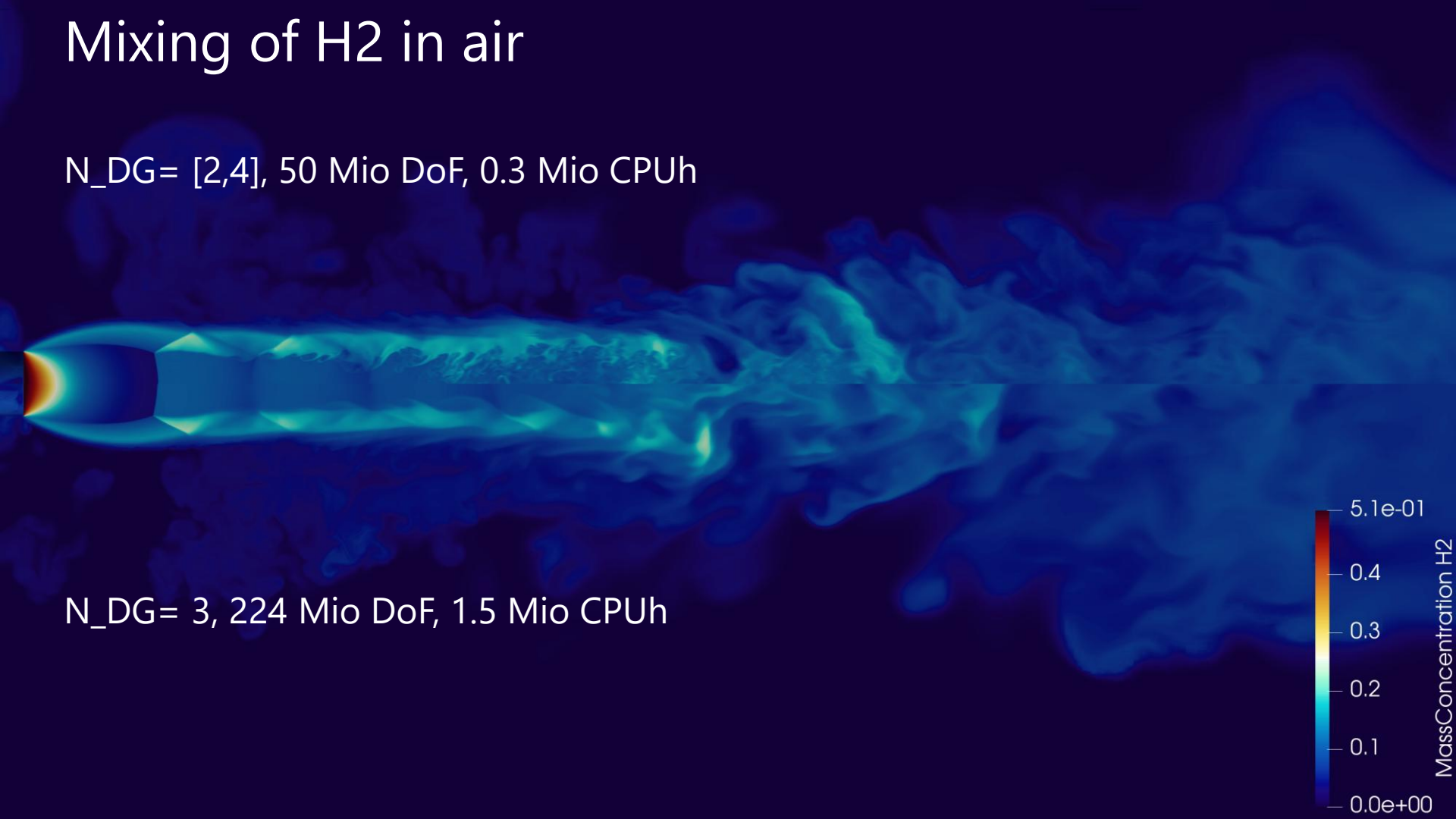

N_DG= 3, 224 Mio DoF, 1.5 Mio CPUh

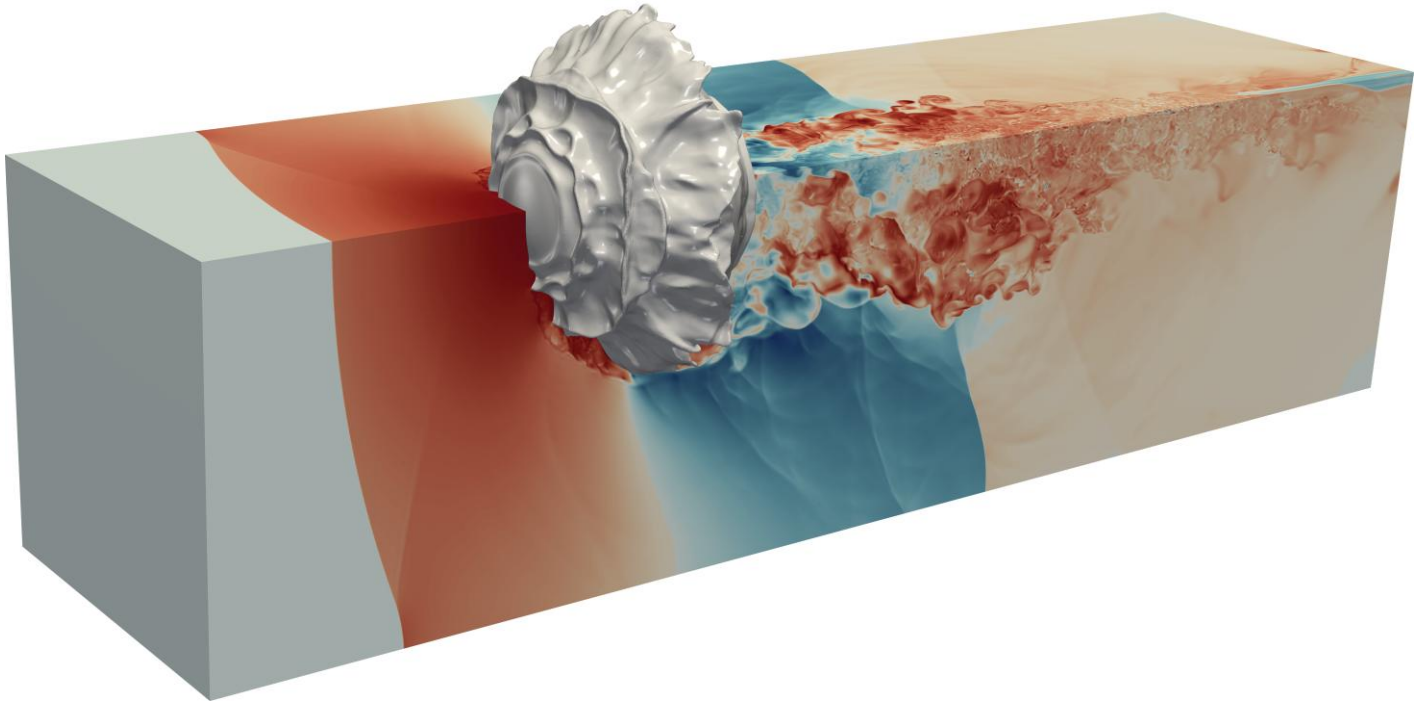

Building Block III: Multi-X

Multi-Method, Multi-Phase, Multi-Code,….

- Arbitrary Lagrangian-Eulerian for mesh movement, coupled for FSI with CG-FEM.

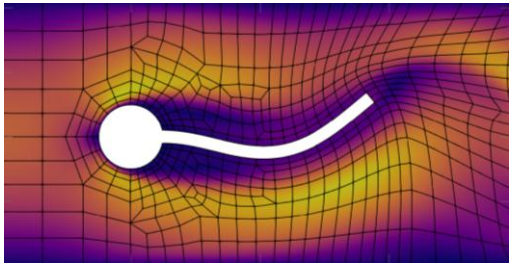

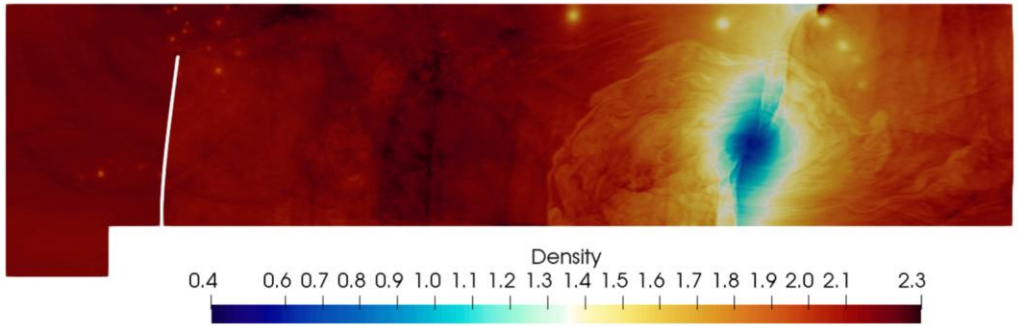

- Direct and hybrid Aeroacoustics

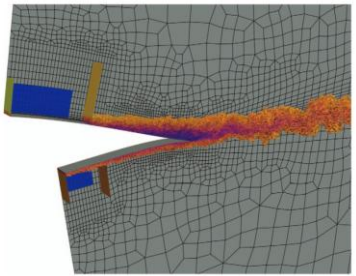

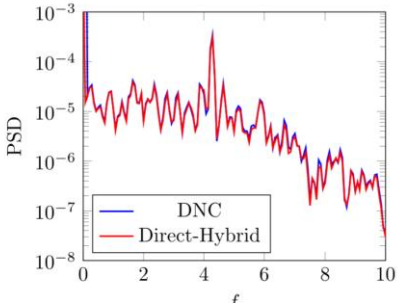

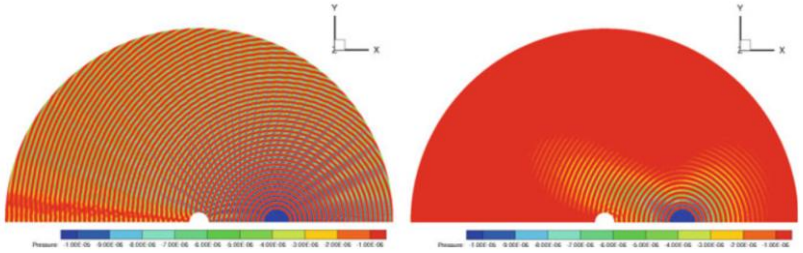

Multi-Method, Multi-Phase, Multi-Code,….

- Intrusive and non-intrusive UQ incl. HPC scheduler

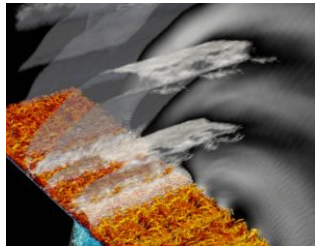

Non-Intrusive / NISP, MLMC

SIAM J. Sci. Comput., 42(4), B1067–B1091. (25 pages)

Computational Methods in Science and Engineering

hp-Multilevel Monte Carlo Methods for Uncertainty Quantification of Compressible Navier--Stokes Equations

Andrea Beck, Jakob Dürrwächter, Thomas Kuhn, Fabian Meyer, Claus-Dieter Munz, and Christian Rohde

Related Databases

Web of Science

Journal of Theoretical and Computational Acoustics | Vol. 27, No. 01, 1850044 (2019) No Access

Uncertainty Quantification for Direct Aeroacoustic Simulations of Cavity Flows

Thomas Kuhn, Jakob Dürrwächter, Fabian Meyer, Andrea Beck, Christian Rohde and Claus-Dieter Munz

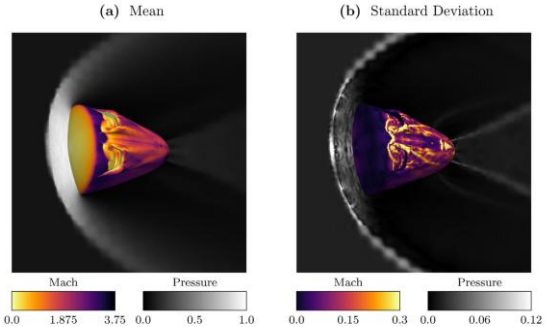

Fig. 6. Spacecraft: mean and standard deviation; Mach number on spacecraft surface, pressure in slice through flow field. Example 5.4.

Intrusive / SG

Contents lists available at ScienceDirect

Computers and Fluids

journal homepage: www.elsevier.com/locate/compfluid

A high-order stochastic Galerkin code for the compressible Euler and Navier-Stokes equations

Jakob Dürrwächter[a,*], Fabian Meyer[b], Thomas Kuhn[a], Andrea Beck[a], Claus-Dieter Munz[a], Christian Rohde[b]

[a] Institute of Aerodynamics and Gas Dynamics, University of Stuttgart, Pfaffenwaldring 21, 70569 Stuttgart, Germany
[b] Institute of Applied Analysis and Numerical Simulation, University of Stuttgart, Pfaffenwaldring 57, 70569 Stuttgart, Germany

Multi-Method, Multi-Phase, Multi-Code,….

- Sharp and diffuse interface method for compressible multiphase flows

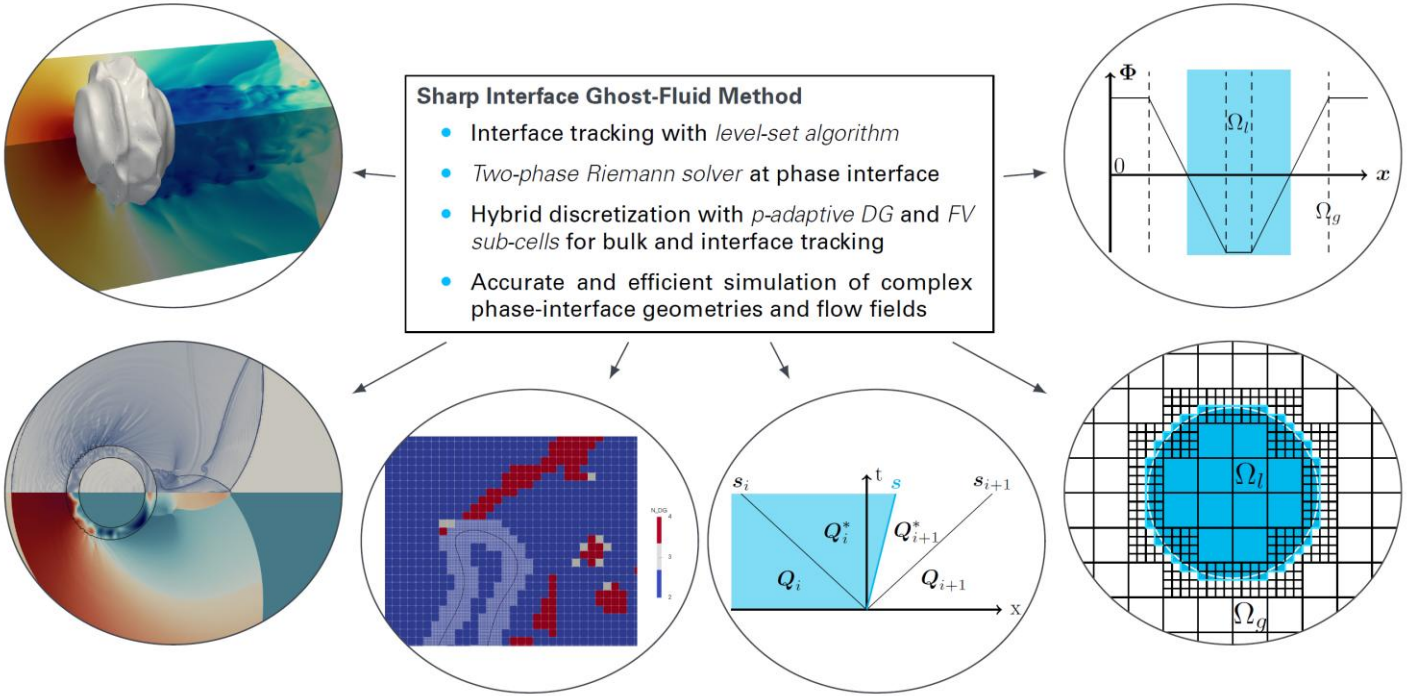

Prediction Erosion in Jet Engines

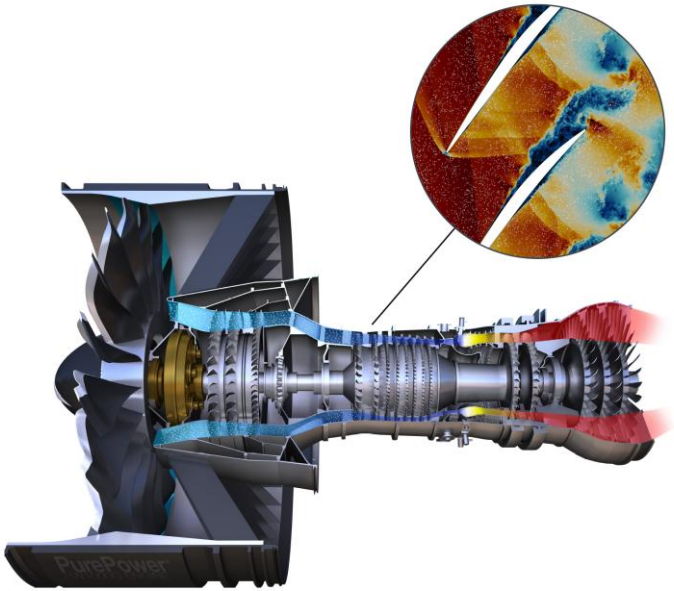

© Pratt & Whitney, MTU

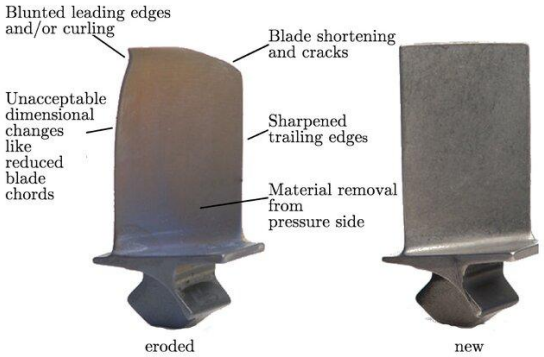

Henning, C., Brodbeck, M., Koch, C., Staudacher, S. and Ricken, T. (2021), Phase-field model for erosion processes. Proc. Appl. Math. Mech., 20: e202000282. https://doi.org/10.1002/pamm.202000282

Numerical Aspects

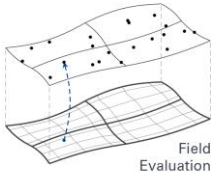

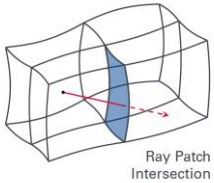

- One-, two- and four way coupling to fluid phase, Maxey-Riley-Gatignol model
- Accurate wall intersections for curved boundaries through ray tracing
- Hybrid (MPI distributed / MPI shared) parallelization for particle load balancing

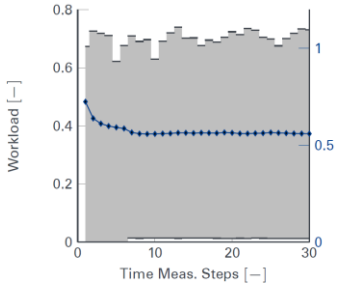

No load balancing

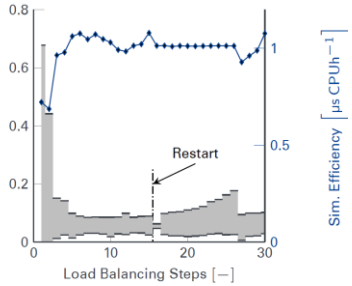

Dynamic load balancing

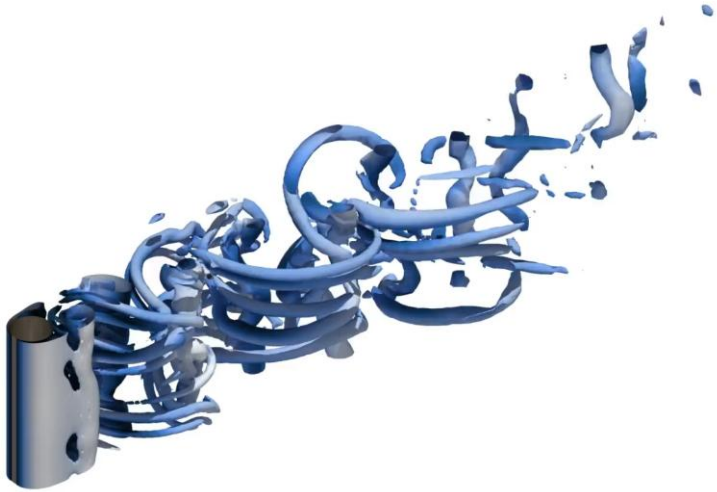

Numerical Aspects

- Conservative projection operators: sliding mesh for rotor / stator interaction
- SotA Wall-interaction models are insufficient: Data-driven, physics-conditioned rebound models through neural networks trained on exp. data

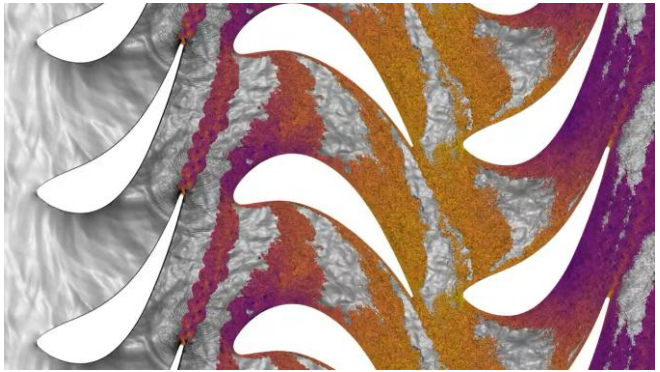

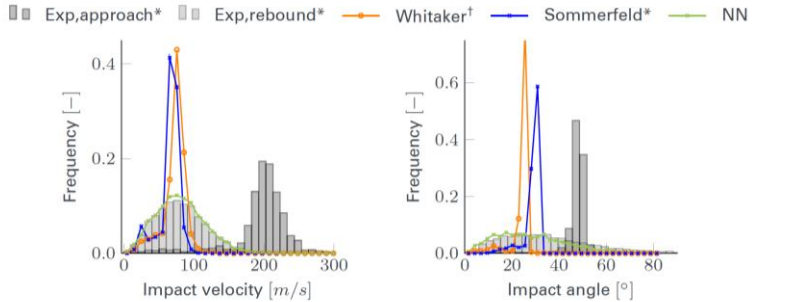

⇒ Neural network (NN) inherently considers the stochasticity and the underlying PDFs are well captured

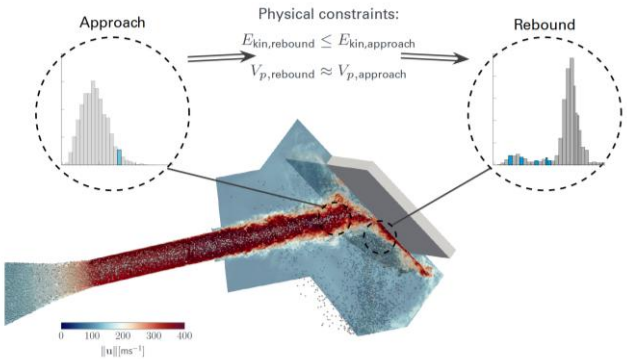

* Sommerfeld2021a
† Whitaker2023

ML-driven, time-resolved erosion simulations

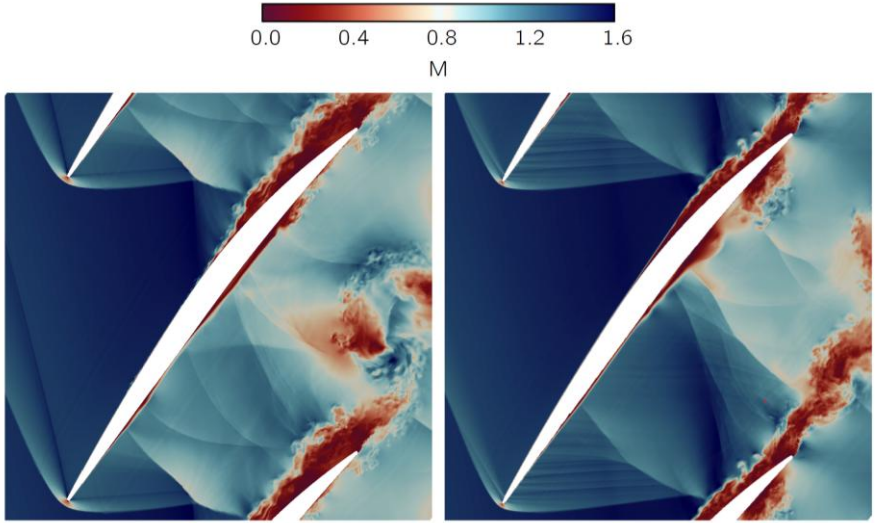

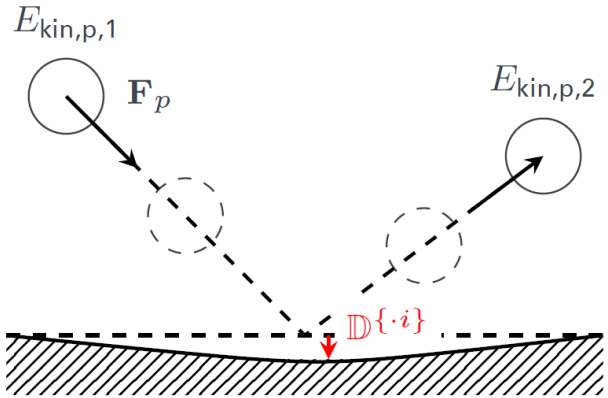

- Wall-Modelled LES
- Erosion modelled on impact energy
- Time-resolved mesh deformation through ALE

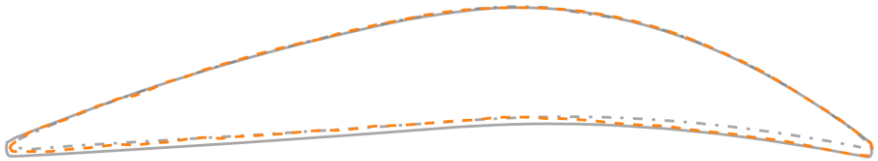

Figure 6.7: Sketch of the rotor blade deformed by the ALE approach (orange) compared to the measured, eroded rotor blade (grey, dashed) given in [125, 70]. The solid, grey line indicates the uneroded blade profile. For reasons of clarity, in the present sketch, the rotor height is scaled by a factor of two compared to the chord length.

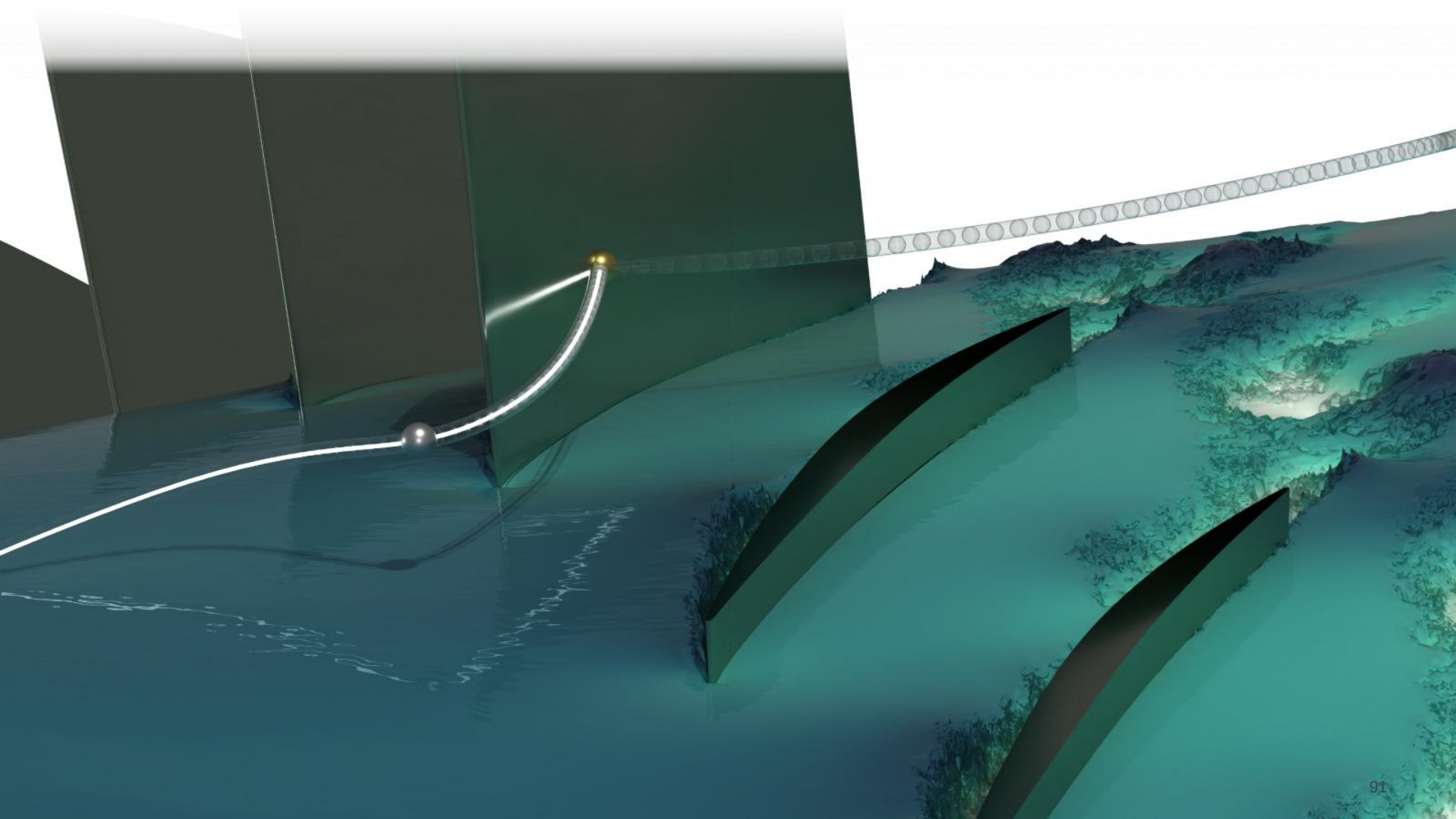

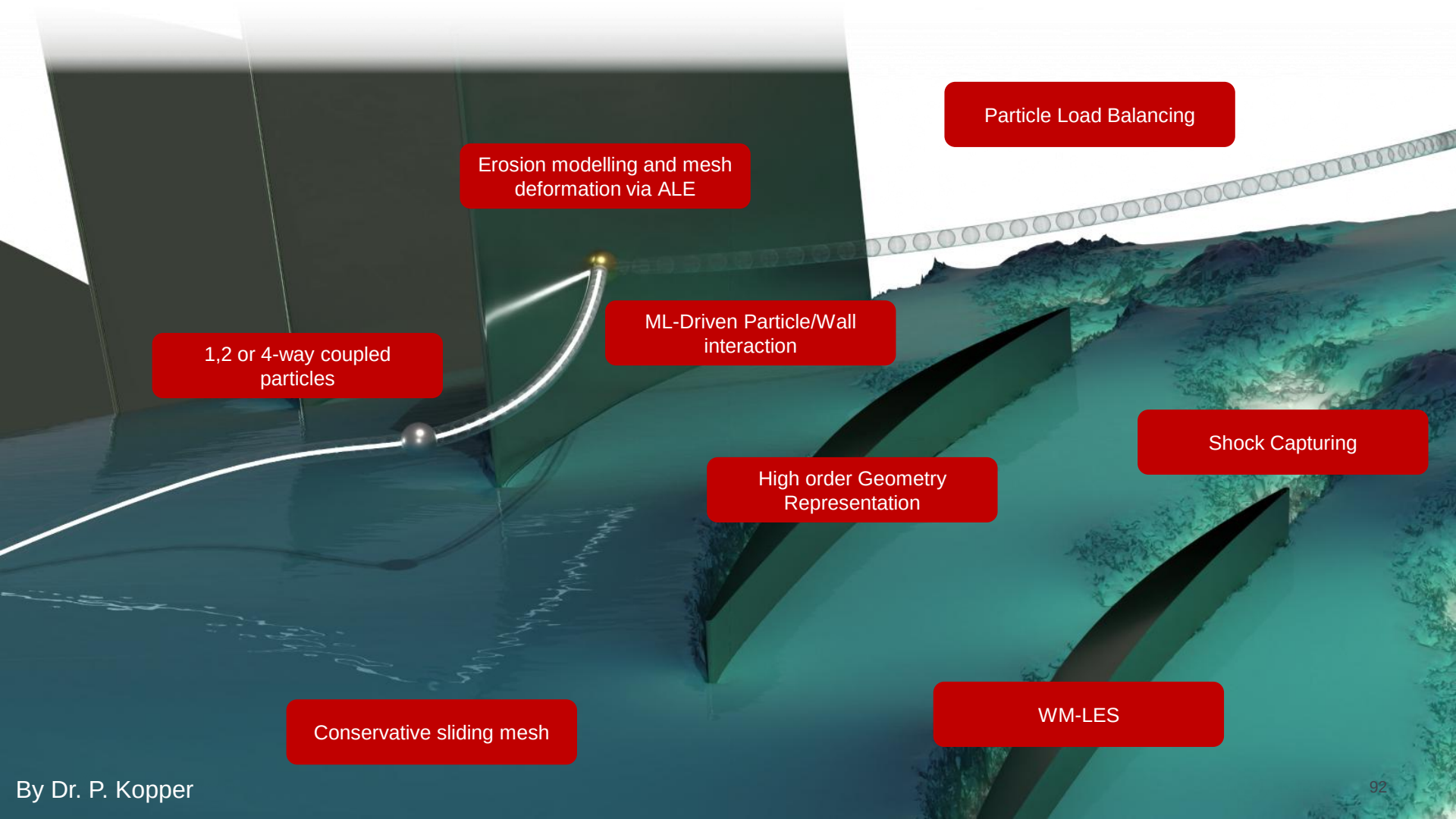

By Dr. P. Kopper

High Performance Computing

- CPU-based systems: HAWK, SuperMUC, LUMI, Leonardo, Mare Nostrum, EuroHPC machines,..
- GPU-based systems: HAWK-AI, JUWELS-Booster, JEDI, JUPITER, HUNTER, LUMI-G, FRONTIER,..

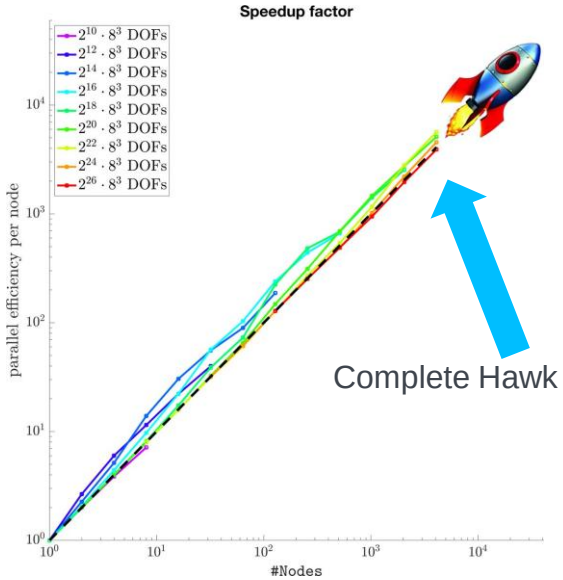

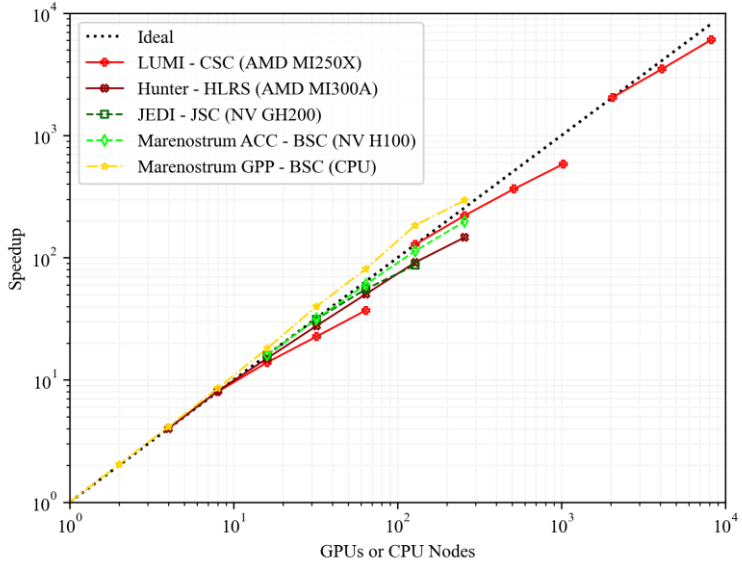

- FLEXI and Galæxi are the lighthouse codes for compressible flows at the EuroHPC Center of Excellence for Exascale CFD

EuroHPC Joint Undertaking

NRG

Simulation software: FLEXI / GALAEXI

[1]www.flexi-project.org

- High-order accurate open source solver[1] with excellent scaling behavior
- Discontinuous Galerkin spectral element method (DG-SEM)
- Focus on DNS/LES of multiscale- and multiphysics problems governed by the compressible Navier-Stokes equations
- Additional features
  - Lagrangian particle tracking (LES/DNS of particle laden flows)
  - Direct & hybrid acoustics
  - Conservative sliding mesh interface for stator/rotor flow
  - Mesh deformation and mesh moving based on ALE formulation
  - hp-adaptivity
  - Intrusive and non-intrusive methods for uncertainty quantification
  - Management framework for optimal scheduling on HPC systems
  - A solver-in-the-loop framework for reinforcement learning

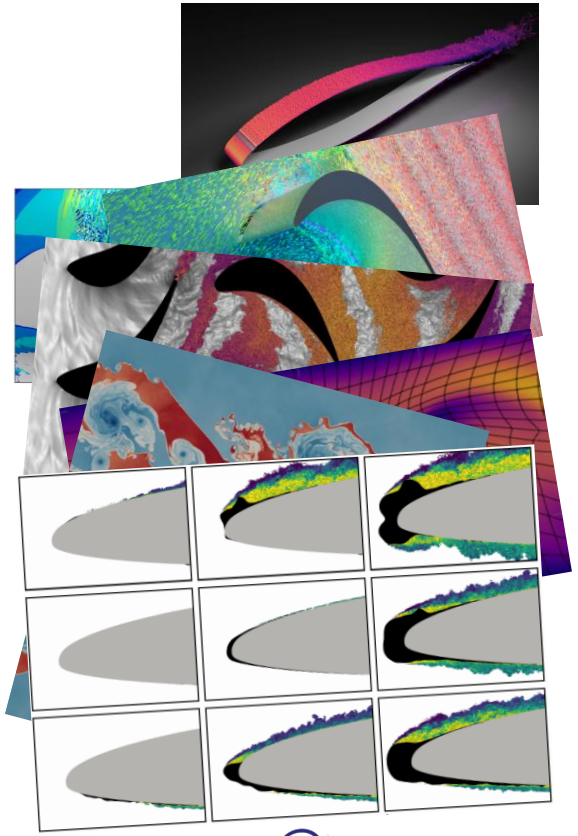

Overview

Motivation

Discretization schemes for multi-X problems

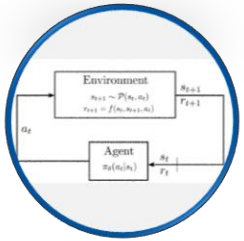

From data-driven to integrated CFD/ML

Observations

- ML / AI methods will not replace PDE solvers
- ML / AI methods will augment PDE solvers, especially for sub-models: hybrid CFD/ML
- A priori performance of ML is vastly superior to a posteriori
- We have successfully combined ML and DG for
  - A limiting strategy for FV (RL)
  - Flow control (RL)
  - Particle / Wall models (SL)
  - Non-linear eddy viscosity models (SL)
  - Subelement shock capturing and HO artificial viscosity
- LLMs?

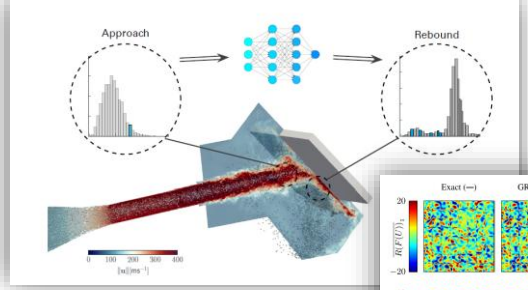

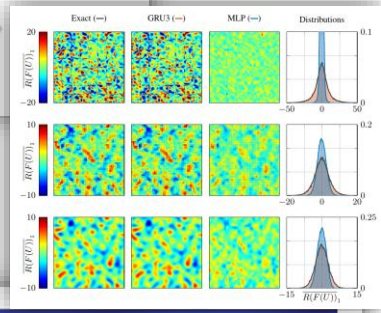

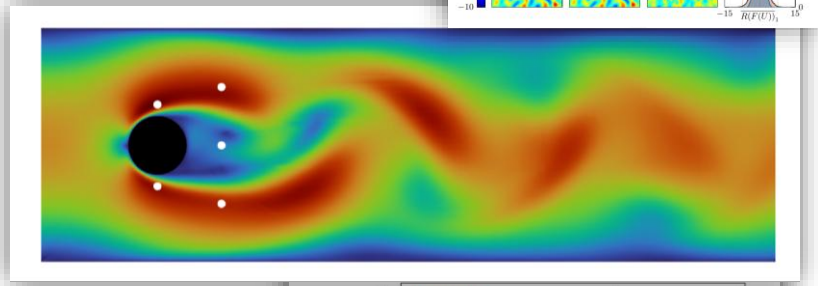

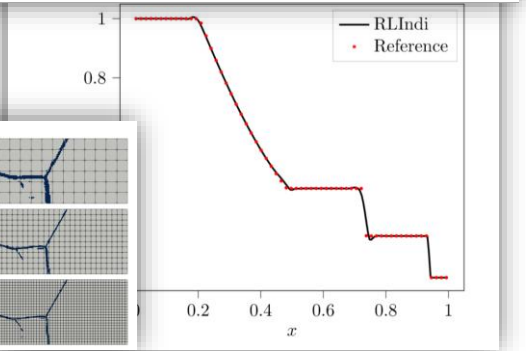

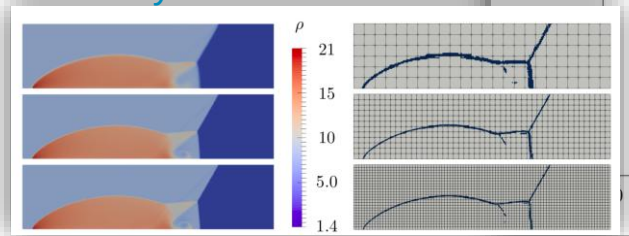

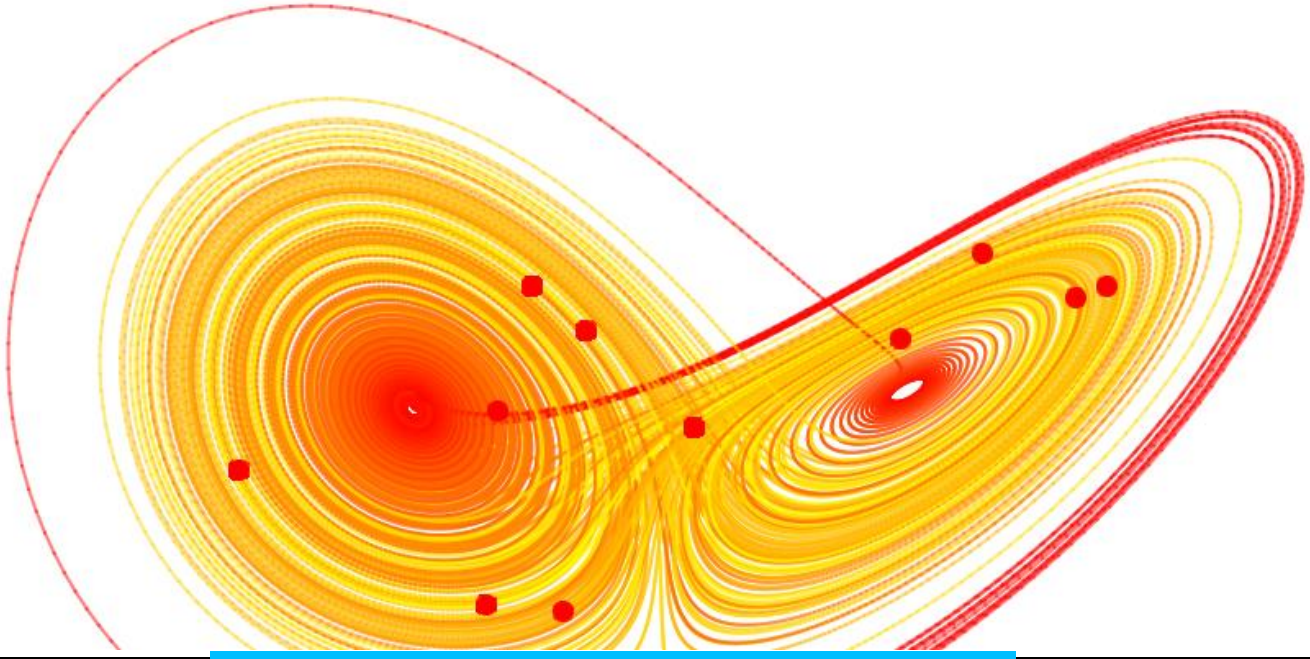

A posteriori-optimal LES models


A350
AIRBUS A350 XWB

The Scale Gap in Turbulence

$$\underbrace{R(U_l, x_l) = 0}_{\text{Governing Equations at level l}} \quad (1)$$

$$0 = R(U_h, x_h) + C(U_l, U_h) \approx \underbrace{R(U_h, x_h,) + \mathbf{M}(\mathbf{U_h})}_{\text{"Closed" Equations at level h}} \quad (2)$$

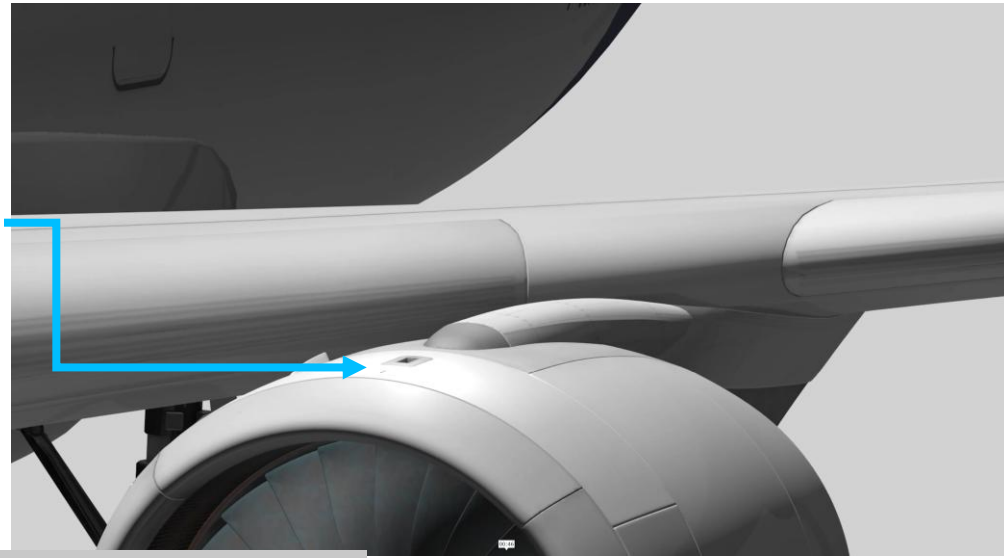

Large Eddy Simulation

- Define a convolution kernel G (in physical or wave space)
  - Properties: linear, isotropic, homogeneous, commutable
  - Filtered / large scale solution

$$\overline{\psi}(x) := F(\psi(x)) = \int_{\infty}^{\infty} k(\xi - x, \Delta)\psi(\xi)d\xi,$$

- Filtering the (incomp.) Navier-Stokes-Equations s.t. these properties

$$\frac{\partial \overline{u}_i}{\partial t} + \frac{\partial}{\partial x_j}(\overline{u}_i \overline{u}_j) = -\frac{1}{\rho}\frac{\partial \overline{p}}{\partial x_i} + 2\nu \frac{\partial}{\partial x_j}\overline{S}_{ij} - \frac{\partial \tau_{ij}}{\partial x_j}$$

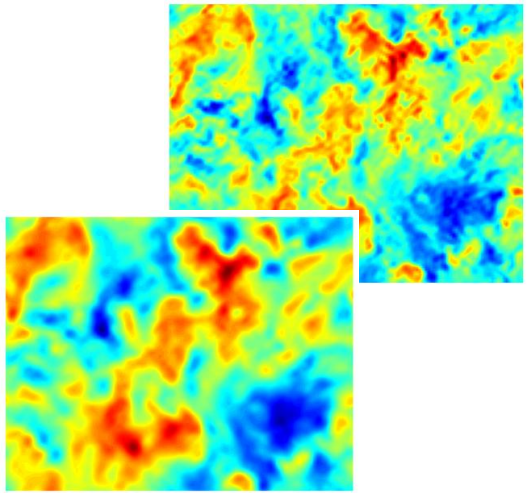

- Closure problem for the explicitly filtered incompressible NSE:

$$\overline{u_i u_j} - \overline{u_i}\,\overline{u_j} = \tau_{ij}$$

Large Eddy Simulation: Explicit Filtering

- A priori application of different filter kernels on a Cartesian grid

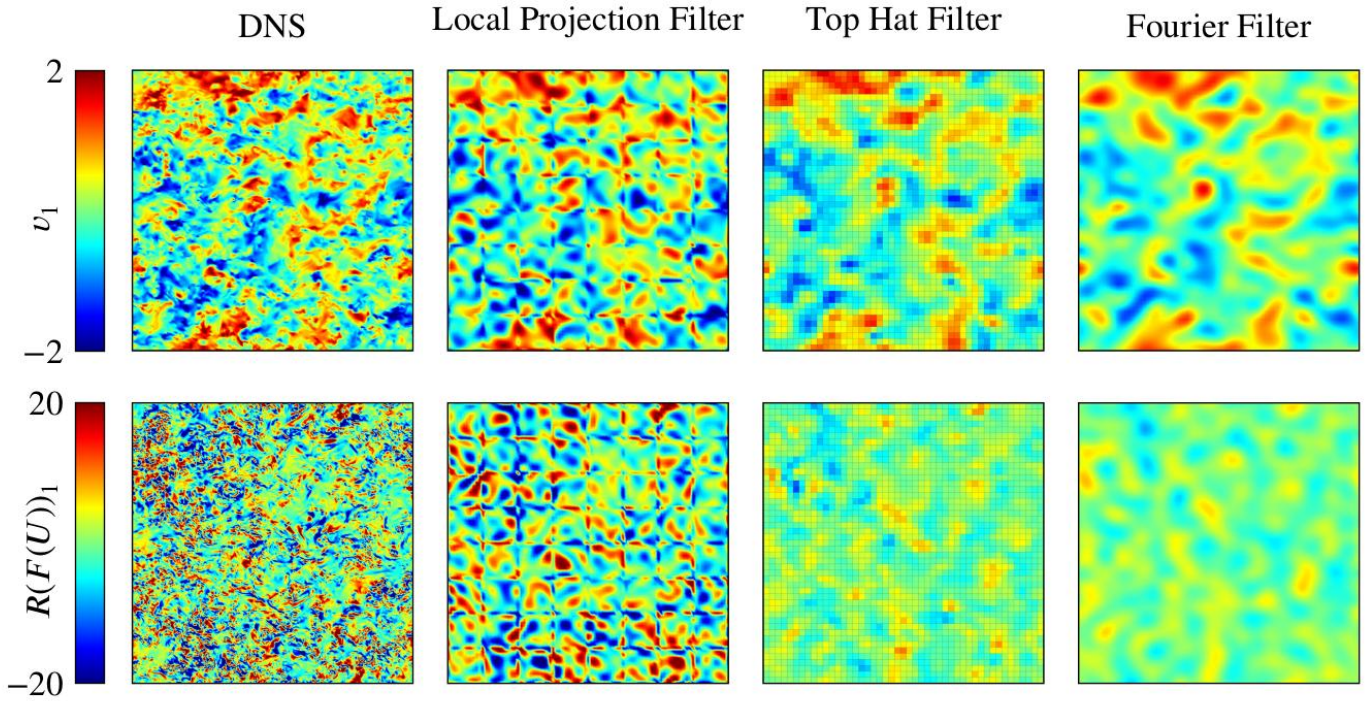

Explicit and implicit filtering for LES

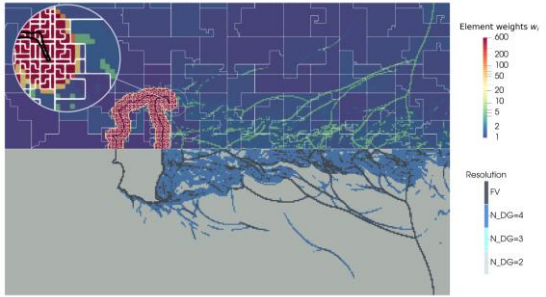

- Filter width Δ, discretization / grid spacing h

- Explicit filtering
  - Separate Δ and h
  - Grid convergence under $h \to 0$
  - Discretization scheme not (very) relevant
  - homogeneity and isotropy, boundary conditions, realizability, commutation…

0.5% on google scholar

- Implicit filtering
  - Joined Δ and h
  - Grid convergence not possible $h \not\to 0$
  - Discretization scheme defines the filter kernel
  - Discretization parameters and errors
  - Additional computational commutation error: Non-linear for a non-linear scheme!

99.5% on google scholar, 100% for “industrial” LES

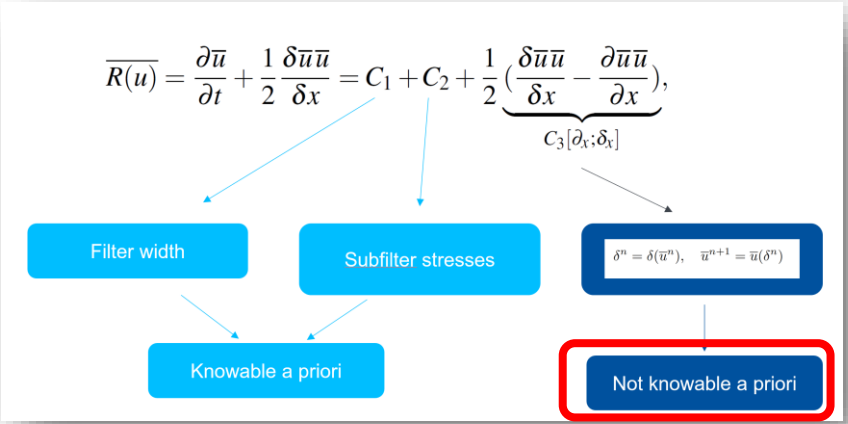

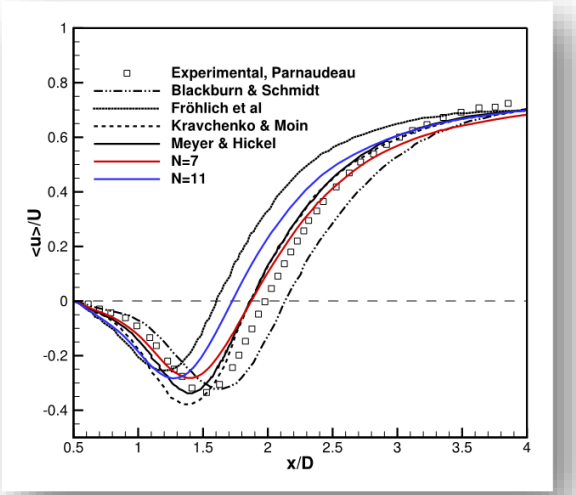

- Computational commutation error can have the same order of magnitude and scaling as the turbulent stress fluxes themselves [GH06]
- “the commutation error arising from the implicit part of the filter has not been well investigated.” (Moser, 2021)
- Computational commutation error is a non-linear function of the discretization and solution
- Optimization-based approach: A posteriori optimal LES

[GH06]: Geurts, Bernard J., and Darryl D. Holm. "Commutator errors in large-eddy simulation." *Journal of physics A: mathematical and general* 39.9 (2006): 2013.

Optimized discretization-consistent closure schemes

Markov Decision Process (MDP)

- Extends Markov chains with actions & rewards
- Discrete-time stochastic control process defined by the tuple of actions, states, rewards and discounts

$$\langle S, A, P(\cdot), R(\cdot), \gamma \rangle, \text{with}$$

$$a \in A : \text{actions}$$
$$s \in S : \text{state of the system}$$
$$\gamma \in \mathcal{R} : \text{discount factor}$$
$$P(s_{k+1} = s' | \langle s_k = s, a_k = a \rangle) : \text{transition probability}$$

- Markovian IFF memoryless:

$$P(s_{k+1} | \langle s_k, a_k \rangle) = P(s_{k+1} | \langle s_0, a_0 \rangle, ..., \langle s_k, a_k \rangle), \ \forall (s_\tau \in S, a_\tau \in A), \ \tau \{1, ..., k\}$$

- Formally solved by a policy: mapping from state-action space to the probability of taking action a when in state s:

$$\pi = S \times A \rightarrow \mathcal{R}, \langle s, a \rangle \rightarrow [0, 1]$$

Markov Decision Process (MDP)

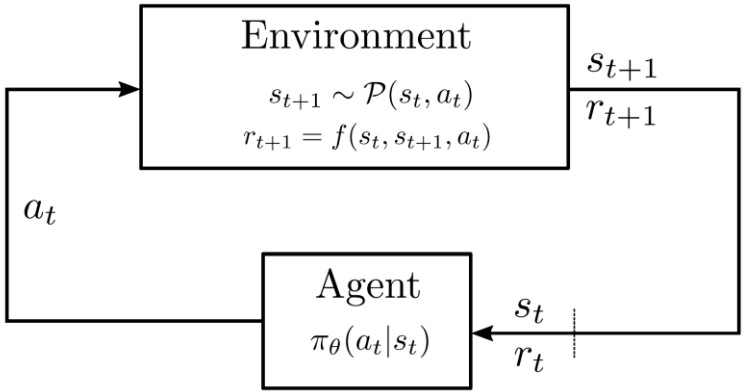

$$\pi = S \times A \to \mathcal{R}, \langle s, a \rangle \to [0, 1]$$

Solved for the optimal policy, e.g. by reinforcement learning

Example: RL for Flow Control

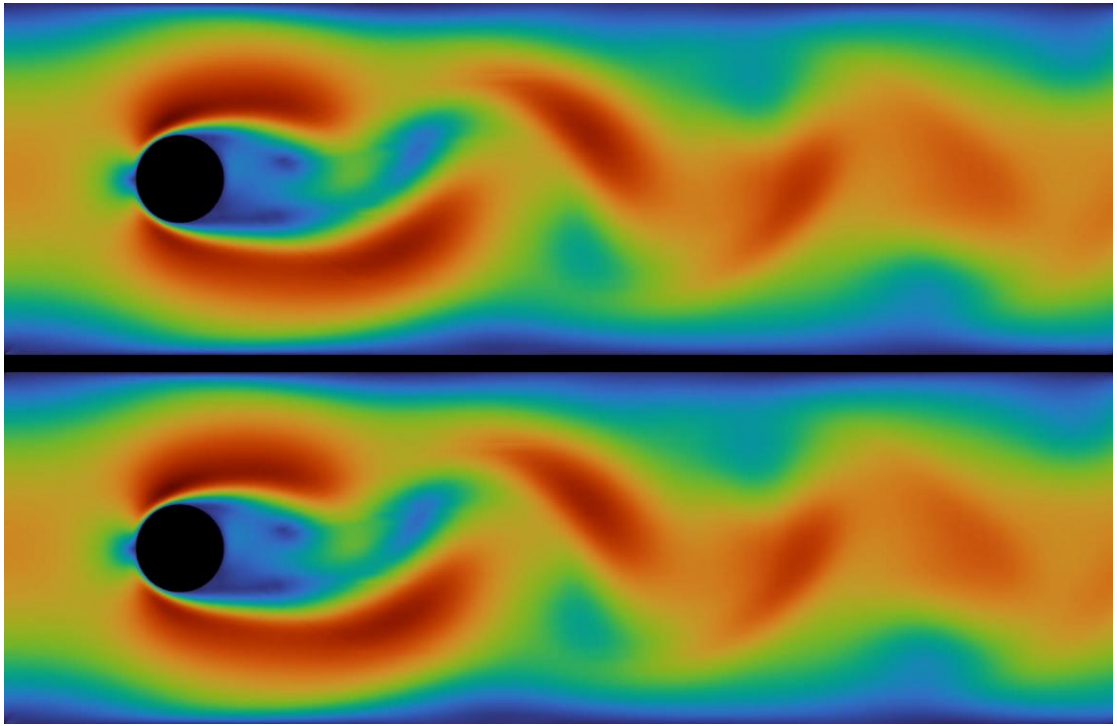

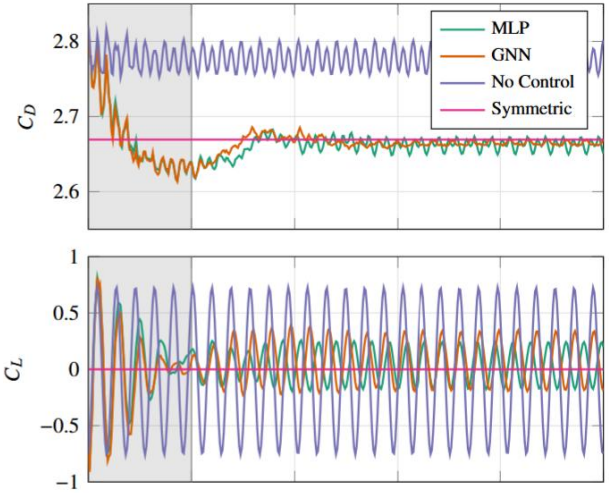

ELSEVIER
Computers & Fluids
Volume 303, 15 December 2025, 106854

Invariant control strategies for active flow control using graph neural networks ☆

Marius Kurz [a 1], Rohan Kaushik [b 1], Marcel Blind [b], Patrick Kopper [b], Anna Schwarz [b], Felix Rodach [b], Andrea Beck [b]

A posteriori optimization

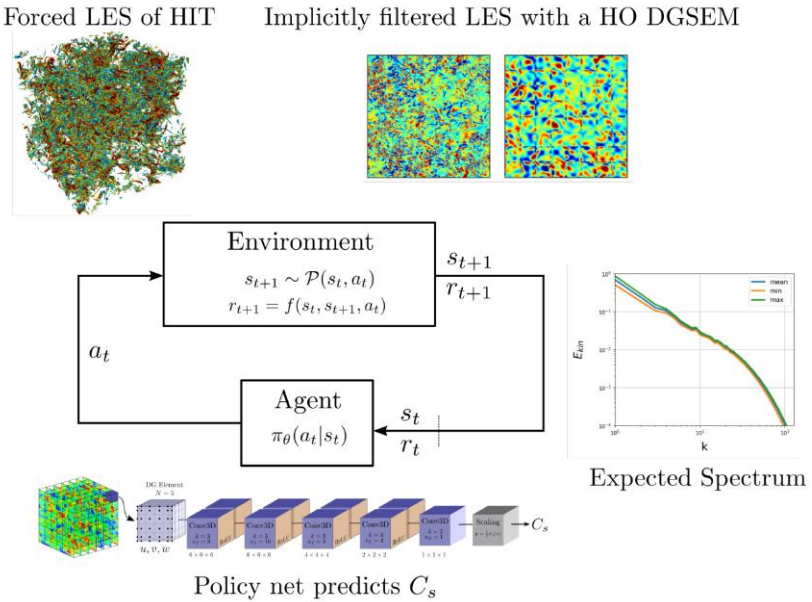

- a posteriori LES, “solver-in-the-loop”,..
- Not optimize for a closure term, but the LES solution
- Formulate optimization as an MDP with a continuous action space, solve by Reinforcement learning method (PPO)
- Environment: Implicitly filtered HO DGSEM
- Reward / Goal: Spectrum
- Agent: Convolutional / Residual / Graph NN
- No DNS data; optimization requires LES runs only

Optimization Details

- Policy gradient based Reinforcement learning (PPO)
  - Gradient ascend to update parameters of agent to maximize reward function J
  - Policy gradient:

$$\nabla_\theta J(\theta) = \mathbb{E}_{\tau\sim\pi_\theta}\Big[\underbrace{\Big(\sum_{k=1}^{N}\gamma^k r_k\Big)}_{\text{Cum. reward over } \tau}\underbrace{\nabla_\theta \log \pi_\theta(\tau)}_{\text{Grad. of the policy}}\Big]$$

  - Approximate expectation by ensemble average of trajectories of MDP

$$\tau^{(1)} = \{(s_0, a_0), (s_1, a_1, r_1), \ldots, (s_N, a_N, r_N)\}$$

  - TRPO:

$$\theta' \leftarrow \text{argmax}_{\theta'}\, \nabla_\theta J(\theta)^T (\theta - \theta'),$$

$$\text{such that } D_{KL}(\pi_{\theta'}(\cdot \mid s) \| (\pi_\theta(\cdot \mid s))) \leq \epsilon \forall s \in S$$

Reinforcement learning framework – ReLeXI[1]: NRG, HLRS & HPE

- Distribution on hybrid HPC systems via the SmartSim Library[2]
- LES instances interactively distributed across multiple CPU nodes („Workers“)
- Communication via in-memory database with the Redis library
- Excellent scaling across CPU / GPU threads

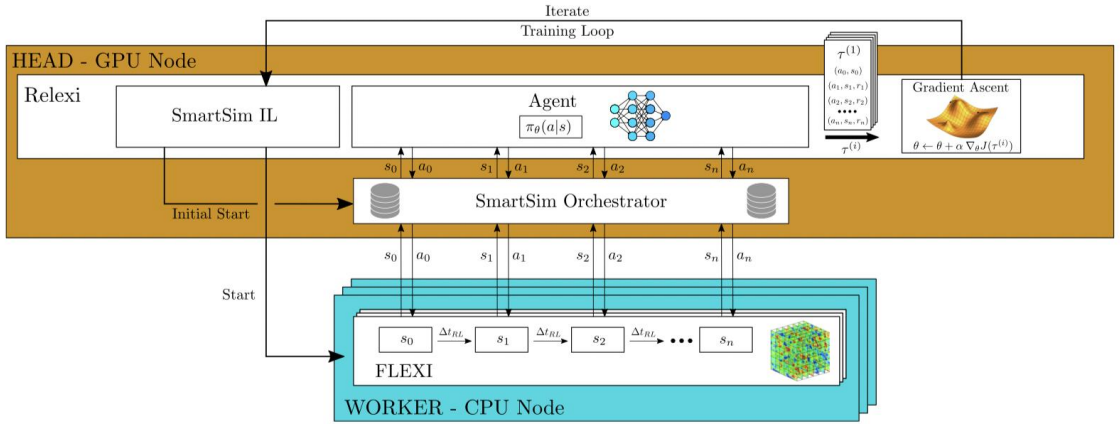

[1]Kurz et al., Relexi—A scalable open source reinforcement learning framework for high-performance computing. Software Impacts, 2022
[2]https://github.com/CrayLabs/SmartSim

State of the Art: Closure Models

Filtered Navier-Stokes equation:
$$\frac{\partial \bar{u}_i}{\partial t} + \frac{\partial \bar{u}_i \bar{u}_j}{\partial x_j} = -\frac{\partial \bar{P}}{\partial x_i} + \frac{1}{\mathrm{Re}} \frac{\partial^2 \bar{u}_i}{\partial x_j \partial x_j} + \frac{\partial \tau_{ij}^R}{\partial x_j}$$

Boussinesq approximation:
$$\tau_{ij}^R = 2\nu_e \bar{S}_{ij}$$

Standard Smagorinsky model:
$$\nu_e = \left(C_s \bar{\Delta}\right)^2 |\bar{S}|$$

Dynamic Smagorinsky model:
$$C_s^2 = \frac{1}{2} \frac{\mathbb{L}_{kl}^R \bar{S}_{kl}}{\mathbb{M}_{mn} \bar{S}_{mn}},$$

$$\mathbb{L}_{ij}^R = 2C_s^2 \left(\tilde{\bar{\Delta}}^2 |\tilde{\bar{S}}| \tilde{\bar{S}}_{ij} - \bar{\Delta}^2 \mid \widetilde{\overline{\bar{S}}_{ij} \mid \bar{S}_{ij}} \right) = 2C_s^2 \mathbb{M}_{ij}$$

No Model approach:
$$\tau_{ij}^R = M(R(.), T(.), \Delta x, \Delta t))$$

Implicit model:
$$\tau_{ij}^R = M(R^{opt}(.), T^{opt}(.), \Delta x, \Delta t))$$

State of the Art: Closure Models on HIT

$$r = 2\exp\left(\frac{\beta}{k_{max}}\sum_{k=1}^{k_{max}}\left(\frac{\overline{E}_{DNS}(k) - E_{LES}(k)}{\overline{E}_{DNS}(k)}\right)^2\right) - 1.$$

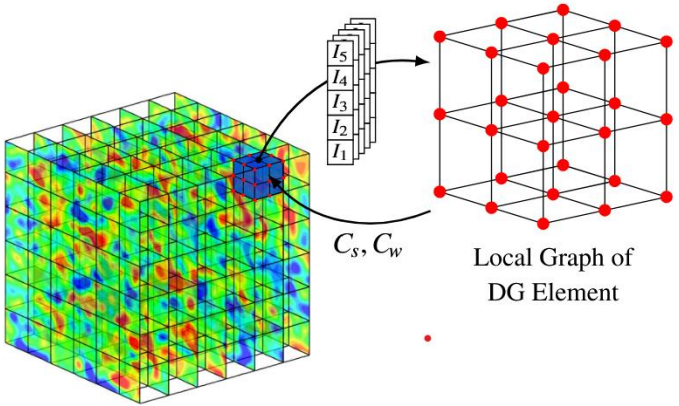

State of the Art: Closure Models on HIT

$$r = 2\exp\left(\frac{\beta}{k_{max}}\sum_{k=1}^{k_{max}}\left(\frac{\overline{E}_{DNS}(k) - E_{LES}(k)}{\overline{E}_{DNS}(k)}\right)^2\right) - 1.$$

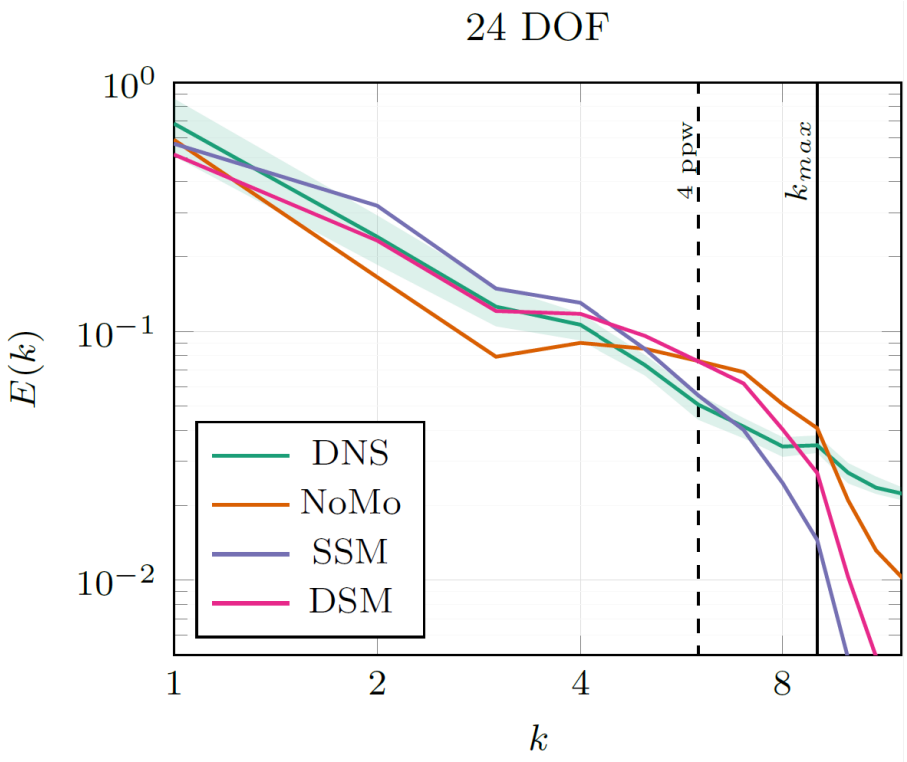

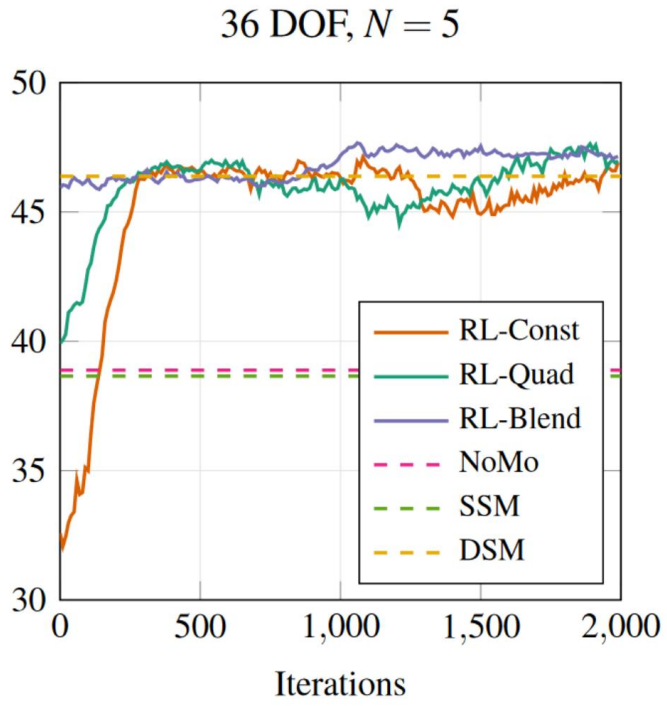

A posteriori optimal LES models: pushing the second frontier

Optimized closures for HIT

Two modelling scenarios: Explicit

Implicit and explicit SGS modeling: Optimal Smagorinsky constant

$$\text{Boussinesq approximation:} \quad \tau_{ij}^{R} = 2\nu_e \bar{S}_{ij}$$

$$\text{Standard Smagorinsky model:} \quad \nu_e = \frac{\mu_{SGS}}{\rho} \left(C_s \bar{\Delta}\right)^2 |\bar{S}|$$

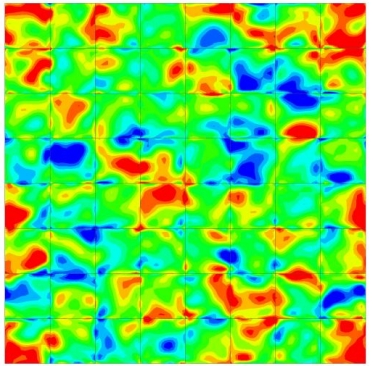

$$\text{SSM: For each grid element } q_{rst} \text{with } r,s,t \in [1, nElems] : C_s^q = C_s = const.$$

$$\text{Cs0: For each grid element } q_{rst} \text{with } r,s,t \in [1, nElems] : C_s^q = C_s(t)$$

$$\text{Cs2: For each grid element } q_{rst} \text{with } r,s,t \in [1, nElems] : C_s^q = \sum_{i,j,k=0}^{2} c_i(t) L_i(x) L_j(y) L_k(z)$$

Results: Explicit Closure with optimized Cs

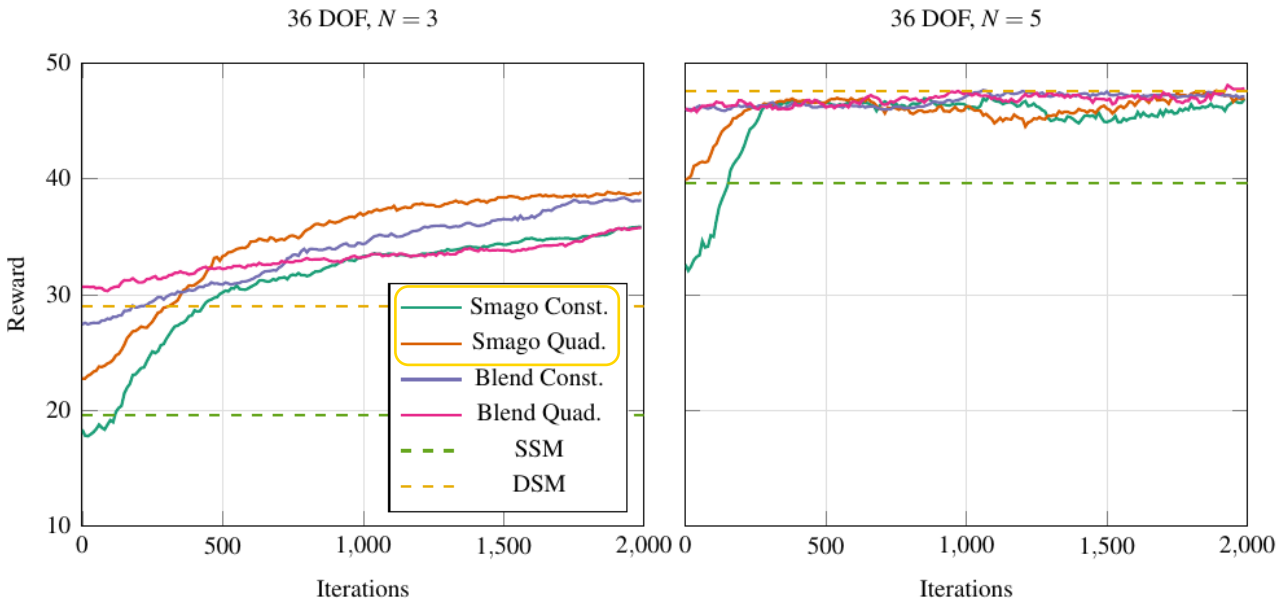

Results: Explicit Closure with optimized Cs

N=5 for different resolutions

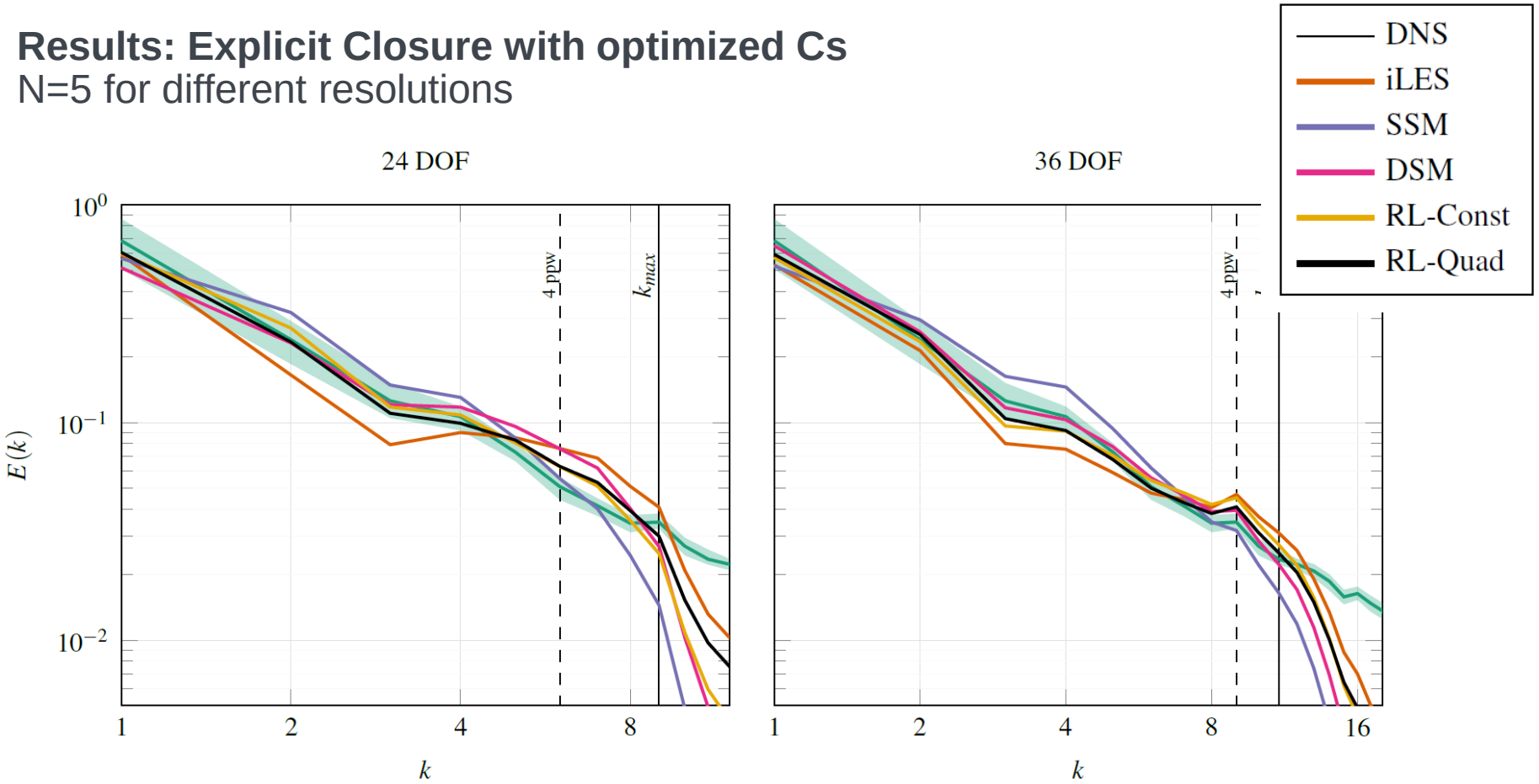

Results: Explicit Closure with optimized Cs

N=5 for different resolutions

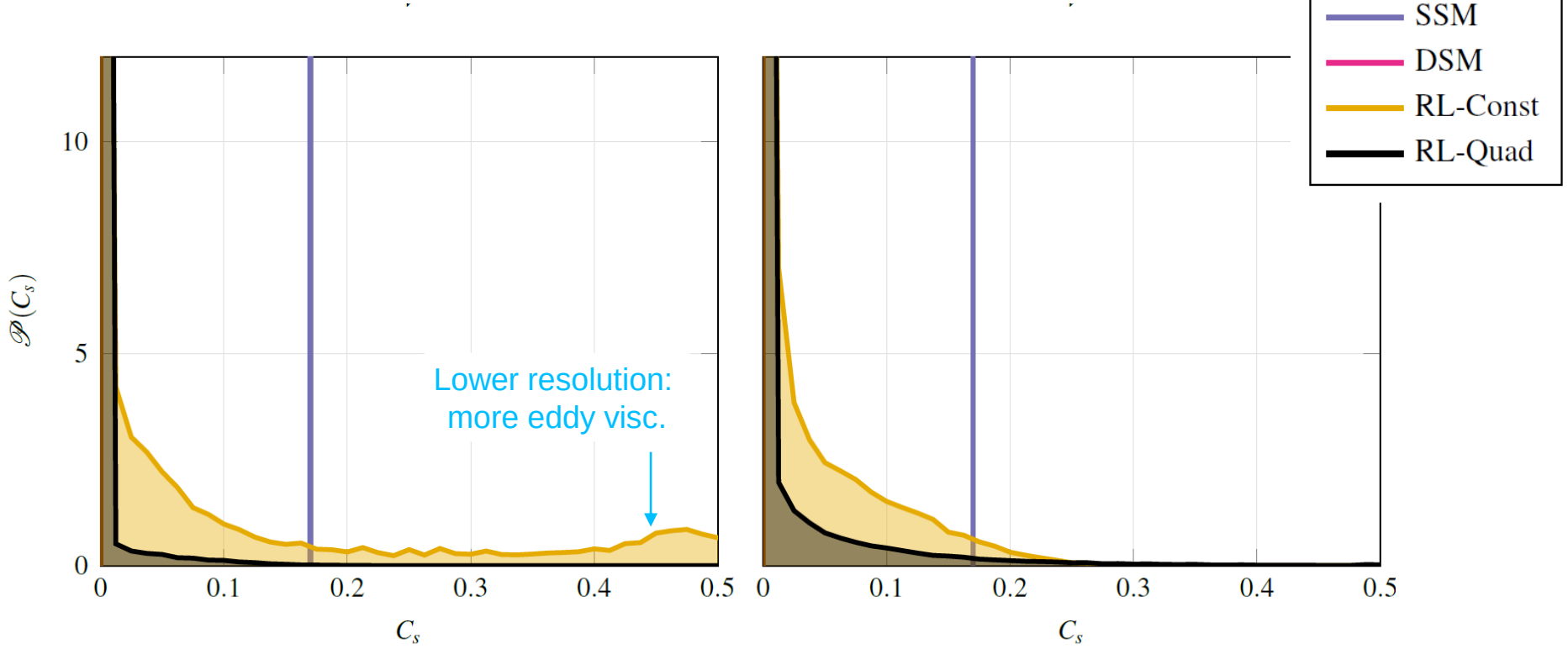

Validity of Boussinesq hypothesis

- Project Subfilter Force Vector (from DNS and the perfect LES idea) onto suitable orthogonal basis
- First basis vector: Viscous flux vector, so coefficient a is the optimal eddy viscosity (actually this tests the Boussinesq hypothesis)

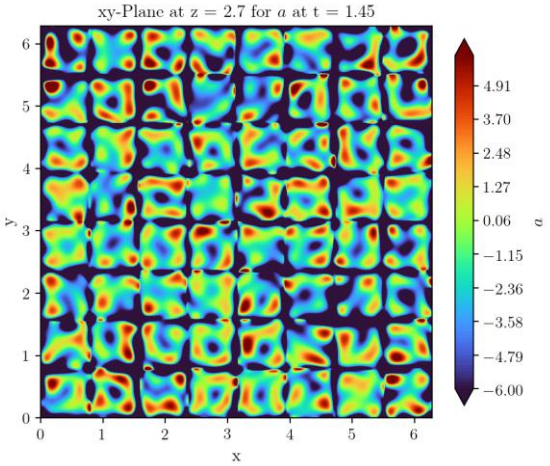

$$\widetilde{R}\left(F^c\left(\overline{U}\right)\right) - \overline{R\left(F^c\left(U\right)\right)} = a\widetilde{R}\left(F^v\left(\overline{U}\right)\right) + b\widetilde{R}\left(F^c\left(\overline{U}\right)\right) + c\left(\widetilde{R}\left(F^v\left(\overline{U}\right)\right) \times \widetilde{R}\left(F^c\left(\overline{U}\right)\right)\right)$$

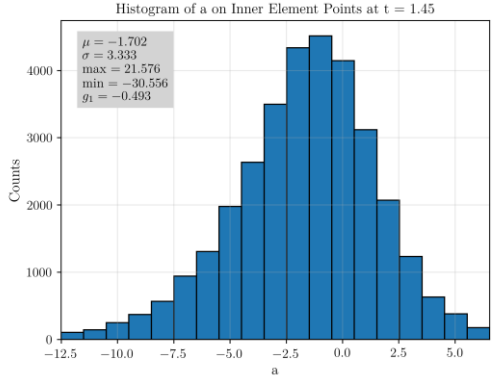

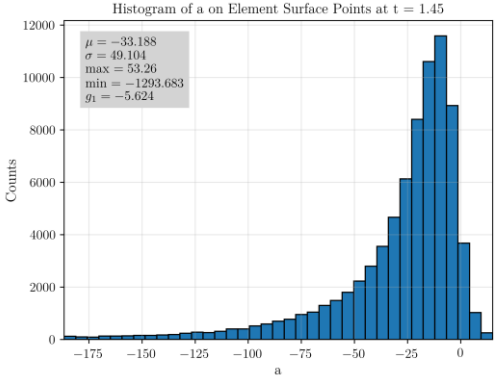

Results: Explicit Closure with optimized Cs

Mean Eddy viscosity field for Cs2

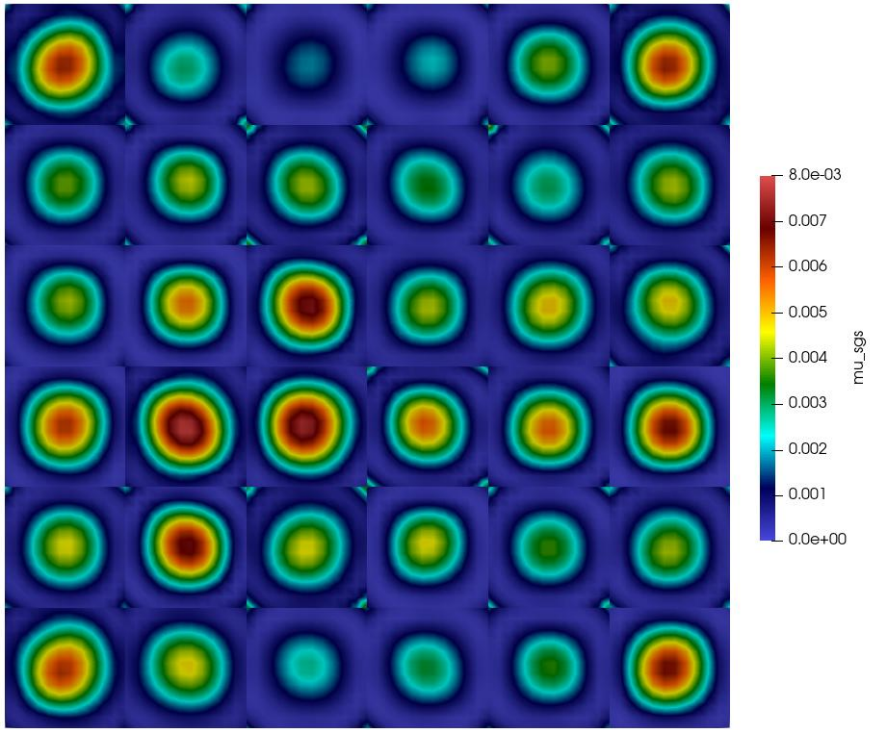

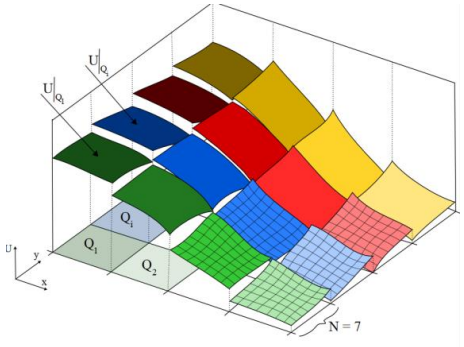

- Average the RL-predicted eddy viscosity coefficient over time
- Observation: „downwards“ oriented parabolas in each grid cell
- RL-optimized closure recognizes filter footprint

Inner-element convex blending of DG and FV I developed for Shock capturing by Henneman et al.

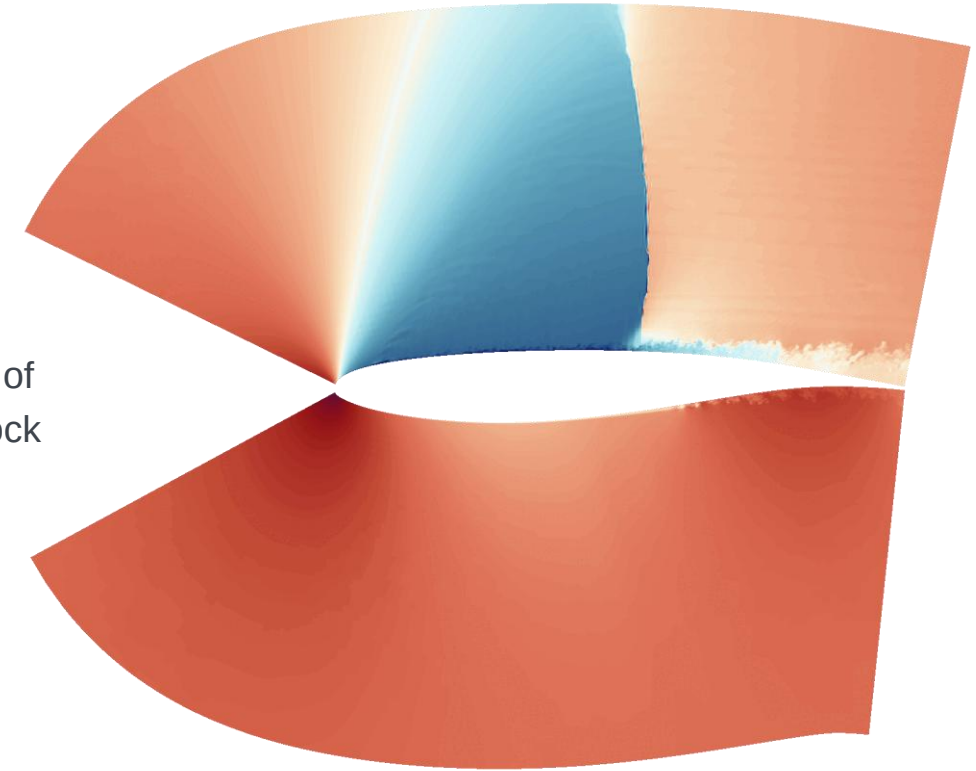

Two modelling scenarios: Implicit

Implicit and explicit SGS modeling: Optimal Operator Blending

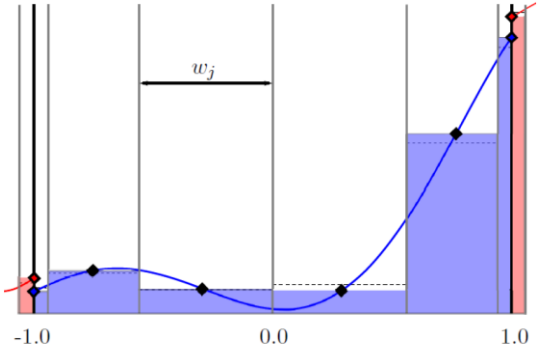

$$\underline{\dot{u}}^{BL} = \underline{\dot{u}}^{DG}\,(1-\alpha) + \underline{\dot{u}}^{FV}\,\alpha$$

A0: For each grid element q_{rst} with $r,s,t \in [1, nElems] : \alpha_s^q = \alpha(t)$

A2: For each grid element q_{rst} with $r,s,t \in [1, nElems] : \alpha_s^q = \sum_{i,j,k=0}^{2} a_i(t) L_i(x) L_j(y) L_k(z)$

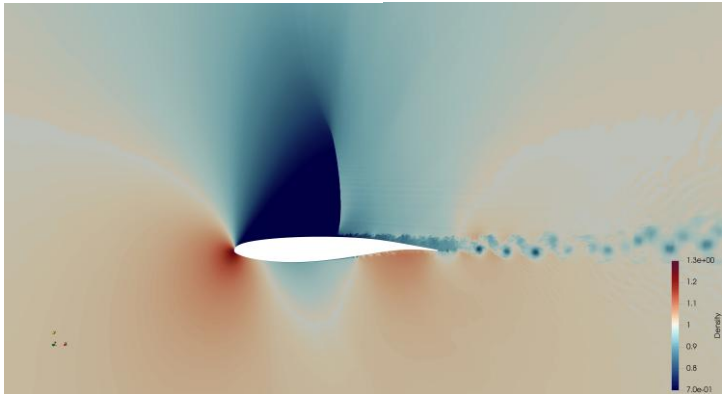

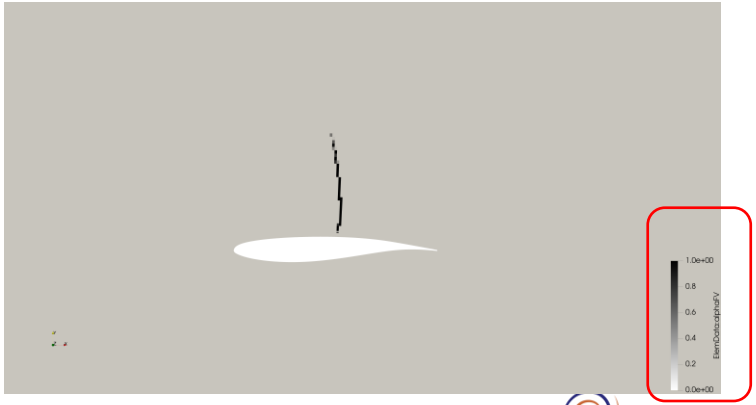

Results: Implicit Closure with optimized Blending

N=5 for different resolutions

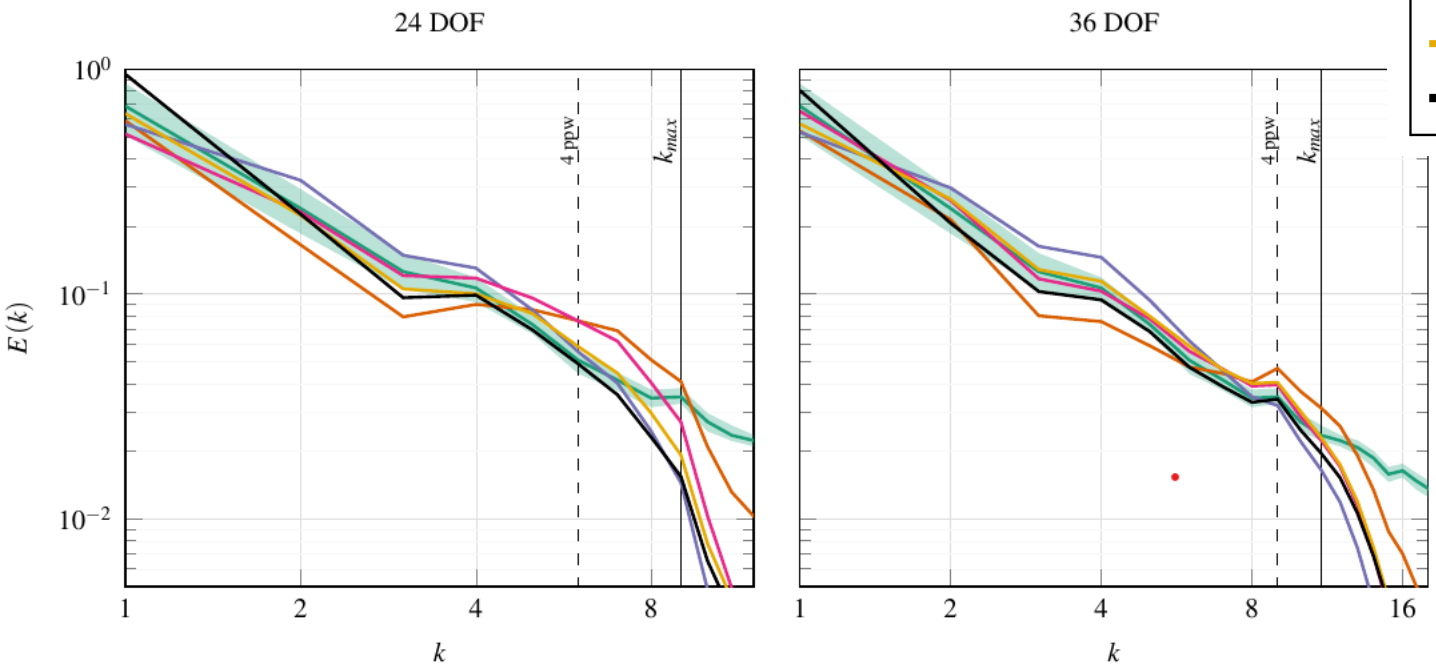

Results: Implicit Closure with optimized Blending

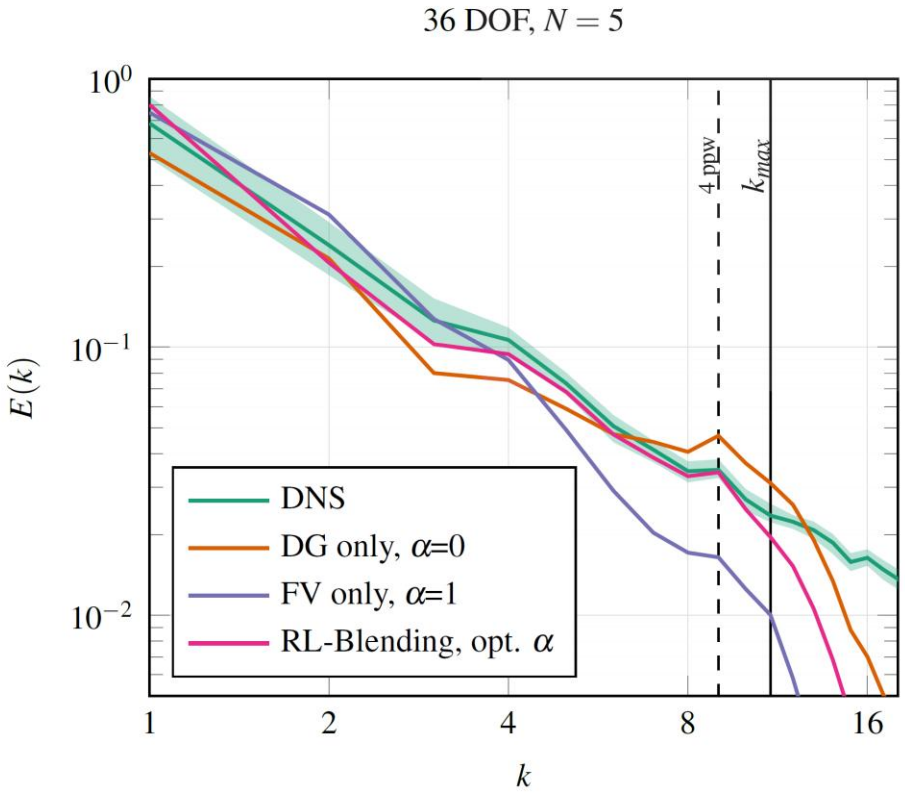

A posteriori optimal LES models: pushing the second frontier

Current Progress

Structure Preserving Closures
Joint work with B. Sanderse

- Symmetries of the NSE (Lie groups):
  - Time translation
  - Rotation
  - Reflection
  - Generalized Galilean transformation
  - Scaling transformation
  - (Pressure translation)

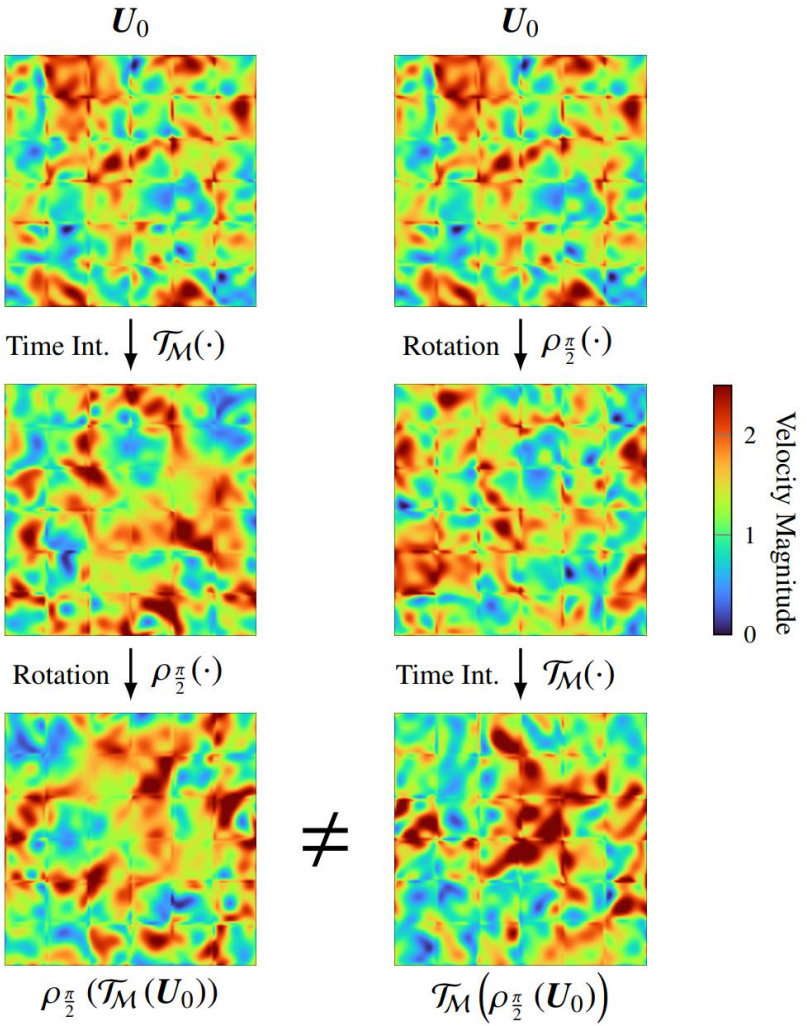

Structure Preserving Closures
Joint work with B. Sanderse

- Graph Convolutional Neural Networks
  - Embed rotational invariance
  - Trained via RL
  - Achieved reward comparable to CNN

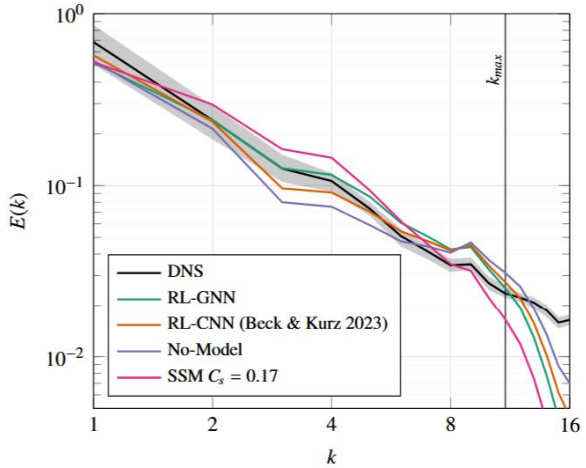

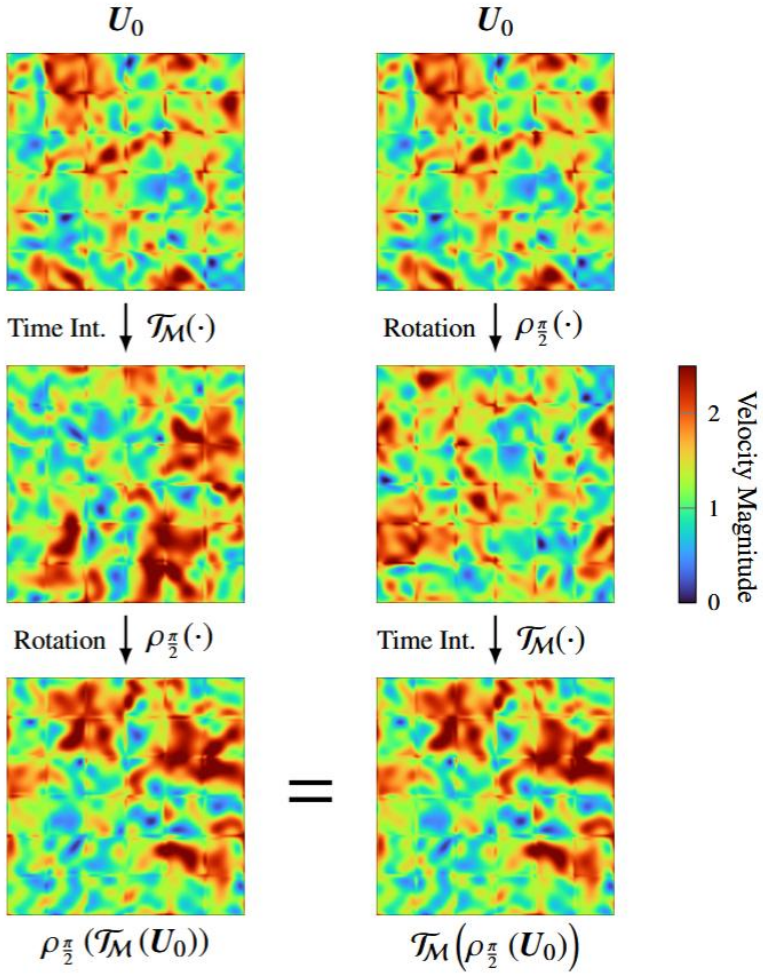

Structure Preserving Closures
Channel flow

- Reward: TBL profile
- Trained via RL

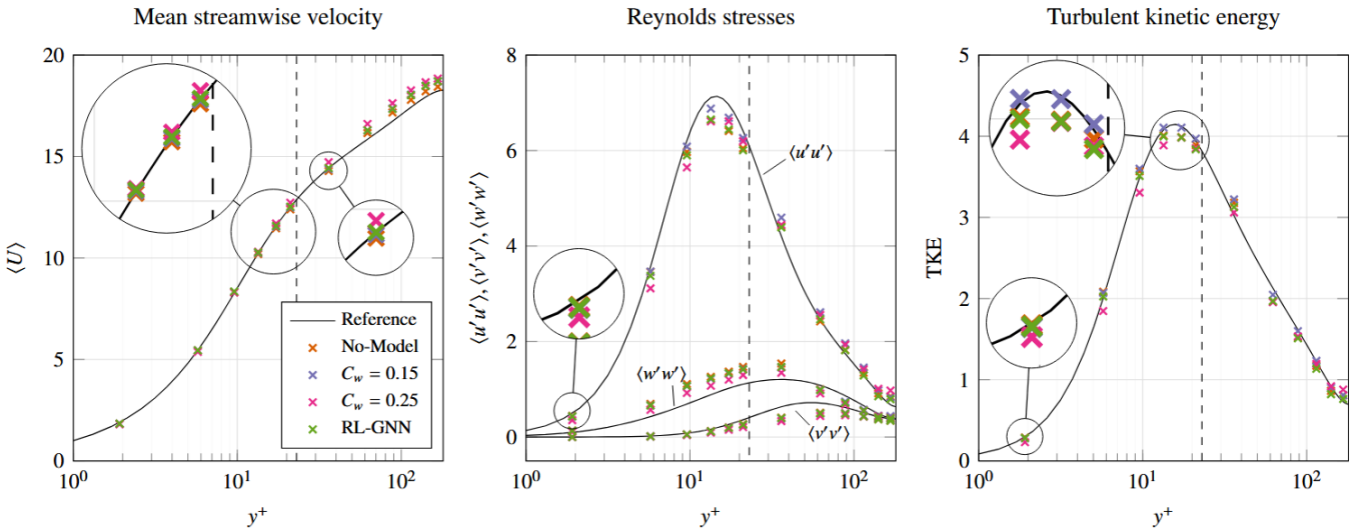

Conclusion

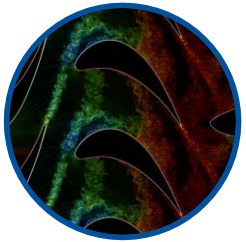

Motivation

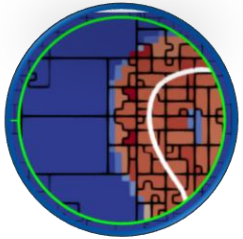

Discretization schemes for multi-X problems

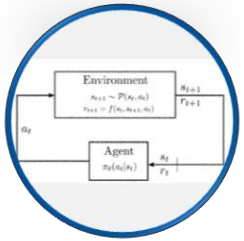

From data-driven to integrated CFD/ML

High Order Numerical Schemes for PDEs

- Are sometimes said to be….
  - Very difficult to analyze, understand, code and parallelize
  - Accurate but really slow
  - For single phase incompressible flows only
  - **Really only good for TBLs on flat plates!**

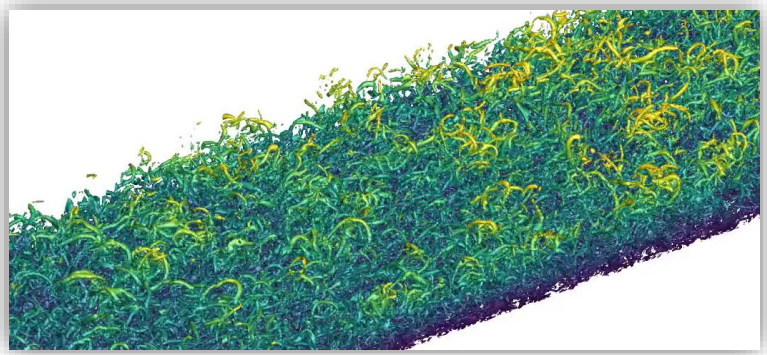

By Wenzel, Rist, Kloker at IAG

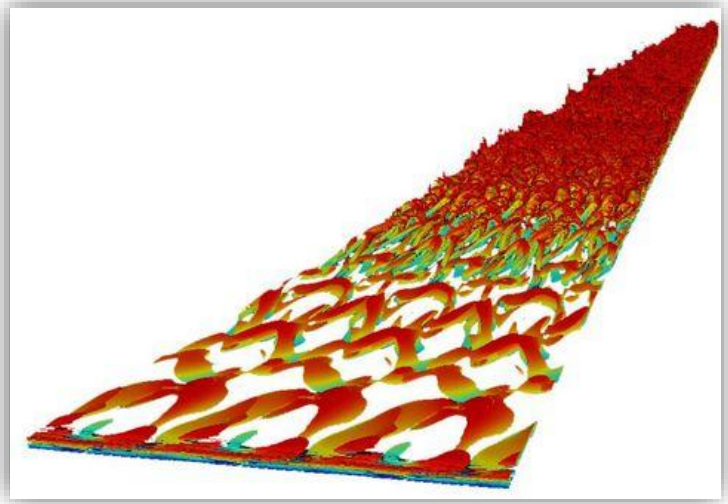

By Atak, Beck, Munz at IAG

High Order Numerical Schemes for PDEs

- Are sometimes said to be….
  - Very difficult to analyze, understand, code and parallelize ✓
  - Accurate but really slow ✗
  - For single phase incompressible flows only ✗
  - Really only good for TBLs on flat plates! ✗

  - High order schemes open up new possibilities and regimes in numerical fluid mechanics! ✓

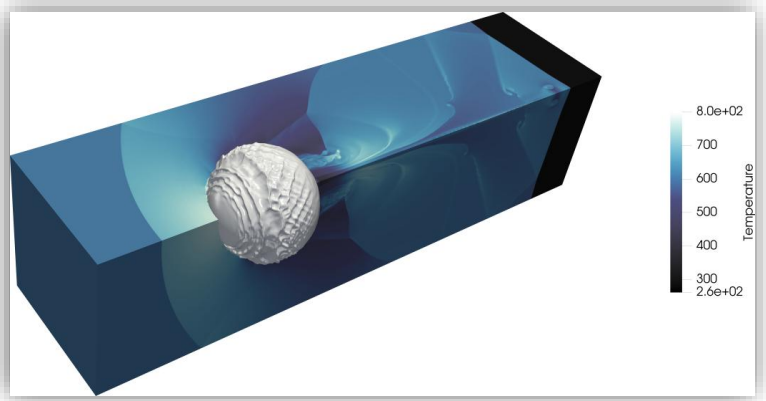

By Mossier, Appel, Keim, Beck at IAG

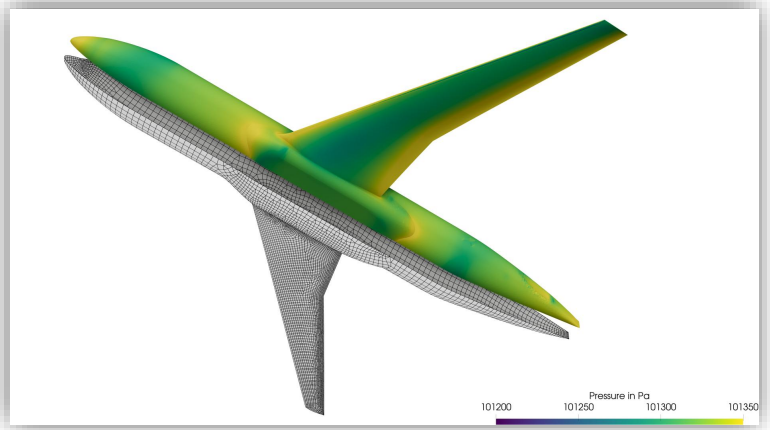

By Schwarz, Keim, Kopper, Blind at IAG

Thank you!

Thank you for your interest and thanks to all my colleagues and co-workers, in particular all present and former members of the Numerics Research Group!

www.numericsresearchgroup.org